Journal of Volcanology and Geothermal Research 417 (2021) 107295

Contents lists available at ScienceDirect

Journal of Volcanology and Geothermal Research

journal homepage: www.elsevier.com/locate/jvolgeores

Invited Research Article

The Independent Volcanic Eruption Source Parameter Archive (IVESPA, version 1.0): A new observational database to support explosive eruptive column model validation and development

Thomas J. Aubry [a,b,*], Samantha Engwell [c], Costanza Bonadonna [d], Guillaume Carazzo [e], Simona Scollo [f], Alexa R. Van Eaton [g], Isabelle A. Taylor [h], David Jessop [e,i,j], Julia Eychenne [j], Mathieu Gouhier [j], Larry G. Mastin [g], Kristi L. Wallace [k], Sébastien Biass [l], Marcus Bursik [m], Roy G. Grainger [h], A. Mark Jellinek [n], Anja Schmidt [a,o]

[a] Department of Geography, University of Cambridge, Cambridge, UK
[b] Sidney Sussex College, Cambridge, UK
[c] British Geological Survey, The Lyell Centre, Edinburgh, UK
[d] Department of Earth Sciences, University of Geneva, Geneva, Switzerland
[e] Université de Paris, Institut de Physique du Globe de Paris, CNRS, F-75005 Paris, France
[f] Istituto Nazionale di Geofisica e Vulcanologia, Osservatorio Etneo, Catania, Italy
[g] U.S. Geological Survey, Cascades Volcano Observatory, Vancouver, Washington, USA
[h] COMET, Atmospheric, Oceanic and Planetary Physics, University of Oxford, Oxford OX1 3PU, UK
[i] Observatoire Volcanologique et Sismologique de Guadeloupe, Institut de Physique du Globe de Paris, F- 97113 Gourbeyre, France
[j] Université Clermont Auvergne, CNRS, IRD, OPGC Laboratoire Magmas et Volcans, F-63000 Clermont-Ferrand, France
[k] U.S. Geological Survey, Alaska Volcano Observatory, 4230 University Dr., Anchorage, AK 99508, United States of America
[l] Earth Observatory of Singapore, Nanyang Technological University, 639798, Singapore
[m] Department of Geology, University at Buffalo, Buffalo, New York 14260, USA
[n] Earth Ocean and Atmospheric Sciences, University of British Columbia, Vancouver, Canada
[o] Department of Chemistry, University of Cambridge, Cambridge, UK

ARTICLE INFO

Article history:
Received 30 October 2020
Received in revised form 14 May 2021
Accepted 19 May 2021
Available online 25 May 2021

ABSTRACT

Eruptive column models are powerful tools for investigating the transport of volcanic gas and ash, reconstructing past explosive eruptions, and simulating future hazards. However, the evaluation of these models is challenging as it requires independent estimates of the main model inputs (e.g. mass eruption rate) and outputs (e.g. column height). There exists no database of independently estimated eruption source parameters (ESPs) that is extensive, standardized, maintained, and consensus-based. This paper introduces the Independent Volcanic Eruption Source Parameter Archive (IVESPA, ivespa.co.uk), a community effort endorsed by the International Association of Volcanology and Chemistry of the Earth's Interior (IAVCEI) Commission on Tephra Hazard Modelling. We compiled data for 134 explosive eruptive events, spanning the 1902-2016 period, with independent estimates of: i) total erupted mass of fall deposits; ii) duration; iii) eruption column height; and iv) atmospheric conditions. Crucially, we distinguish plume top versus umbrella spreading height, and the height of ash versus sulphur dioxide injection. All parameter values provided have been vetted independently by at least two experts. Uncertainties are quantified systematically, including flags to describe the degree of interpretation of the literature required for each estimate. IVESPA also includes a range of additional parameters such as total grain size distribution, eruption style, morphology of the plume (weak versus strong), and mass contribution from pyroclastic density currents, where available. We discuss the future developments and potential applications of IVESPA and make recommendations for reporting ESPs to maximize their usability across different applications. IVESPA covers an unprecedented range of ESPs and can therefore be used to evaluate and develop eruptive column models across a wide range of conditions using a standardized dataset.

* Corresponding author at: Department of Geography, University of Cambridge, Cambridge, UK.
E-mail address: ta460@cam.ac.uk (T.J. Aubry).

https://doi.org/10.1016/j.jvolgeores.2021.107295

1. Introduction

1.1. Eruptive column models: key tools for linking eruption source parameters and characterizing explosive volcanic plume dynamics

Numerical models of volcanic columns or plumes, referred to as eruptive column models (ECMs) hereafter, are fundamental to the understanding of explosive eruption dynamics, characterizing the relationship between a variety of eruption source parameters (ESPs) and, in turn, our ability to assess and manage hazards from explosive volcanic eruptions. ECMs have a range of complexity, from three-dimensional (3D) ECMs that can resolve the large-scale turbulent structure of a volcanic column but are computationally expensive, to one-dimensional (1D) integral ECMs that parameterize the turbulent entrainment of ambient air into the column and are inexpensive to run (Costa et al., 2016a). The simplest form of model consists of theoretical (e.g. Morton et al., 1956; Sparks, 1986; Wilson and Walker, 1987) or empirical (e.g. Settle, 1978; Wilson et al., 1978; Sparks et al., 1997a; Mastin et al., 2009) relationships linking the mass eruption rate (MER), and the column height. These scaling relationships, sometimes referred to as 0th order relationships or 0D ECMs, have become popular tools due to their simplicity.

The value of ECMs has become apparent during the 21st century due to an increased use of volcanic ash transport and dispersion models (VATDMs) to forecast the dispersion of ash clouds in the atmosphere and ash deposition on the ground. VATDMs have proved crucial for mitigating hazards to civil aviation (e.g. Heffter and Stunder, 1993; D'Amours, 1994; Versteegeri et al., 1995; Stohl et al., 1998; Draxler and Hess, 1998; Searcy et al., 1998) and hazard-sensitive land use planning (e.g. Barberi et al., 1990a). VATDMs require an estimate of plume height, generally constrained using satellite or ground-based observations, and an estimate of either total airborne mass of ash or the rate at which ash is injected into the atmosphere, commonly assumed to be a fraction of the MER (Gouhier et al., 2019). MER is generally estimated from the eruption column height using the 0D ECM between MER and column height. Increasingly, 1D ECMs are being coupled with VATDMs used in operational response to forecast ash dispersion (e.g. Bursik et al., 2012).

The last two decades have also seen an increased recognition that the relation between MER and plume height is complicated by a variety of factors, such as atmospheric wind velocity, the plume water content, and ash aggregation and the total grain size distribution (TGSD), among other factors (e.g. Degruyter and Bonadonna, 2012; Girault et al., 2014). 0D models, linking plume height to the MER, will thus always result in a large data scatter (e.g. Mastin et al., 2009; Mastin, 2014). They remain limited compared to 1D and 3D ECMs, which can account for the impact of vertically-resolved atmospheric conditions on plume dynamics as well as other parameters such as TGSD. As well as being able to link MER to column height, these ECMs can also make additional predictions (depending on their complexity), such as the conditions under which a volcanic column will collapse, the evolution of plume properties with height, and the distribution of ash versus gas in the volcanic column.

1.2. Overview of datasets available for the evaluation and development of eruptive column models

A requirement of datasets produced for validation of ECMs is that the ESPs serving as inputs and outputs to ECMs are constrained independently, and without reliance on any eruptive column modelling. Independent observations of the MER and column height are essential minimal requirements to constrain scaling relationships (0D) between these two parameters, which are also required to evaluate more sophisticated (1D, 3D) ECMs. However, gathering independent constraints on MER and height is challenging. Estimates of column height before the beginning of the satellite era (late 1970's/early 1980's) are, for example, sparse. MER can be estimated from field studies of deposits by dividing the erupted mass (derived from the measured volume using an appropriate bulk deposit density) by the eruption duration. However, volume estimates exist for only a relatively small fraction of eruptions in the geological record and timing information can be difficult to constrain. Table 1 lists some of those datasets with independent MER and plume height estimates available, as well as their main features. The number of events (i.e. eruption or eruption phases for which ESP are constrained) in these datasets has generally increased as new data became available (e.g. Sparks et al., 1997b; Mastin et al., 2009), aided by improvements in observations with time. For example, for column height, the use of satellite observations has become much more systematic, and community efforts such as the International Association of Volcanology and Chemistry of the Earth's Interior (IAVCEI) Remote Sensing Commission (https://sites.google.com/site/iavceirscweb/Home) have greatly improved the availability and communication of satellite observations of volcanic columns.

In the wake of eruptions such as that of Eyjafjallajökull (2010, Iceland), the following decade saw an increased recognition of the key role played by atmospheric conditions in column dynamics. A greater number of plume height scaling (0D) models began accounting for vertically-averaged atmospheric conditions (e.g. Aubry et al., 2017a and references therein). 1D ECMs also included vertical profiles of

Table 1
Overview of the key features of the main existing datasets with independent estimates of the MER (or erupted and duration) and plume height. "-" and "✓" symbols mean that the feature is not and is incorporated, respectively.

Reference or dataset name	Number of eruptive events	Strictly independent ESPs[1]	Atmospheric data[2]	Total grain size distribution	Uncertainties	Community-wide effort	Online, open access dataset	VATDM parameters[3]
Wilson et al. (1978)	8	✓	-	-	-	-	-	-
Carey and Sigurdsson (1989)	45	-	-	-	-	-	-	-
Sparks et al. (1997b)	26	✓	-	-	-	-	-	-
IAVCEI THM dataset (2001)	9	-	✓	✓	-	✓	✓	✓
Mastin et al. (2009)	35	-	-	-	-	✓	-	-
Mastin et al. (2013a)	5	-	✓	✓	-	✓	✓	✓
Mastin (2014)	25	-	✓	-	-	-	-	-
Girault et al. (2014)	10	-	-	✓	-	-	-	-
Aubry et al. (2017a)	94	✓	✓	-	✓	-	-	-
IVESPA v1.0 (this study)	134	✓	✓	✓	✓	✓	✓	-

[1]*Column height and MER were derived from independent methods for the full dataset. For example, erupted mass could not be inverted from column height using an ECM and height could not be inverted from isopleth data.* [2]*Atmospheric data means the dataset provides vertical atmospheric profiles of wind, temperature and humidity.* [3]*Also include parameters required for evaluating VATDMs, such as spatially-resolved deposit information.*

atmospheric properties (e.g. Costa et al., 2016a and references therein). As a consequence, ESP datasets which previously focused on gathering only independent estimates of MER and height plume have evolved to also compile atmospheric conditions including Mastin, 2014 and Aubry et al., 2017a. More sophisticated 1D ECMs (e.g. Girault et al., 2014) as well as most 3D ECMs account for the role of particle size (e.g. Cerminara et al., 2016) and sometimes particle aggregation (Van Eaton et al., 2015), thus also requiring TGSD as input. To date, only one dataset aimed at evaluating ECMs contains independent estimates of MER, plume height, and TGSD (Girault et al., 2014), but atmospheric conditions provided with this dataset are highly simplified. A few datasets have been developed for VATDM evaluation and contain all ESPs required for evaluation of ECMs, including TGSD and atmospheric conditions. However, the additional parameters required for VATDM evaluation (e.g. spatially resolved information on the deposit) mean these datasets only provide ESPs for a handful of events - five in the case of Mastin et al. (2013a), and nine in the IAVCEI Commission on Tephra Hazard Modelling's (THM) original ESP dataset (https://thm.iavceivolcano.org/repository/datasets.html). These datasets do not include many other parameters that are required by 1D and 3D models, for example eruptive temperature, water mass fraction and exit velocity, which are difficult to retrieve in real-time.

1.3. Motivation for the Independent Volcanic Eruption Source Parameter Archive (IVESPA)

Despite the increase in available ESP datasets, we still lack a standardized reference dataset to specifically evaluate and develop ECMs, from simple 0D models to sophisticated 3D models. Existing datasets aimed at ECM evaluation, including those of Mastin et al. (2009); Girault et al. (2014); Mastin (2014) and Aubry et al. (2017a), do not include all of the following parameters (Table 1): MER, column height, atmospheric conditions, and TGSD. Most of these datasets also contain a relatively small number of events compared to those available in the wider literature (e.g. Mastin, 2014; Girault et al., 2014). Furthermore, they represent the work of only a handful of researchers (e.g. Girault et al., 2014; Aubry et al., 2017a) rather than harnessing a broader community-wide consensus. Critically, despite the very large uncertainties associated with ESPs, only one dataset (Aubry et al., 2017a) has attempted to quantify uncertainties in a systematic manner (Table 1). ESP datasets are rarely made available in online websites, like the IAVCEI THM commission database (http://www2.ct.ingv.it/iavcei/index.htm or https://thm.iavceivolcano.org/repository/datasets.html), and even more rarely maintained. Constructing open-access datasets is also challenging because it relies on the willingness of the authors to openly share their data. Scientists commonly use these datasets without acknowledging the effort involved in its compilation. A data policy for the use of data is, therefore, required.

Illustrating the potential value of a robust validation dataset, the eruptive column model intercomparison project (Costa et al., 2016a; Suzuki et al., 2016) examined output from 0D, 1D and 3D ECMs, but did not directly test model performance against observations. This study was the first of its kind for ECMs, and the primary objective was to understand key differences between numerical parameterisations. However, such evaluation is a gold standard of intercomparison projects in other scientific communities (e.g. Coupled Model Intercomparison Project in climate science, Eyring et al., 2016a, 2019). Developing a reference observational dataset for ECM evaluation constitutes a first step towards reaching this goal.

To address these challenges, we have created the Independent Volcanic Eruption Source Parameter Archive (IVESPA). The primary objective of IVESPA is to foster the evaluation and development of ECMs (0D, 1D, 3D), and it has been developed with five main specifications:

1. Provide an exhaustive compilation of eruptive events with published estimates of MER, plume height, and atmospheric conditions that are independent from each other and independent from plume modelling constraints.
2. Include other ESPs when they are available, including TGSD which is required as input to some 1D and 3D ECMs.
3. Include uncertainties for each parameter.
4. Establish a robust and transparent quality control of the data provided.
5. Provide an online database that is easily accessible, updatable, consistently maintained, and open to the community (ivespa.co.uk).

IVESPA is the result of a collaboration between multiple research centers, geological surveys, and volcano observatories, and builds on decades of efforts in compiling observational datasets. It has been endorsed by the IAVCEI THM Commission and is supported by the Global Volcano Model and the British Geological Survey, which hosts the database website (ivespa.co.uk). In the present contribution, we introduce the methodology used to create this first version (v1.0) of IVESPA, then provide an overview of the data collected and used. We investigate in detail the uncertainties in the information collected, which is an important distinction of this new dataset. We use insights gained while gathering ESP information from the published record to provide suggestions on making field data more useful for numerical modelling purposes. Finally, we discuss future development and applications of IVESPA.

2. Methodology

In this section, we first give a general overview of the methodologies followed in the selection of events to populate the database and the presentation of information on their ESPs (section 2.1). Following this general description, we provide definitions, and detail the challenges and specificities of the data collection for each ESP (section 2.2).

2.1. Methodology

2.1.1. Condition of entry for IVESPA events

One of our main aims is to provide a database supporting model assessment in the case of explosive volcanic eruptions that generate a buoyant eruptive column or plume, originating from a vent. As a consequence, pure collapse events that only produce pyroclastic density currents (PDCs), and resulting co-PDC plumes were not considered for version 1.0 of IVESPA despite proving valuable in testing ECMs, and in particular their ability to capture the transition from a stable eruptive column to a collapsing one (e.g. Degruyter and Bonadonna, 2013; Jessop et al., 2016; Aubry and Jellinek, 2018; Koyaguchi et al., 2018; Koyaguchi and Suzuki, 2018; Michaud-Dubuy et al., 2018; 2020). We collect all parameters that represent independently estimated inputs and outputs to ECMs, and all parameters gathered must have been estimated without the use of any ECMs.

The key input that ECMs require is the MER, whose time-averaged value can be determined from the total erupted mass of tephra-fallout (TEM) and the duration of the eruption. The TEM is often derived by integrating isomass or isopach maps (see section 2.2.1). Other methods to estimate the MER or TEM exist, but the vast majority result from inverting observations, such as the column height, using a scaling relationship or a more sophisticated ECM, and can thus not be used for the purpose of testing and informing these same models. A few methods are independent from the application of ECMs but remain rarely applied and are very different in nature from TEM estimates based on field deposits, e.g. methods based on the umbrella cloud growth rates (e.g. Costa et al., 2013a; Pouget et al., 2013; 2016a; Hargie et al., 2019) or radar measurements (e.g. Gouhier and Donnadieu, 2008; Marzano et al., 2016, 2019; Ripepe et al., 2013; Freret-Lorgeril et al., 2018). The validation or calibration of these methods also sometimes rely on ECMs (e.g. Freret-Lorgeril et al., 2018). For simplicity and consistency, we thus restrict version 1.0 of IVESPA to eruptive events for which

both a deposit-derived TEM estimate and a duration estimate were available in the literature.

In addition to the MER, the vast majority of plume models now require atmospheric conditions (density profiles, wind speed and direction) from ground level up to the height reached by the plume as inputs. While direct observations of atmospheric conditions near the eruptive vent are not systematically available, even for relatively recent events, the development of multiple climate reanalysis (section 2.2.4) means that model estimates of atmospheric conditions derived from observations from at least 1979 and in some cases as far back as 1600-1900 are commonly available. To guarantee that atmospheric data from at least two different reanalyses using a relatively dense array of observations were available, we only consider volcanic events that occurred since 1900 or later for this first version of the database. Last, we require all events of IVESPA to have at least one type of measurement of the eruptive column height and allowed for three different types defined as in section 2.2.3.

To summarize, we impose the following conditions for any eruptive event to be included in IVESPA:

1. An estimate of the TEM derived from the tephra deposit is available.
2. An estimate of the duration is available.
3. An estimate of at least one of the three types of eruption column height considered (see section 2.2.3) is available.
4. The event occurred in 1900 or later, guaranteeing the availability of estimates of atmospheric conditions from well-constrained climate reanalyses.
5. All above estimates must be independent of any ECMs.
6. All above estimates must be independent of each other.

We refer to the first three parameters listed above (TEM, duration, eruptive column height) as basic "key" ESPs, as together they enable constraint of the input (MER, obtained from TEM and duration) and output (height) common to all ECMs (0D, 1D, 3D). We refer to any sequence of an eruption fulfilling the list of above criteria as an "event". A specific volcanic eruption may thus contribute several "events" to the database if distinct estimates of key ESPs exist for each event. Last, we made a number of exceptions to the sixth criteria listed above:

- Column heights obtained from satellite-measured brightness temperature and an atmospheric temperature profile (inducing a dependence between the plume height and atmospheric conditions) can be used.
- Column heights obtained from the inversion of the ash or sulphur dioxide (SO_2) dispersion patterns and wind field using a trajectory model (inducing a dependence between the column height and atmospheric conditions) can be used.
- Eruption chronologies established on the basis of shifts in wind direction and differences in tephra layer dispersal direction (inducing a dependence between the duration and atmospheric conditions above vent) can be used.
- Event duration constrained using observations of the volcanic plume (inducing a dependence between duration and column height) can be used.

While commonly encountered in estimates of ESPs, these dependencies would result in negligible biases for understanding the relationships between ESPs and evaluating ECMs.

2.1.2. Data sources

This study undertook an extensive search of the published literature and of other sources, such as bulletins of the Global Volcanism Program (GVP), and reports from volcano observatories to compile ESPs. Table 2 summarizes the 340 sources used. The published peer-reviewed literature in the English language accounted for 66% (225 articles) of our sources, with several journals unsurprisingly dominant such as *Journal of Volcanology Geothermal Research* (73), and a total of 43 different journals spanning the period 1949 to the present day. Other types of sources used include online reports (particularly the GVP, which alone was referenced for 58 separate events); books (7 entries in the database); student theses (3 entries); reports from volcano observatories, meteorological offices and national geological surveys (e.g. USGS reports, 15 entries); personal communications reporting direct (i.e. field) or indirect measurements (e.g. analysis of satellite data) (7 entries); and non-reviewed scientific publications such as technical reports and conference proceedings (13). The full reference list is available in Appendix A and on the online database website (ivespa.co.uk).

Table 2
List of the different types of sources used in compiling ESPs for IVESPA.

General type	Journal name or type	Count
Peer-reviewed journal article in English (total = 225)	Journal of Volcanology and Geothermal Research	73
	Bulletin of Volcanology	39
	Journal of Geophysical Research: Solid Earth	17
	Geophysical Research Letters	9
	Journal of Geophysical Research: Atmospheres	9
	Earth and Planetary Science Letters	6
	Atmospheric Chemistry and Physics	5
	Earth, Planets and Space	5
	Geochemistry, Geophysics, Geosystems	5
	Journal of Volcanology and Seismology	5
	Science	5
	Other journals (32)	47
Other sources (total = 115)	Global Volcanism Program	58
	Geological Survey or Meteorological Office reports or communications (USGS=15)	23
	Conference abstracts or articles	13
	Books	7
	Personal communications	7
	PhD/MSc thesis	3
	Other	4

2.1.3. Best estimate, uncertainty, and interpretation flags

ESP estimates are commonly subject to large uncertainties and are used to initiate and test numerical models which themselves are limited by uncertainties (e.g. understanding of the underlying process) propagating uncertainties further. Yet, ESP uncertainties are not systematically rigorously documented in the literature and are even less commonly reported in ESP datasets (Table 1). To make progress, in addition to providing a best estimate for all numerical parameters, we also provide an uncertainty for all relevant parameters of the database. In general, the uncertainties provided in IVESPA are meant to be representative of a high confidence level, calculated as a 95% confidence interval when the available data enables it. We provide a single value for uncertainty, with the underlying assumption that uncertainty is symmetric around the best estimate value provided. The only exception is for TEM for which we decided to provide both a lower and upper bound uncertainty because studies which have rigorously quantified uncertainty on this parameter commonly show strongly asymmetric probability distributions for the true value of TEM (Bonadonna et al., 2015a). We describe parameter-specific challenges encountered when providing uncertainty in section 2.2.

Most databases describing volcanic activity are built on information gathered from the published record, e.g. the LaMEVE (Crosweller et al., 2012), DomeHaz database (Ogburn et al., 2015), or the GVP database, and that is also the case for IVESPA. When gathering ESPs from the published record, information on the data provided (e.g. what parameter was exactly measured, how and when) and its uncertainties may be incomplete or unclear. As a consequence, experts compiling databases on volcanic activity must commonly interpret sources, i.e. make assumptions on missing information, to estimate the most appropriate value

of an ESP best estimate or uncertainty. For example, a paper may provide a clear estimate for the column height, but be unclear whether the height quoted is above vent, ground (e.g. plains surrounding volcano used as a reference point to measure the height) or sea level (a.v.l., a.g.l. and a.s.l.). The level of interpretation required to provide ESP estimates may directly affect their reliability and, in turn, the use or weight given to specific events in ECM evaluation studies. However, this interpretation is rarely discussed and never documented in ESP datasets. To move forward, we systematically provide an interpretation flag for both best estimate and uncertainty values associated with all key ESPs provided in the database (i.e. TEM, duration, and the three column heights). Interpretation flags can take values of 0, 1 or 2, and Fig. 1 illustrates how these values were attributed. Flag 0 corresponds to parameters which required negligible interpretation of the literature, and/or for which required interpretation had a negligible influence on the parameter value. In contrast, flag 2 corresponds to parameters which required significant interpretation or educated guess, and/or for which this interpretation exerted a major influence on the final value attributed. Flag 1 corresponds to intermediate levels of interpretation. The type of sources used to derive the value of an ESP (see section 2.1.2) also influenced the choice of interpretation flag values, with information not issued from the peer-reviewed literature leading to higher values of interpretation flags because of the lack of peer-reviewed/objective information on which to rely for estimating an ESP value. Detailed examples of choices made for flag values for all parameters are provided in section 2.2.

Last, we do not provide uncertainty or interpretation flags on categorical parameters (e.g. eruption style), some trivial parameters consisting of a single numerical value (e.g. latitude of eruptive vent) and quantitative parameters consisting of more than one numerical value (atmospheric conditions and TGSD). For atmospheric conditions, two profiles issued from two different families of reanalysis are systematically provided (section 2.2.4). For TGSD as well as for TEM, the only key ESP for which uncertainty could not always be constrained, we provide "metadata" (see section 2.2) describing the deposit sampling quality. This metadata can then be used to infer the uncertainty on these deposit-derived ESPs.

2.1.4. Initial quality control of key eruption source parameters

IVESPA is downloadable as datasheets and is accessible through a searchable website (ivespa.co.uk) on which database users can post comments, suggestions, and feedback which may lead to correction of initially provided ESP values and new entries in the database. Ultimately, we hope that community contributions will result in a database in which values provided are consensual across the volcanology community. To ensure that values initially provided represent a reasonable consensus, we implemented an initial quality control by at least two "data contributors" (DCs), who are members of the IAVCEI THM commission working group tasked with the creation of IVESPA and co-authors of this paper. DCs were asked to independently provide estimates of the best value, uncertainty, and associated interpretation flags (Fig. 1) of all key ESPs for each event of the database. This process was 'blind' in that none of the DCs were aware of the data sources referenced by the other DCs, nor of the estimated values. DCs could choose to use any data source (see section 2.1.2) for providing ESPs. This helped to maximise the range of publications and to thus sample from as many sources as possible. The DCs then compared and discussed their values until they reached a consensus. The consensual values reached are the final values provided in IVESPA. However, we also made available values initially proposed by individual DCs as well as spreadsheets with detailed comments tracking how consensual values were reached from values initially provided by two or more DCs. In the future, new entries to IVESPA will undergo the same procedure with at least two experts providing key ESPs values and reaching a consensus before inclusion in the database. Documents summarizing core discussions between DCs are available via the IVESPA website (ivespa.co.uk), and detailed notes on each event are available upon request from the corresponding author.

The number of references available for each ESP may greatly influence discrepancies between different DCs. For eruptions with a large number of references, it is unlikely that DCs will perform an exhaustive search of ESP estimates throughout all references available and differences in their ESP estimates may reflect preferences for certain references. For eruptions with a small number of references, some references may be particularly challenging to find and failure to do so

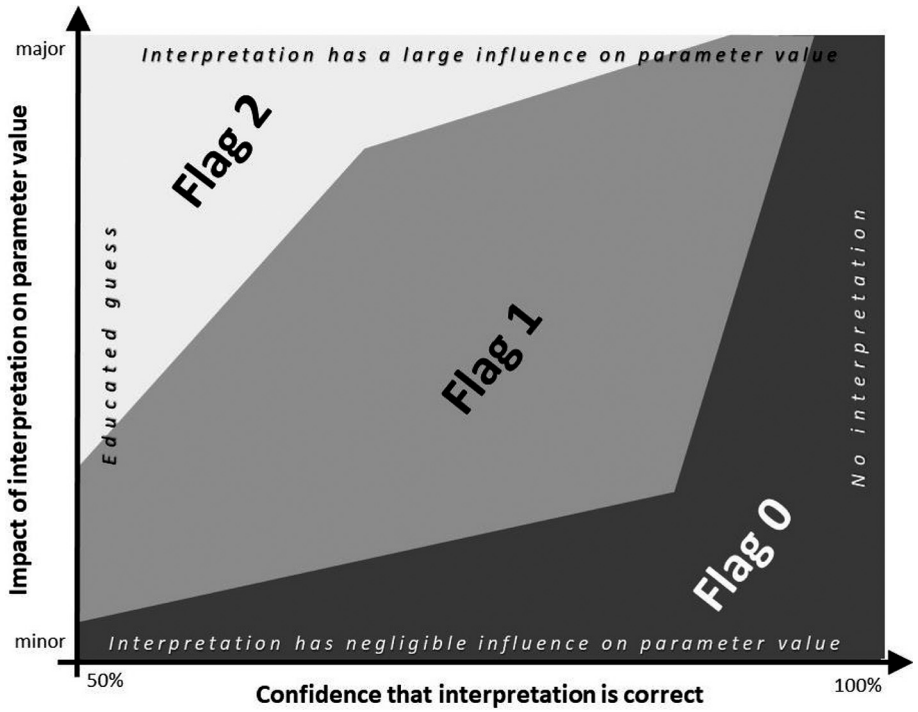

Fig. 1. Chart illustrating how interpretation flag values relate to the confidence in our interpretation and its impact on parameter value.

may result in very different ESP estimates due to scarcity of information. To better assess how much ESP estimates may differ depending on the expert compiling data from the literature, we extended the above quality control procedure to eight DCs for two example eruptions in the database. For this purpose, we chose the 2015 eruption of Calbuco and the 1971 eruption of Fuego, which are respectively representative of eruptions with a relatively large and small number of dedicated studies. A detailed analysis of discrepancies between the different ESP estimates and of the final consensual value chosen is provided in section 4.

2.2. Parameters collected

In this subsection, we provide a definition and overview of all parameters collected. For our three key ESPs (sections 2.2.1, 2 and 3), we first provide the parameter definition before discussing in detail two examples of events which represent challenging and ideal cases for the compilation of that ESP, along with explanation for the values chosen in IVESPA to illustrate the data collection process.

2.2.1. Total erupted mass of tephra-fallout deposits

2.2.1.1. Parameter definition. The total erupted mass (TEM) of tephra-fallout deposits is one of our key ESPs and was collected solely from sources that used the properties of the tephra-fallout deposit to derive its volume or mass. In theory, both can be estimated based on the field mapping of the deposit thickness (volume) or mass per unit area (mass), which are then contoured into isopach or isomass maps, respectively. The final volume or mass can then be obtained by integrating the square root of the area of each contour against the contour's value on a semi-log plot (e.g. Pyle, 1989). In practice, this process is complicated by sources of uncertainties that can be classified into four broad categories. First, various uncertainties are related to the deposit's properties, e.g. its accessibility and preservation, which affect the density and spatial distribution of samples, or the natural variability of emplacement processes, which affect how representative a given sample is of the surrounding local conditions (Engwell et al., 2013). Second, a subjective component is inherent to the measurement of thickness and or mass per unit area values (e.g. Engwell et al., 2013). Third, some uncertainties can be associated with the contouring of the deposit's thickness or mass per unit area. Although semi-empirical methods have been proposed to minimize the subjective component of the contouring processes, most values of mass and volume in the literature inferred from deposit geometries rely on hand-drawn contours (e.g. Klawonn et al., 2014a, 2014b). A number of techniques for automating construction of isopach maps have been produced (e.g. Engwell et al., 2015; Yang and Bursik, 2016) however these also typically involve the choice of some fit parameter. The fourth source of uncertainty relates to the strategy chosen for computing the final value of volume or mass (e.g. Bonadonna et al., 2015a). On the one hand, various empirical approaches have been proposed to describe the variable thinning rates of tephra deposits and extrapolate the deposit in regions where it is either inaccessible (e.g. proximal regions) or removed (e.g. distal regions). Each approach's strengths and weaknesses have made them more appropriate in different contexts and, as a result, deposit volumes or masses are often reported in the literature as a range bounded by the estimates provided by the different models. On the other hand, the field measurement of the deposit thickness is easier and more time efficient in case of old deposits than measuring a mass per unit area. In contrast, sampling of tephra fallout in real time or quasi real time (i.e. within a few hours or days from the eruption) is more efficient in mass per unit area. Consequently, estimates of the TEM are frequently only a simple product of the volume of the deposit by a single generic value of density assumed to be constant over the entire deposit and vice-versa. For some deposits, numerous measurements of deposit density are available at different distances from vent, making the conversion between mass and volume more accurate.

Whenever distinct mass or volume estimates were provided in the literature, the TEM includes only the mass of fallout deposits from a vent-sourced stable volcanic column only, and an estimate for the deposit mass derived from PDCs is provided separately. Accompanying the TEM estimate, we provide a categorical parameter indicating whether the TEM was directly obtained from measurements of mass per unit area, or whether it was obtained from the deposit volume and density. We also provide the value of the deposit bulk density, which was assumed to be 1000 kg m^{-3} when no estimate was available in the literature, with this default value being representative of the average density for events across which it is available (e.g. Scasso et al., 1994; Andronico et al., 2014a). In contrast to event duration and column height, uncertainty information on TEM in the published record is commonly not provided and hard to infer from contextual information, so that it is the only key ESP for which we did not systematically provide an uncertainty. However, we provide a set of "metadata" on the deposit, including

- The number of sampling sites at which the thickness or mass per unit area was measured.
- The minimum and maximum distance of sampling sites from the eruptive vent.
- The number of lines drawn on the isopach or isomass map.
- The minimum thickness or mass per unit area value among these lines.
- A subjective estimate of the fraction of the deposit lost to sea or ocean, expressed as a categorical parameter taking values "negligible", "some" and "significant".
- The delay between the eruptive event and the data collection.

These metadata complement the uncertainty estimate, when provided, and interpretation flags in providing users with information on the quality of the deposit dataset and TEM estimate provided. Ultimately, investigating the relationship between these metadata and the uncertainty on TEM may enable us to make informed estimates of TEM uncertainty for events for which it is not constrained in the literature.

2.2.1.2. Examples of challenging and ideal events to collect the parameter. To illustrate some of the data collection process for TEM, we discuss two eruptions included in the database. The Cordón Caulle 2011 eruption (Chile) represents a case for which TEM collection was relatively straightforward thanks to excellent data presentation in Pistolesi et al. (2015) and Bonadonna et al. (2015b). The sampling of the deposit and the stratigraphy is clearly presented in Pistolesi et al. (2015) and the authors included isopach maps (showing both the thickness contours and the sampling locations) and thinning trend plots for all stratigraphic units which represent different events within the eruption for which a volume and TEM could be constrained. Multiple strategies were used to integrate thinning trends and obtain a volume, and the authors provided values obtained from each of these strategies as well as averages and standard deviations across all strategies in a table. The bulk deposit density for each event was also clearly constrained with distance from the vent enabling confident derivation of mass estimates (Bonadonna et al., 2015b). Last, the role of PDCs is also clearly discussed and their volume was constrained, enabling us to confidently provide distinct estimates for our TEM parameter and the erupted mass derived from PDCs. As a result of the clear data presentation, there was excellent agreement between the TEM parameter values compiled independently by the two DCs in charge of this eruption, and interpretation flags for both the TEM best estimate and uncertainty were chosen to be 0 (no or negligible interpretation, see Fig. 1). The only minor discrepancy related to uncertainty, with one DC choosing the one standard deviation values quoted in Pistolesi et al. (2015) and Bonadonna et al. (2015b), and the other one doubling them. The latter option is more consistent with our aim to provide uncertainties representative of a 95% or

"high" confidence level and it was thus chosen as the consensual value after minimal discussion. TEM uncertainty estimates can be slightly more refined than those from the Cordón Caulle 2011 eruption. For example, TEM uncertainty of some events in the database accounted for uncertainties in drawing of the isopach map or the bulk density of the deposit. However, the choice of the thinning trend integration strategy is one of the dominant causes of TEM uncertainty (Bonadonna et al., 2015a) and the Cordón Caulle 2011 eruption represents a nearly ideal case for TEM collection from published literature.

In contrast, the Sarychev Peak (Russia) 2009 eruption took place on a remote island, and therefore most of the deposit was lost to sea and field analysis of land deposits, and estimation of TEM, proved very challenging. As a consequence, one of the only references with information on the deposit (Rybin et al., 2011) did not include any detailed information on the sampling conducted, nor any plot or data on isopach map or thinning trend. The authors mention a preliminary estimate of the bulk volume of 0.4 km^3 with no further justification. The minimal description provided at least gave confidence that this estimate was based on field data and not, for example, on inversion of plume height via plume modelling. The thickness of the deposit was apparently sampled on distant islands which also suggests that this estimate is not based solely on the proximal deposit on the Matua Island where Sarychev Peak is located. A second reference (Rybin et al., 2012) quotes volume estimates between 0.1 and 0.4 km^3, but we could not access any of the references quoted and no additional information on how these estimates were obtained was provided. To obtain a TEM estimate for the Sarychev Peak 2009 eruption based on this information, both DCs working on this event chose to use the volume estimate of 0.4 km^3 and an arbitrarily assumed density of 1000 kg m^{-3} (e.g. Scasso et al., 1994). An interpretation flag value of 1 was given to the TEM best estimate, although the possibility of using a flag 2 was discussed. Ultimately, there was only one volume estimate available in the peer-reviewed literature (Rybin et al., 2011) so that even if it is poorly informed, no interpretation was required in choosing a volume estimate. DCs had to make an educated guess for the bulk deposit density, but volume uncertainty is expected to be the dominant contribution to the TEM uncertainty so that DCs did not deem that a flag 2 was justified for the TEM best estimate. However, in the absence of any other information, no TEM uncertainty (and no interpretation flag for the uncertainty) was provided for this event.

2.2.2. Event duration

2.2.2.1. Parameter definition. Duration is one of the key ESP collected for each volcanic event of the IVESPA database because it is required to obtain the MER from the TEM. To be as consistent as possible in the calculation of the MER, we define duration of an event in IVESPA as the duration of the sustained eruptive phase(s) during which most of the tephra volume was erupted by the volcano. This parameter was particularly challenging to define owing to a variety of factors:

1. Various definitions for the duration of a volcanic event are used in the literature, and it is often unclear which definition was used in original references and the extent to which it is compatible with the definition we use in IVESPA. For example, duration may be defined as the period of time when a volcano is erupting volcanic material (e.g. Gunn et al., 2014). However, it is well known that an eruption can show different phases (e.g. explosive, effusive) and styles (e.g. Strombolian, Vulcanian), sometimes separated by periods of quiescence. During some of the eruption phases, the emitted material (e.g. volcanic gas, lava, minor/sporadic ash during ash venting or vent clearing events) may not be relevant to the emplacement of the tephra fallout deposit from a sustained column, and such phases were excluded when estimating event duration for IVESPA.
2. A large variety of methods can be applied to measure the duration of an event, and these methods result in different estimates and sometimes impose different definitions of the eruption duration. These methods include image analysis from visual and thermal cameras, satellite observations, ground-based radar, and analysis of infrasound signals and volcanic tremor. It is also common that the only source of information is visual reports from local witnesses (non-expert observers). We also considered events for which the only source of information on duration is indirect observations, such as reports on the noise of the eruption or the glow of the eruptive vent/column at night, as well as ashfall reports (e.g. Hill et al., 1998). Such observations may be poorly representative of the duration during which most of the tephra was emitted, e.g. ashfall timing, even when corrected for ash transport and settling, is a very uncertain proxy for ash emission at the vent. Accordingly, uncertainties and flag values are generally particularly high when using indirect evidence to estimate duration.
3. For eruptions for which multiple events can be constrained, each event corresponds to a distinct layer of the tephra deposit whose properties were measured to provide an estimate of the volume or mass of that specific layer. Layers are often separated based on either the properties of the deposited tephra (e.g. size distribution, componentry or color) or the main direction of dispersal governed by wind direction at the altitude at which most of the ash was injected into the atmosphere. Thus, determining the timing of emplacement of each layer requires observations of the corresponding transitions in eruption style or in wind direction (e.g. Gudmundsson et al., 2012). The exact timing of such transitions is often challenging to constrain.

2.2.2.2. Examples of challenging and ideal events to collect the parameter. While it represented a nearly ideal case for TEM collection, the 2011 eruption of Puyehue Cordón Caulle is a typical example of an eruption for which the duration of individual eruptive events was particularly hard to estimate. The volume of four distinct groups of tephra layers is constrained by Pistolesi et al. (2015) (layers A-B, A-F, H, and K2). However, we could not find any constraint on the time at which the activity associated with layer B finished, which prevented estimating two key ESPs, the duration and the height. Consequently, we could only provide ESPs for three eruptive events for this eruption corresponding to layers A-F, H and K2. For layers A-F, Bonadonna et al. (2015c) provide detailed estimates of the duration but these are based on the ratio between the TEM and the MER as inverted from plume height using an ECM; as such, these estimates do not fit our set of entry conditions (see section 2.1.1) and were ignored. By comparing deposit dispersal and satellite images, Pistolesi et al. (2015) estimated a duration of roughly 24-30 hours. A compatible duration of 27 hours is mentioned in Jay et al. (2014), but this reference is a conference presentation and does not include any detail on the methodology. Consequently, DCs decided to use a duration of 27 hours with an uncertainty of 3 hours, but to attribute a flag 2 (see Fig. 1) to both the best estimate and the uncertainty. The duration of the second event of this eruption, corresponding to layer H, was equally hard to constrain. Pistolesi et al. (2015) attributed various satellite images to different layers deposited by the eruption, based on the correlation between the deposit dispersal direction and the wind direction. They could not attribute any satellite image to layer H but one image at 19:45 (local time) on June 6 is attributed to layer G (preceding layer H) and one at 13:28 on June 27 to layer K2 (following layer H). This suggests that the maximum duration of the phase (or event) depositing layer H was ca. 17 hours. Furthermore, they state that the phase depositing layer H started during the night of June 6 and that the phase depositing layer K2 (the layer above layer H) started in the morning of June 7. Assuming that a night start was before 3:00 at the latest and a morning end after 6:00 at the earliest, the minimum duration of the event depositing layer H was 3 hours. Bonadonna et al. (2015c) also state that the maximum duration of the event that deposited layer H was 12 hours. Based on interpretation of published information, the minimum duration of the event depositing layer H could thus be ca. 3 hours and the maximum duration could be 12 hours, possibly up to 17 hours. One

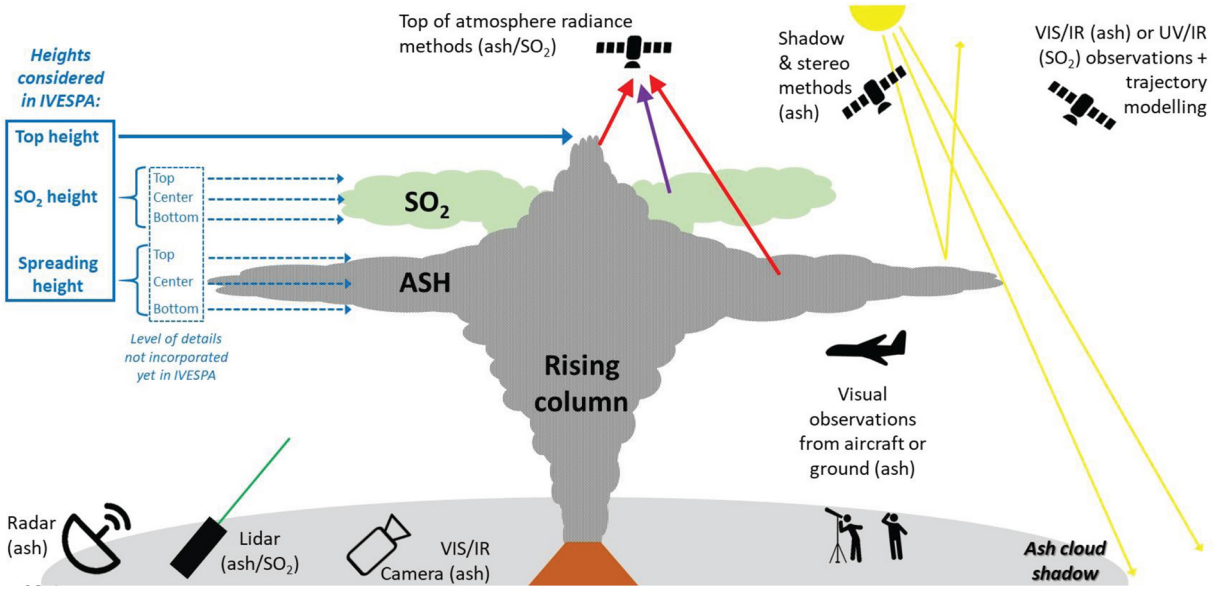

Fig. 2. Cartoon illustrating the three column heights considered in IVESPA (box to left), as well as the various measurement techniques constraining values in the database. We also illustrate more refined height definitions not yet incorporated in IVESPA v. 1.0 (box with dashed line). The cartoon shows a strong plume with separation of volcanic ash and SO_2; note that these two phases are not always decoupled, and that for a weak plume (bent-over by the wind with no overshooting top), the top height equals that of the top of the spreading umbrella cloud. IR, VIS and UV stand for infrared, visible and ultraviolet, respectively.

DC with no a priori knowledge of the eruption thus proposed a duration of 7.5 hours with an uncertainty of 4.5 hours, and interpretation flag values of 2 for both the best estimate and uncertainty. However, the second DC had first-hand knowledge of the eruption that provided insight that the duration was between 6 and 12 hours for this event. The final consensual value for the duration of this event was thus 9 hours with an uncertainty of 3 hours, and we retained interpretation flag values of 2 given the minimal amount of information available in the literature and the substantial role of interpretation and expert judgement required to provide an estimate of the duration.

Contrary to the 2011 Puyehue Cordón Caulle events, duration was straightforward to constrain for the 22 April phase of the 2015 Calbuco eruption. Based on seismic signals, visual observations, and satellite observations, available references place the start of the eruption between 21:04 UTC and 21:06 UTC, and the end between 22:32 UTC and 22:35 UTC (Romero et al., 2016b; Van Eaton et al., 2016; Global Volcanism Program, 2015a; SERNAGEOMIN, 2015). Based on the eruption description in these references, we are confident that sustained ash emission occurred between these time stamps, and Vidal et al. (2015a) also state that the most energetic phase of the eruption lasted 90 min. We chose the latter estimate as the best estimate for the duration of this event, with an uncertainty of 4 min covering the duration range of 86-91 min informed by the start/end time. No interpretation of the literature was required to come up to these estimates and we thus chose interpretation flag values of 0 for both the best estimate and uncertainty.

2.2.3. Column heights

2.2.3.1. Parameter definition. The column (or plume) height is the main output common to all ECMs. Its estimation is key for characterizing the explosivity of volcanic eruptions (Newhall and Self, 1982) and to evaluating the level of the plume injection used by Volcanic Ash Advisory Centers (VAACs) to forecast volcanic ash dispersion during a volcanic eruption (e.g. Witham et al., 2007). This value is also essential to run plume gas and aerosol retrievals (Prata and Grant, 2001; Corradini et al., 2018). While volcanological studies - including those compiling ESP datasets - often mention "the" plume height without explicit definition, multiple metrics for the vertical extent of an eruptive column exist (Fig. 2) and the discussion of column height is increasingly nuanced in the literature. The most common distinction is between the maximum or "overshoot" height reached by a volcanic column, referred to as the top height hereafter, and the height at which an umbrella cloud is spreading, referred to as the spreading height hereafter (Fig. 2). Because most early measurements of volcanic plume vertical extent were based on visual observations, the first estimates of the top height and spreading height available refer to the ash-rich part of a volcanic column. However, volcanic columns are fundamentally multiphase flow, and as remote sensing methods to measure plume height have developed, the height of dispersion of SO_2 is now a standard measurement during volcanic eruptions (e.g. Carboni et al., 2016). In particular, it has become clear that the ash and gas phase of a volcanic plume can separate and disperse at different altitudes (Schneider et al., 1999; Prata et al., 2017). In addition to being observed, these different types of plume heights can also be distinct outputs of some ECMs, and using more than one height enables to improve the evaluation and/or predictions of ECMs (e.g. Suzuki and Iguchi, 2019).

Consequently, in version 1.0 of IVESPA, where possible we compile height data for three different types of plume (Fig. 2):

- "Top height": the top height of the tephra phase of the plume, i.e. its maximum height in a spatial sense (not in a temporal sense, see below).
- "Spreading height": the spreading height of the tephra phase of the plume.
- "SO_2 height": the height of dispersion of SO_2.

Each event in the database has at least one of these three measurements available (section 2.1.1). As key ESPs, all three types of height collected systematically include a best estimate, an uncertainty, and interpretation flags for both values (see section 2.1.3 and Fig. 1). The distinction between these different types of height represents a major improvement over previous ESP datasets where a single height was compiled, sometimes loosely defined (e.g. Sparks et al., 1997b; Mastin et al., 2009; Aubry et al., 2017a; IAVCEI THM database). Because of the dominance of satellite-measured height in the data collected, we provide height in km a.s.l. However, we systematically provide the altitude

of the eruptive vent (see section 2.2.6) so that IVESPA users can easily convert these heights to km a.v.l., which is a more meaningful metric for plume dynamics. We aim to provide heights that are representative of the time-averaged value over the duration of volcanic events. Previous datasets have sometimes compiled heights that are more representative of the maximum height reached during an event (e.g. Sparks et al., 1997b; Mastin et al., 2009). However, MER values derived from the TEM (section 2.2.1) and duration of sustained ash emission (section 2.2.2) are representative of the time-averaged MER (as opposed to a peak MER). Thus, providing time-averaged plume heights is more consistent with the definition of the other key ESPs collected. All heights provided are also aimed to be representative of the vertical extents of the column near the vent, before transport and radiative processes affect the vertical distribution of volcanic products initially determined by the eruptive column dynamics. For the spreading height of any type of plume, a few studies (e.g. Van Eaton et al., 2016) sometimes provide detailed information on whether their measurements are representative of the top, center or bottom of the spreading height layer (Fig. 2). Such distinction can in turn be crucial for rigorous ECM evaluation, in particular for weak plumes (e.g. Mastin, 2014; Devenish, 2016; Aubry et al., 2017a). However, this distinction is challenging to make and rarely presented in the literature so that we did not include it in version 1.0 of IVESPA (Fig. 2).

Fig. 2 summarizes some of the different techniques used to measure plume height in the sources from which we compiled ESPs. For the events in the database that occurred before the beginning of the satellite era (late 1970's/early 1980's), the most common type of plume height measurement is visual report from experienced observers (e.g. observatory staff) and witnesses from the ground - sometimes using video camera - as well as aircraft pilot visual reports. However, for the majority of events that occurred during the satellite era, the column heights have been estimated using different satellite-based remote sensing techniques (Fig. 2; also see table 1 in Taylor et al., 2019). For example, the correlation of 11-μm brightness temperature of the plume top observed from satellite (e.g. MSG-SEVIRI) with the atmospheric temperature profile of a nearby radiosonde is the most commonly used method for top height estimation. This method, referred to as Cloud-Top-Temperature (CTT) in the literature is routinely used by VAACs and volcano observatories (Gouhier et al., 2020). From the ground, the column dimensions may be estimated by weather radar (e.g. Marzano et al., 2019), lidar (e.g. Scollo et al., 2015), auto-calibrated webcams (e.g. Scollo et al., 2014), or video image analysis (e.g. Arason et al., 2011). The heights obtained from different techniques (Fig. 2) may differ largely because they measure different parts of the plume (e.g. top vs. bottom of the umbrella cloud), use fundamentally different techniques, are obtained at different times after the eruption and/or distances from the volcanic vent, and because each technique is subject to its own uncertainty (e.g. Tupper and Wunderman, 2009). For example, the cloud-top-temperature method is limited by the quality of the radiosonde profile used and the fact that for columns with heights close to the tropopause, two heights estimates are possible because of the temperature inversion. Last, it is important to note that we excluded any plume height estimate obtained from inversion of deposit data using a modelling approach, including the method of Carey and Sparks (1986) and its recent extensions (e.g. Rossi et al., 2019) which invert the plume height from clast size isopleths. Such methods clearly violate the criteria of independence among ESPs and the rejection of any method making use of eruptive column modelling (section 2.1.1).

Given the large variety of techniques applied in measuring plume height, their limitations, and the differing levels of confidence that a database user may have in them, we complement parameters provided for each of the three plume height types by a categorical variable named "method" which includes the following categories:

- "v": visual observation of the plume, whether from the ground or from an airplane.
- "g": ground-based observation of the plume using instrumentation such as radar, lidar or calibrated cameras.
- "s": satellite-based observation of the plume, such as cloud-top-temperature, shadow technique or backward trajectory modelling.
- "o": other, which include some of the least conventional methods used to place constraints on plume height. For example, when very few plume height estimates are available, the tropopause height is used as a lower bound on the SO_2 height when the eruptive event led to significant perturbation of the stratospheric aerosol optical depth or to significant deposition of sulfate in polar ice-core.
- "u" = unknown.

We generally use all available estimates to propose a best estimate and uncertainty on plume height, so that this categorical variable often includes several methods.

2.2.3.2. Examples of challenging and ideal events to collect the parameter. The 1902 eruption of Santa Maria is one of the IVESPA events for which we have the least information on plume height. The only estimates are reports from two ship captains found by Williams and Self (1983), one of which places the "column height" at 27-29 km using a sextant and the other one at 48 km using an unknown method. It is unclear whether these heights should be considered as a.s.l. or a.v.l. estimates, although the former option is more likely for a sextant measurement, and given the much higher height of the column compared to the altitude of the eruptive vent (3.8 km). It is also unclear whether these heights likely correspond to the top height or the spreading height. Both DCs for this eruption chose 28 km as the best estimate because the measurement technique is documented, and both assumed it was likely representative of the plume top measured a.s.l. An interpretation flag 1 was chosen by both DCs for this value even though a flag 2 could have been considered given that the measurement could relate to the spreading height. For the uncertainty, one could consider the 48 km estimate as an upper bound which would give an uncertainty of 20 km. This eruption is also associated with sulfate deposition at the pole and stratospheric aerosol optical depth perturbation (Rose, 1972), so it seems unlikely that the top height was below the tropopause, i.e. 16-17 km, which would give an uncertainty of 12 km. Here the DCs chose to attribute a 50% uncertainty, i.e. 14 km, which falls in the 12-20 km range that could be inferred from the minimal information available. An interpretation flag of 2 was given to the uncertainty as it consists mostly of an educated judgement.

In contrast, eruptive events associated with the 2010 eruption of Eyjafjallajökull represent a nearly ideal case for collecting plume height. The Icelandic Meteorological Office had a weather radar and several cameras monitoring the eruption from which the top height could be estimated (Arason et al., 2011). Multiple satellite sensors, including the Infrared Atmospheric Sounding Interferometer (IASI), the Global Ozone Monitoring Experiment (GOME)-2 and the Spinning Enhanced Visible and Infrared Imager (SEVERI), were also used to track the eruptive column and estimate the spreading height and the SO_2 height (Stohl et al., 2011; Flemming and Inness, 2013; Carboni et al., 2016). Most of the column height data consisted of time series as opposed to a single or handful of values so that we could rigorously calculate time-averaged values of plume heights for each event. The extraordinary interest of the volcanology community in this eruption also means that publications in which we found plume height data included more information on measurement limitations than for most eruptions. The large number of publications also enabled us to compare height values across multiple references and to be confident in uncertainty values provided. As a result, whether for the top height, spreading height or SO_2 height, all best estimates of heights for this eruption have been attributed an interpretation flag of 0, and uncertainty estimates were either given flag values of 0 or 1.

2.2.4. Atmospheric conditions

Atmospheric conditions have been demonstrated to exert substantial influence on the dynamics of eruptive columns and have become a standard input to most ECMs (e.g. Costa et al., 2016a; Aubry et al., 2017a). As a consequence, for each eruptive event in the database, we

provide vertical profiles (as a function of the altitude a.s.l.) for the atmospheric pressure, temperature, zonal and meridional wind speed, and relative humidity up to 50 km a.s.l. The most convenient type of dataset from which to obtain these profiles are atmospheric reanalyses, in which meteorological and climate observations are assimilated in a global climate model. Atmospheric reanalysis data are gap free, available on a global scale, and contain a large number of outputs including the five variables required in IVESPA. Two of the most popular atmospheric reanalyses are the ERA5 reanalysis (Hersbach et al., 2020) produced by the European Centre for Medium-Range Weather Forecasts (ECMWF) and the NCEP-NCAR R1 reanalysis (Kalnay et al., 1996) produced by the National Centers for Environmental Prediction (NCEP) and the National Center for Atmospheric Research (NCAR). In order to better inform uncertainties related to atmospheric conditions and their impact on ECM evaluation, we provide atmospheric conditions issued from both the ERA5 and NCEP-NCAR R1 datasets in IVESPA. One caveat is that the ERA5 reanalysis only covers years 1979 onwards (to be extended to 1950 onwards), and the NCEP-NCAR R1 reanalysis only covers years 1948 onwards. Consequently, we complement these two reanalyses with two reanalyses covering the full 20th Century: the ERA-20C reanalysis (Poli et al., 2016) produced by the ECMWF, and the 20CR reanalysis (Compo et al., 2011) produced by the National Oceanic and Atmospheric Administration (NOAA), of which NCEP is part. For each event in the database, we then provide one set of atmospheric profiles from an ERA-family reanalysis (ERA-20C for events older than 1979 and ERA5 otherwise) and one set of atmospheric profile from a NOAA-family reanalysis (20CR for events older than 1948 and NCEP-NCAR R1 otherwise). Table 3 briefly summarizes some of the main characteristics of the four reanalysis datasets used, and in particular the spatial and temporal resolution of the output used. Note that the atmospheric conditions retrieved from different atmospheric reanalyses are not strictly independent, e.g. because some of the observational datasets assimilated in the climate models are used by several of the four reanalyses in Table 3. However, we show in section 3 that important differences exist in the atmospheric parameters derived from these reanalyses so that using two different reanalysis families is still valuable for assessing uncertainty in atmospheric conditions.

Regardless of the reanalysis dataset used, we followed a unique methodology to extract time-average atmospheric profiles at the time and location of any event of IVESPA. Temporally, we extract reanalysis data between the time step of the reanalysis that immediately precedes the event start and the time step that immediately follows the event start date to which we added the best estimate for the duration. Spatially, for all vertical levels, we find the reanalysis grid point closest to the volcano location and extract reanalysis data corresponding to that grid point and the eight immediate neighbours at the same vertical level. For each vertical level and time step, we then perform a linear 2-dimensional interpolation of extracted data at the volcano location. This method provides us with the time series of atmospheric profiles at the volcano location. We then simply averaged these atmospheric profiles to produce the time-average atmospheric profiles during the event. For events for which duration is short compared to the temporal resolution of the reanalysis output - which we arbitrarily defined as events for which less than four time steps were extracted - we first interpolate the available profiles as hourly profiles between the start and end of the event before calculating the time average. Last, in addition to time-averaged atmospheric profiles, we also provide all atmospheric profiles extracted for each reanalysis product (i.e. atmospheric profiles at each time step of the reanalysis product during each event).

In addition to providing atmospheric profiles for each event in IVESPA, we also provide the average atmospheric Brunt-Väisälä frequency ($\overline{N}$) and the average wind speed ($\overline{W}$) for each event. These two parameters enable quantification at zero order of the effect of atmospheric conditions on plume rise and are used in many scaling relationships relating the MER to plume height (e.g. Degruyter and Bonadonna, 2012; Woodhouse et al., 2013; Aubry et al., 2017a) as well as in calculating dimensionless parameters governing the dynamical regime in which volcanic columns erupt (e.g. Degruyter and Bonadonna, 2013; Carazzo et al., 2014; Aubry et al., 2017a). We first calculated altitude-dependent values of these parameters as

$$W(z) = \sqrt{u(z)^2 + v(z)^2} \quad (1)$$

for wind speed where u is the zonal wind speed, v the meridional wind speed, and z the altitude, and

$$N(z) = \sqrt{\frac{g}{\theta} \times \frac{d\theta}{dz}} \quad (2)$$

for the Brunt–Väisälä frequency, where g is Earth's gravitational constant and θ is the potential temperature calculated from the temperature and pressure. We then calculated the vertical average of W (z) and N(z) to obtain $\overline{N}$ and $\overline{W}$ by using the vent altitude as the lower integration limit and the best estimate of the top height as the upper integration limit. When no estimate of the top height was available, we used the umbrella height instead. We provide $\overline{N}$ and $\overline{W}$ for each event and for each of the two families of climate reanalysis used.

Table 3
Summary of the main characteristics of the atmospheric reanalysis used to provide atmospheric profiles for each volcanic event in IVESPA.

Family	ERA reanalysis		NOAA reanalysis	
Name	ERA-20C	ERA5	20CR	NCEP-NCAR R1
Period	1900-2011	1979-present	1850-2014	1948-present
Volcanic events for which reanalysis is used in IVESPA	1900-1978	1979-present	1900-1947	1948-present
Domain	global	global	global	global
Model spatial resolution	T159 (125 km), 91 levels	TL639 (31 km), 137 levels	T62 (210 km), 28 levels	T62 (210 km), 28 levels
Output maximum altitude	100 Pa (ca. 50 km)	100 Pa (ca. 50 km)	100 Pa (ca. 50 km)	1000 Pa (ca. 30 km)
Output spatial resolution used	1.0° x 1.0°, 37 levels	0.25° x 0.25°, 37 levels	1.0° x 1.0°, 28 levels	2.5° x 2.5°, 17 levels
Output temporal resolution used	Three hours	One hour	Three hours	Six hours
Reference	Poli et al. (2016)	Hersbach et al. (2020)	Compo et al. (2011)	Kalnay et al. (1996)
Website from which data was retrieved	https://www.ecmwf.int/en/forecasts/datasets/reanalysis-datasets/era-20c	https://www.ecmwf.int/en/forecasts/datasets/reanalysis-datasets/era5	https://psl.noaa.gov/data/gridded/data.20thC_ReanV3.pressure.html	https://psl.noaa.gov/data/gridded/data.ncep.reanalysis.pressure.html

2.2.5. Total grain size distribution

The TGSD describes the distribution of the grain size of particles emitted during an eruptive event. TGSDs provide key insights into the eruption process, for example fragmentation mechanisms, but are also crucial for application of ECMs and VATDMs, and subsequent hazard assessment. We systematically collected TGSDs when they were available for IVESPA events, and provided them as comma separated value files for each event, with the first two columns of the file corresponding to grain size diameter in phi unit and mm, and the third column corresponding to the weight fraction in weight % (wt.%). One categorical variable in IVESPA informs whether a TGSD is available for each event.

While imaging techniques have been developed to estimate the grain size of particles within a rising column (e.g. Freret-Lorgeril et al., 2019) these techniques have typically been applied to a small number of volcanoes and for low-intensity eruptions, and are not able to produce the full distribution of particles emitted during an event as imagery cannot penetrate through the rising material to capture all particles within the rising column. Ash collection instruments have been developed to collect and enable analysis of tephra grain size at a given location in real time during an eruption (Shimano et al., 2013), however these are not widely used as they require access to the areas being impacted by ash fall, and for correct positioning during an eruptive event. Therefore, information on deposit grain size is typically gathered from post-eruption field analysis of deposits, whereby deposits are sampled and a grain size distribution at a given location is estimated through sieving of coarse fractions (typically at phi or half phi intervals), and laboratory analysis of fine fractions (for example using laser diffraction methods). Given these methods rely on identification and analysis of a deposit, very distal deposits where thickness is less than a few millimetres are commonly not preserved and identified, therefore biasing grain size analysis to coarser fractions. Increasingly, deposit information is supplemented with grain size information gathered from analysis of satellite imagery (Gouhier et al., 2019) which is able to account for fine ash transported over great distances which may not be observed when on final deposition.

To produce a TGSD requires integration of the grain size measurements from across the deposit extent (Bonadonna and Houghton, 2005; Costa et al., 2016b; Pioli et al., 2019). grain size can be highly variable across a deposit, depending on the complexity of the eruption and weather patterns. To estimate TGSD, a deposit extent is commonly divided spatially, with each section assumed to have the grain size of the closest measurement, and the Voronoi Tesselation statistical method (Bonadonna and Houghton, 2005) being the most common method for dividing deposit extent. The Voronoi Tessellation is a good statistical strategy to average non-uniform distribution of data; nonetheless, it cannot account for missing parts of the deposit, such as very distal fines. As a result, the critical element to consider when compiling a representative TGSD is the exposure, and therefore sampling, of the deposit; the parts of the deposit that correspond to the transition of fallout regimes especially need to be sampled (e.g. Alfano et al., 2016; Pioli et al., 2019). Deposit preservation and access issues are common and the coarse proximal and/or fine distal portions of a deposit tend to be poorly represented in existing data (e.g. Andronico et al., 2014a). In application of statistical methods to assess TGSD, an assumption is made on the extent over which the analysis is conducted, i.e. the location of the zero-isomass line, and choice of this can produce large uncertainties in the final result (Volentik et al., 2010).

In comparison to other parameters, where multiple observations are made of a parameter and presented in different publications, there are fewer events for which TGSD has been calculated because of the effort to estimate TGSD, and limited examples where multiple TGSD are presented for the same events in different publications or from different authors. However, a number of the publications from which TGSD was gathered do contain in-depth analysis of potential uncertainties, and show the impact of number of measurements, and their location on resultant TGSD (Volentik et al., 2010). Given the nature of grain size methods, we did not assign uncertainty, and interpretation flags were not allocated. Therefore, for this study, we present grain size information as gathered from the published record, alongside a number of metadata consisting in the number of measurements and their minimum and maximum distance from the vent to allow the user to evaluate potential uncertainties. Publications describing TGSDs often contain several TGSDs produced using various different methods, and in some cases combining model data with measured grain size data. For consistency, the distributions chosen and presented herein relate to those defined from analysis of the deposit. Where multiple TGSD were presented for the same event (e.g. Volentik et al., 2010; Rose et al., 2007), we extracted the distribution that required least interpretation and supplementation of the field dataset. For these examples, we recommend that the user refers to the referenced paper to understand the range of possible TGSDs.

2.2.6. Other parameters

In addition to the three key ESPs (TEM, duration and column height) and atmospheric conditions provided for all events, the TGSD provided when available, and their companion parameters (e.g. uncertainty, interpretation flags, deposit metadata), we provide a number of parameters that enable further characterization of volcanic events. Table 4 lists these additional parameters and some of their characteristics.

Some fundamental parameters were provided for all events, such as the volcano name, the eruptive vent latitude, longitude and altitude, or the event start date. To facilitate cross-references between IVESPA and other volcanological datasets, we also provide the volcano and eruption number as retrieved from the Global Volcanism Program Volcanoes of the World database (https://volcano.si.edu/). The combination of these two numbers is not unique across events of IVESPA, as we commonly gather ESPs for multiple events that occurred during a single eruption from one volcano. Consequently, we also provide an IVESPA identification number (ID) unique to each event, which we use, for example, for naming files that contain atmospheric profiles and TGSD of individual events. For each event, a list of references used to constrain ESPs is provided. The complete list of references used in IVESPA is available in Appendix A of this paper and on the IVESPA website (ivespa.co.uk).

When we could constrain them from the literature, we provide two categorical parameters: the “eruption style” and the “plume morphology”. The eruption style consists of the “magmatic”, “phreatomagmatic” and “phreatic” category and is intended to inform the extent to which external water was involved in an eruption, an important consideration when modelling plume dynamics (e.g. Van Eaton et al., 2012). When it was not possible to define an eruption type, the field was left blank. The plume morphology consists of the “weak” and “strong” categories, when ash disperses only downwind, or downwind and upwind of the eruptive vent. Providing these categorical parameters will enable physical volcanologists to distinguish categories of events with distinct dynamics when investigating the relationship between ESPs, developing/evaluating ECMs, and estimating hazard. In particular, the assumptions upon which the 1D ECM are built are more reasonable for weak plumes than strong plumes (e.g. Costa et al., 2016a) so that plume modellers using IVESPA may want to distinguish between strong and weak plumes when evaluating their models (e.g. Aubry and Jellinek, 2018). Note that the plume morphology parameter was provided solely on the basis of direct observations of the plume, such as pictures, videos and eyewitness reports. Multiple studies have proposed dimensionless parameters that describe the transition from weak to strong plumes, but these parameters are dependent on ESPs and sometimes ECMs (e.g. Degruyter and Bonadonna, 2013; Carazzo et al., 2014; Aubry et al., 2017b). We thus decided not to use them so that IVESPA can also be used to further investigate the dependence of plume morphology on ESPs.

Lastly, when they are available in the literature, we provide a number of quantitative parameters such as the deposit mass issued from PDCs. We tried to provide an uncertainty on these parameters but did not provide any interpretation flag. The magma water content

Table 4
List of parameters compiled, when available, other than the key ESPs and related parameters listed in sections 2.2.1-2.2.5

Parameter name	Provided for all events? (y/n)	Quantitative (Q) or categorical (C) parameter?	Unit	Uncer-tainty provided? (y/n)	Comment
Volcano name	y	C			As obtained from the Volcanoes of the World database of the Global Volcanism Program (GVP)
Event year	y	Q	CE	n	
Event label	y	C			Generally the month or day the event occurred, or the name of the phase or tephra deposit layer as named in the literature
IVESPA ID	y	C			A unique ID for IVESPA consisting of three first letters characteristic of the volcano name followed by the event year, an underscore, and a two-digit number (e.g. ETN2001_02)
Start date & time	y	Q	UTC	n	Specified as MM/DD/YYYY HH:MM:SS
GVP volcano number	y	Q		n	As obtained from the Volcanoes of the World database of the Global Volcanism Program (GVP)
GVP eruption number	y	Q		n	As obtained from the Volcanoes of the World database of the Global Volcanism Program (GVP)
Vent latitude	y	Q	degree N	n	As obtained from Volcanoes of the World database of the Global Volcanism Program (GVP)
Vent longitude	y	Q	degree E	n	As obtained from Volcanoes of the World database of the Global Volcanism Program (GVP)
Vent altitude	y	Q	m a.s.l.	n	As obtained from reference papers for the vent specific to the eruptive event, or from the Volcanoes of the World database of the Global Volcanism Program (GVP) if not specified in any reference.
Eruption style	n	C			Classified as either "magmatic", "phreatomagmatic" or "phreatic" (White and Valentine, 2016)
Plume morphology	n	C			Classified as either "weak" or "strong" (e.g. Carazzo et al., 2014)
Mass of PDC	n	Q	kg	y	Obtained from the distribution of PDC deposits
Vent Diameter	n	Q	m	y	If available from volcanological observations
Exit velocity	n	Q	m s^{-1}	y	Obtained from ballistic trajectory modelling or remote sensing measurements such as Doppler radar or thermal cameras (Marzano et al., 2020)
Magma water content	n	Q	wt.%	y	Representative of dissolved volatiles; obtained from measurement of the water content of melt inclusions
Magma temperature	n	Q	degree C	y	Obtained from petrological studies
References	y	C			List of references used to provide information for the event. The reference list is available on the IVESPA website and in Appendix A of this paper.

(dissolved volatiles) and temperatures, where available, were obtained from petrological studies (e.g. Métrich et al., 2004). The vent diameter and exit velocity estimates provided rely only on measurementd independent of ECMs and key ESPs such as the TEM, the plume height, or the MER. Constraint on these two parameters are typically very crude, with vent diameter generally obtained from visual observations (e.g. Calvari et al., 2011) and exit velocity generally obtained from a camera recording or ballistic estimates (e.g. Marzano et al., 2020).

2.3. Access to data and data policy

The information in the dataset is intended for use in evaluating ECMs by providing the required inputs for initiating models, and outputs for testing results against observations. The information may also be used to investigate relationships between eruption and environmental (e.g. atmospheric) characteristics and key eruption parameters such as column height. The data was originally compiled as a spreadsheet, with atmospheric profiles and TGSD information held within separate csv files. The dataset has been converted into a relational database to hold the data in a structured manner for structured querying using volcano and other characteristics. The creation of the database is undertaken by British Geological Survey as part of the Global Volcano Model. A searchable interface will be made available in the future using the relational database to allow easy access to the data such that it can be searched according to these parameters.

The dataset can be downloaded as a single excel spreadsheet from ivespa.co.uk, providing all eruption information in one place. TGSD and atmospheric information can also be downloaded as separate files. For transparency, we also provide spreadsheets containing all key ESP values initially suggested by individual DCs, as well as summarizing discussions that led to choices of consensual values used in IVESPA. To facilitate updates and allow community interaction with the dataset, there is contact form to allow suggestion of further eruptions for consideration in the database or to provide feedback on existing entries.

When using any data from IVESPA, we require users to cite IVESPA following the latest citation and acknowledgement policy provided on the IVESPA website (ivespa.co.uk). The production of the database used information from a large number of resources, with the parameters often requiring considerable effort to constrain (for example see discussions on TEM and TGSD in section 2.2). Consequently, we strongly encourage IVESPA users to cite the data sources and references cited within the IVESPA when simulating a particular event or comparing a small number of events using information within IVESPA. When using atmospheric information from the database, we also recommend that users cite the reference paper for climate reanalyses (see Table 3) and use appropriate formulas in the acknowledgement (see Acknowledgements section of this study).

3. Overview of collected data

Following the methodologies described in section 2, we collected ESPs for 134 explosive volcanic events between 1902 and 2016 that fulfilled the entry criteria of the database. Fig. 3 shows the spatial and temporal distribution of these eruptive events. They are associated with 45 different volcanoes and 70 distinct eruptions, using the GVP eruption number to distinguish eruptions. The two volcanoes contributing the most events to the database are Mount Redoubt (Alaska, USA) with 24

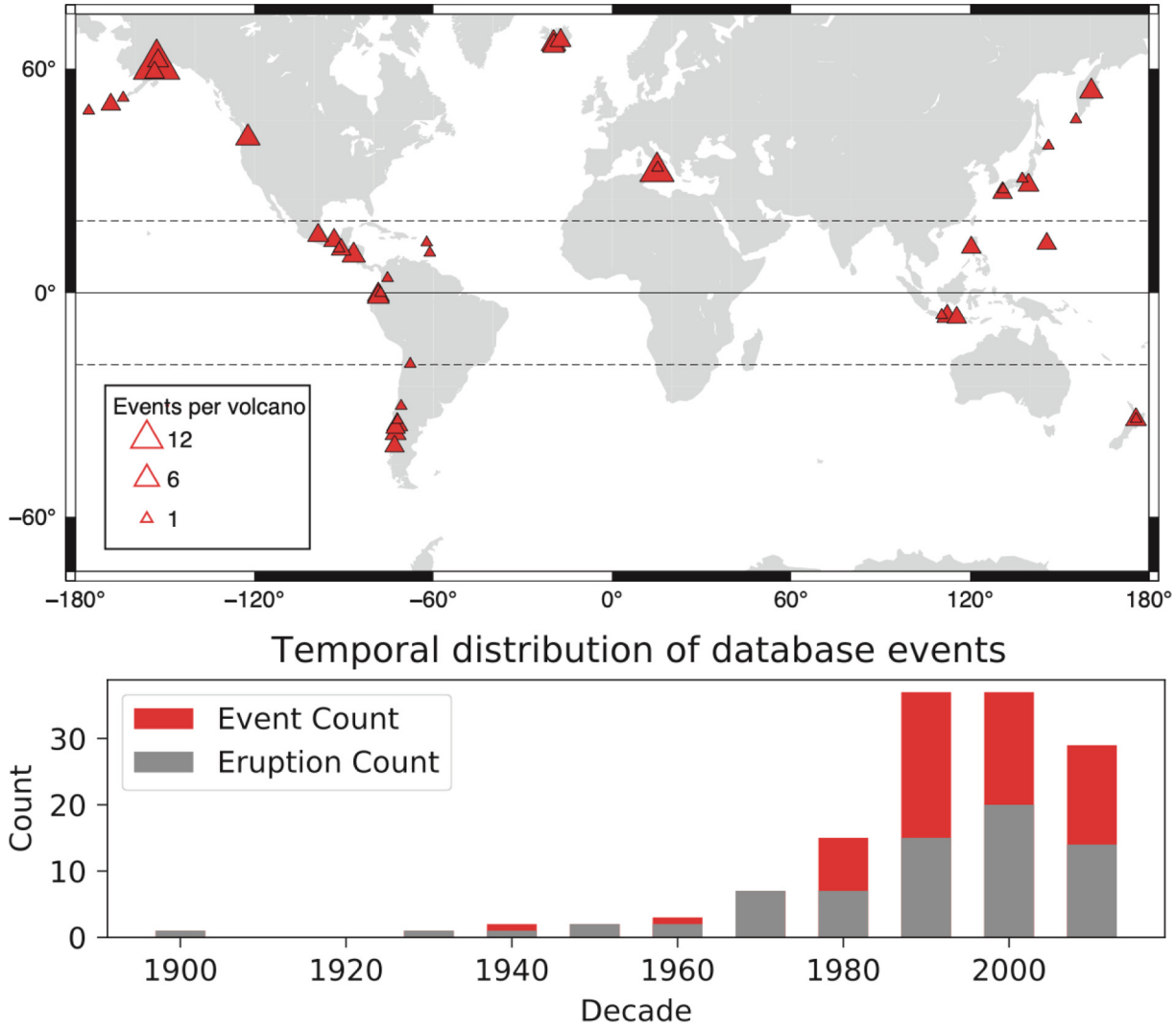

Fig. 3. Top: Location of volcanoes with eruptive events that are included in IVESPA. Symbol size is larger for volcanoes with more included events. Bottom: Number of included eruptions and eruptive events per decade since 1900.

events and Mount Etna (Italy) with 14 events. The 1989-1990 eruption of Mount Redoubt alone contributed 18 events with distinct sets of key ESP estimates available. The number of events in specific geographical areas in the new database is now comparable to the total number of events in some recent ESP datasets with atmospheric conditions (e.g. 10 events in Girault et al. (2014), 25 events in Mastin (2014)). For example, Central America contributes 22 events from 9 volcanoes, Iceland contributes 13 events from 3 volcanoes and Chile contributes 12 events from 6 volcanoes. However, the database still contains only a handful of events that occurred in the Southeast Asia/Oceania region despite it being a highly active volcanic region (Jenkins et al., 2012). Heights of eruptive plumes of major eruptions in this area are commonly available (e.g. Tupper and Wunderman, 2009; Syahbana et al., 2019), but tephra volume or mass derived from the deposit are rarely quantified.

Unsurprisingly, the number of events for which data is available has increased in recent decades, with the only exception being the 2010's because of the lag between eruptive events and the time of publication of papers documenting ESPs, in particular the mass or volume of the deposit. With the beginning of the satellite era (late 1970's/early 1980's), the number of events in the database strongly increases as plume height estimates based on remote sensing became almost systematically available (Engwell et al., 2021). The main limitation for volcanic events to fulfil our database entrance criteria is then the availability of deposit-derived mass or volume estimates required to obtain the TEM. Before the satellite era, in addition to fewer deposits being studied and less mass/volume estimate being available, plume height was commonly only constrained by the isopleth method (Carey and Sparks, 1986). Such estimates were not included in this database because of dependence on the deposit, atmospheric conditions, and plume modelling (section 2).

A key advance over previous work is the distinction of three different column heights (top height, spreading height and SO_2 height), with at least one of these being available for each event. Fig. 4 shows the fraction of events for which each of these heights is available. The top height of the plume is available for 97% of the events, whereas the spreading and SO_2 heights are constrained for only 31% and 21% of the events respectively. The availability of other select ESPs is also shown in Fig. 4. Two parameters that are frequently constrained are the PDC mass (81% of events) and the mass fraction of water vapor (54% of events). The TGSD, whose importance for plume and dispersion dynamics is increasingly recognized, is only available for 21% of the events. However, this still represents a total of 28 events for which duration, erupted mass, plume height, atmospheric conditions and TGSD are available which is three times more than in Girault et al. (2014) or the database of the IAVCEI THM. Parameters such as the vent radius and exit velocity,

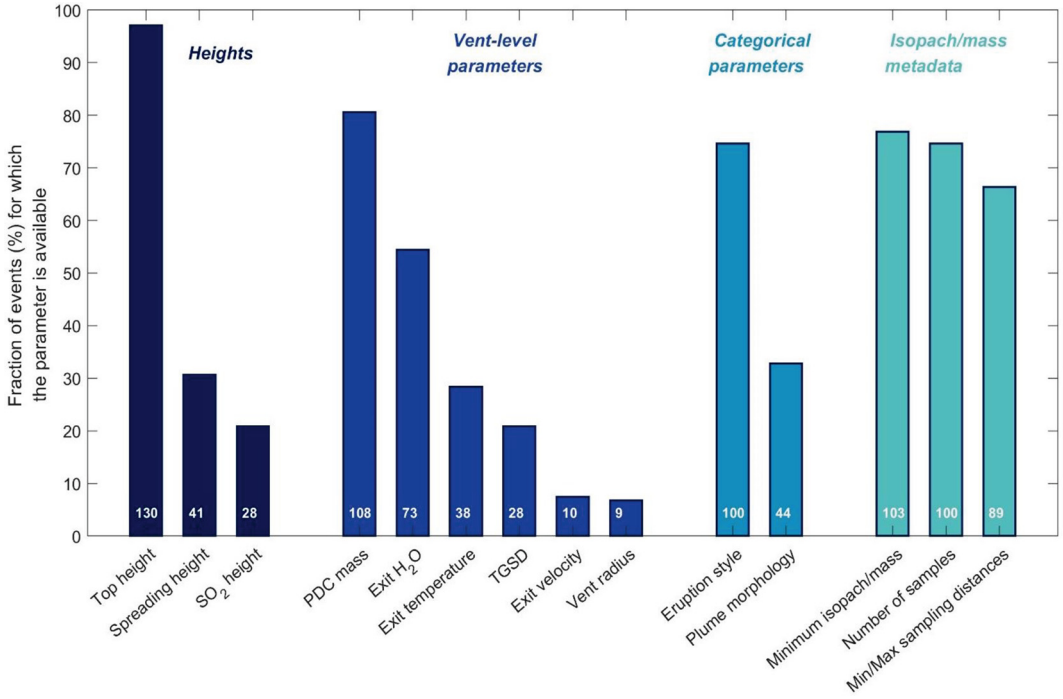

Fig. 4. Availability of select parameters collected in the database. White numbers in each bar provide the number of events (out of 134) for which the parameter is available. Note that for all eruptive events, we were able to document at least one of the three column heights (See Fig. 2 for definitions).

which are particularly important for understanding the stability of volcanic columns, are rarely constrained (<10% of events). Whereas the eruption style (magmatic, phreatomagmatic or phreatic) is commonly explicitly characterized in the literature (75% of events), the plume morphology (weak or strong) is characterized for only 33% of the events. This represents an important challenge for 1D plume modelling as assumptions underlying the models are not valid in the umbrella region of a strong plume, and distinguishing weak versus strong plumes is useful when evaluating and calibrating these models (e.g. Aubry and Jellinek, 2018). Lastly, even though a mass or volume estimate is required for an event to be considered, metadata on the deposit and its mapping (such as the number of samples, spatial distribution and distance from the vent) is available for around 70% of the events.

Fig. 5 shows distributions of the three key ESPs, as well as their uncertainties and associated interpretation flag values (Fig. 1). TEM values cover six orders of magnitude and event duration values cover five orders of magnitude. Their ratio, the MER, covers seven orders of magnitude. Whereas many large magnitude events were characterized in previous datasets (e.g. Mastin et al., 2009; Mastin, 2014; Aubry et al., 2017a), our extensive compilation means that almost half of the events in our database erupted less than 10^{10} kg of tephra. The new database thus provides a much more complete range of events to characterize plume dynamics and evaluate ECMs. Fig. 5 also shows distributions of uncertainties for TEM, duration and plume height. Unsurprisingly, the ESP subject to the highest uncertainty is the TEM, with relative uncertainty commonly between 200 and 500%. Height uncertainties are as high as 80%. Duration uncertainty is generally below 65%. However, in contrast to the TEM and heights for which the frequency of events clearly decreases with higher uncertainty, the distribution of duration uncertainty is more uniform. This reflects the multiple challenges encountered when estimating duration from the literature (see section 2.2.2).

For all key ESPs, the distribution of interpretation flags is skewed to higher values for uncertainties, while flags for best estimates are skewed to lower values. This reflects difficulties in finding rigorous constraints on uncertainties on ESP values quoted in the literature, but a confidence from DCs in extracting an estimate for the best value. For TEM, the best estimate flag is 0 for over 80% of events, reflecting a relatively well-established methodology for calculation and presentation of this parameter. However, flag values for TEM uncertainty are polarized between 0 and 2. This reflects that rigorous uncertainty quantification has often not been attempted with authors commonly providing rough estimates with limited justification in most examples. However, in recent years, increased efforts have been devoted to quantifying uncertainties in TEM (Biass and Bonadonna, 2011; Bonadonna and Costa, 2012, 2013; Engwell et al., 2013; Klawonn et al., 2014a, 2014b; Bonadonna et al., 2015a) and estimates for recent events more often include a rigorous uncertainty quantification, at least of the uncertainty related to the integration method used to convert thinning trends into a volume or mass. In contrast with the TEM best estimate, flags for duration best estimate show the lowest fraction of flags 0 and the highest fraction of flag 2, a consequence of the multiple challenges encountered when compiling duration as discussed above and in section 2.2.2. When assessing plume height, only ca. 60% of events have a flag 0 for the best estimate. In addition to difficulties related to sparse information for older events, recent events are commonly affected by: i) a lack of clarity on which kind of height is reported in the literature (e.g. spreading height vs. top height); and ii) a lack of temporal and contextual information accompanying plume height estimates, making it challenging to provide an estimate for the height averaged over the duration of the event.

In addition to the three key ESPs discussed above, atmospheric profiles from two different climate reanalysis are available for each event, and we derived the vertically-averaged Brunt-Väisälä frequency (eq. 2) and wind speed (eq. 1) from these profiles (section 2.2.4). The distribution of these parameters and their uncertainties is shown in Fig. 6. Thanks to the large span of locations (Fig. 3) and seasons (not shown) covered by events in the database, both parameters vary over a large range, with the average Brunt-Väisälä frequency varying between 0.008 and 0.02 s^{-1} and the average wind speed varying between 3 and 40 m s^{-1}. Differences in the Brunt-Väisälä frequency between the two reanalyses do not exceed a few percent. However, differences in wind speed are up to 45%, with a large number of events having differences in wind speed over 10%. This suggests that

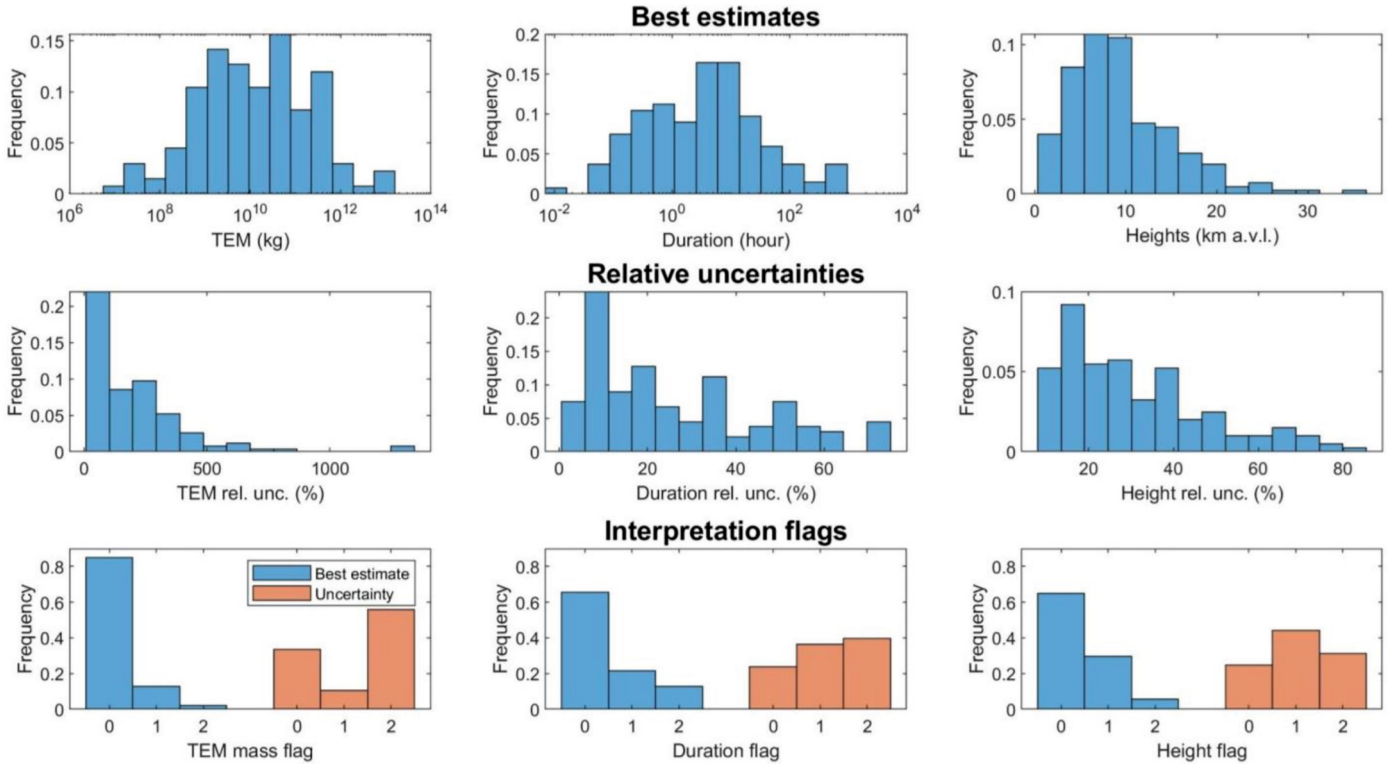

Fig. 5. Distributions of best estimate (top), relative uncertainty (middle) and their flags (bottom) for the total erupted mass (TEM, left), duration (centre) and heights (right, including top height, spreading height and SO_2 heights altogether) in IVESPA.

compiling atmospheric conditions from multiple sources is important for quantifying ESP uncertainties and their propagation through plume modelling.

Finally, Fig. 7 shows the TGSD of the 28 events for which it is available in the database. There are only 24 distinct TGSDs because, for the eruptions of Etna in 2002 and Grímsvötn in 2004, only a single TGSD

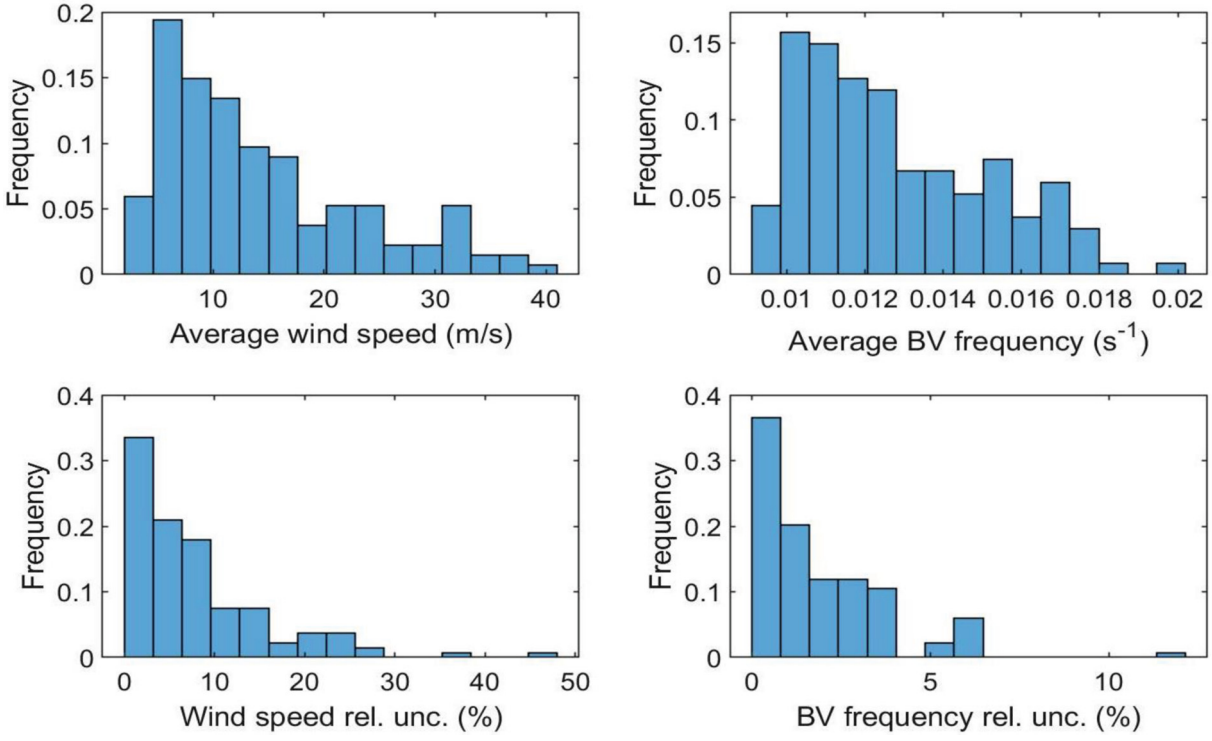

Fig. 6. Distributions of the vertically-averaged wind speed (left) and Brunt-Väisälä (BV) frequency (right) across all events in the database. Top panels show the mean of values obtained from the NOAA reanalyses and ERA reanalyses (see section 2.2.4), and the bottom panels show their relative differences.

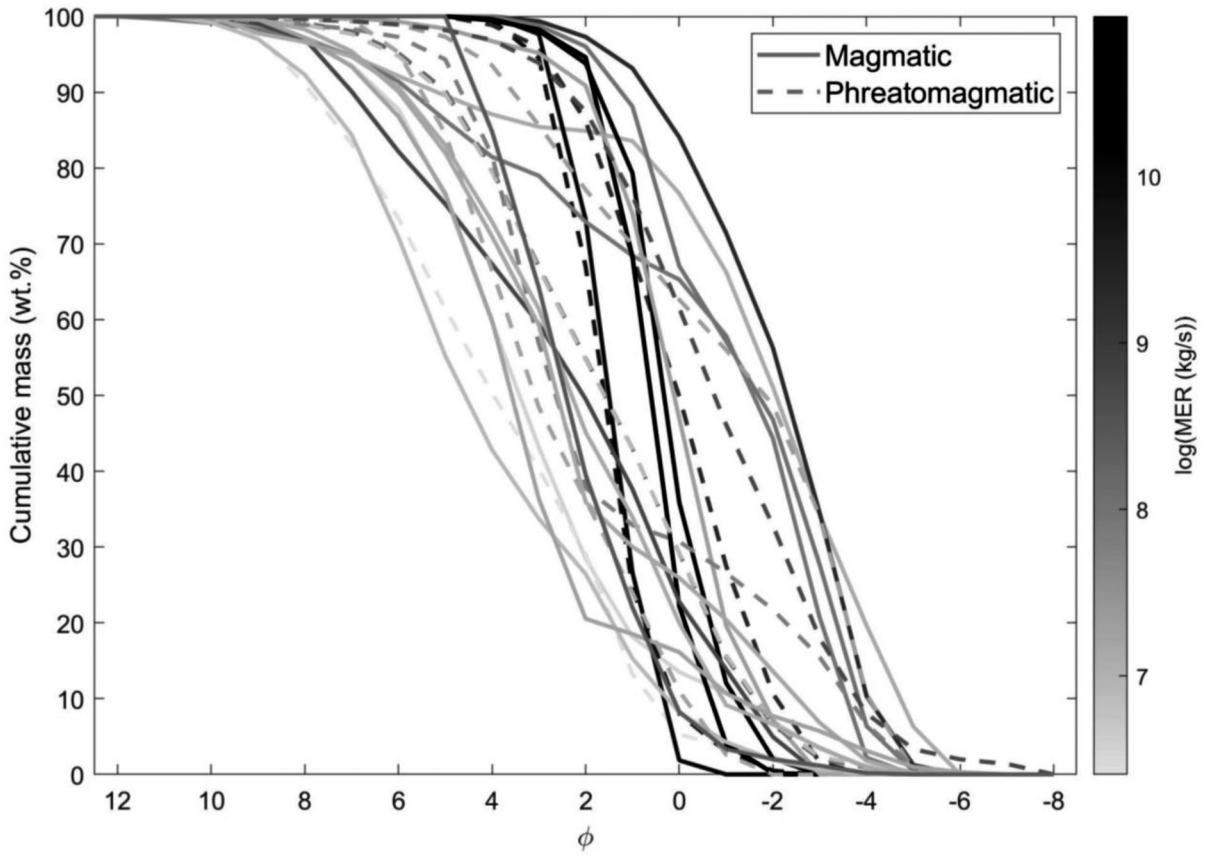

Fig. 7. Total grain size distributions of all eruptive events in the database, shown as the cumulative mass percent coarser than each size class in phi units. Magmatic events are plotted with solid lines, phreatomagmatic with dashed lines. Darker lines correspond to events with higher mass eruption rates.

was reconstructed for the whole eruption. However, each eruption contained multiple events in the sense used in this paper, i.e. with key ESPs independently constrained (Jude-Eton et al., 2012; Pioli et al., 2019). For comparison, most ESP datasets do not include TGSDs (Table 1); the IAVCEI THM database included 7 events with TGSD in addition to other key ESPs. A number of the TGSDs show discontinuous trends, associated with bimodal distributions. TGSDs of the database events show tremendous variability with the median grain size varying between φ=2 and φ =-4 (i.e., 0.25 mm & 16 mm). All in all, IVESPA covers an unprecedented range of MER, atmospheric conditions and TGSDs which should be particularly valuable to test and develop ECMs across a wide range of eruptive conditions.

4. Uncertainty in collection of key ESPs

4.1. Differences among estimates for two case studies: Calbuco 2015 and Fuego 1971

In gathering data for IVESPA, we investigated DC assumptions during data collection by asking eight DCs to provide key ESPs along with their uncertainties and flags for two eruptions: Calbuco 2015 and Fuego 1971. These two eruptions were chosen because they cover the spectrum of well-observed (Calbuco) and poorly observed (Fuego) eruptions. No guidance was provided regarding the resources to use, but DCs were asked to strictly follow the definition of key ESPs given in section 2.2. Fig. 8 shows the ESP value given by each DC, with symbol shape showing the interpretation flag for the best estimate and the symbol colour showing the interpretation flag for uncertainty (section 2.1.3). For both the Calbuco 22nd April and 23rd April 2015 events and the Fuego 1971 eruption, data on TEM, duration and top height were collected. Information on spreading height and SO_2 height were also collected for the Calbuco events.

The results in Fig. 8 show that estimates for duration and spreading height are consistent across the different contributors for the Calbuco examples. Interestingly, this consistency stems from very different reasons for both parameters. For the duration, all DCs were in excellent agreement and used low-value of interpretation flags thanks to a large number of sources agreeing on duration estimate (see section 2.2.2). In contrast, all DCs used the same reference for the spreading height (Van Eaton et al., 2016), so that the agreement comes from having only one published source. Final flag values chosen for the uncertainty on the spreading height was 2, reflecting the fact that we had no other source providing an estimate for this parameter and that little information on uncertainty was provided in Van Eaton et al. (2016).

In comparison to duration and spreading height, the results for TEM, plume top height, and SO_2 height are more variable, with fewer contributors providing data for these parameters. The latter fact reflects that a particularly thorough search of the literature was required to find estimates for these parameters, so that some DCs could not find any value. This highlights the value in having two DCs independently compiling key ESP for each event in the database. For TEM, while parameters were provided by most contributors, the uncertainties for these parameters were high, and a number of contributors indicated that their estimates required some interpretation of the literature (flag 1), while one contributor noted that their response required significant interpretation of the literature (flag 2). In terms of uncertainties, the majority of contributors gave an uncertainty flag of 1, indicating that their estimates required interpretation of the literature; two contributors gave an uncertainty flag of 2, indicating that significant interpretation of the literature required. Interestingly, the final consensual value has a flag 0 for the uncertainty. The reason is that there was variety in both the

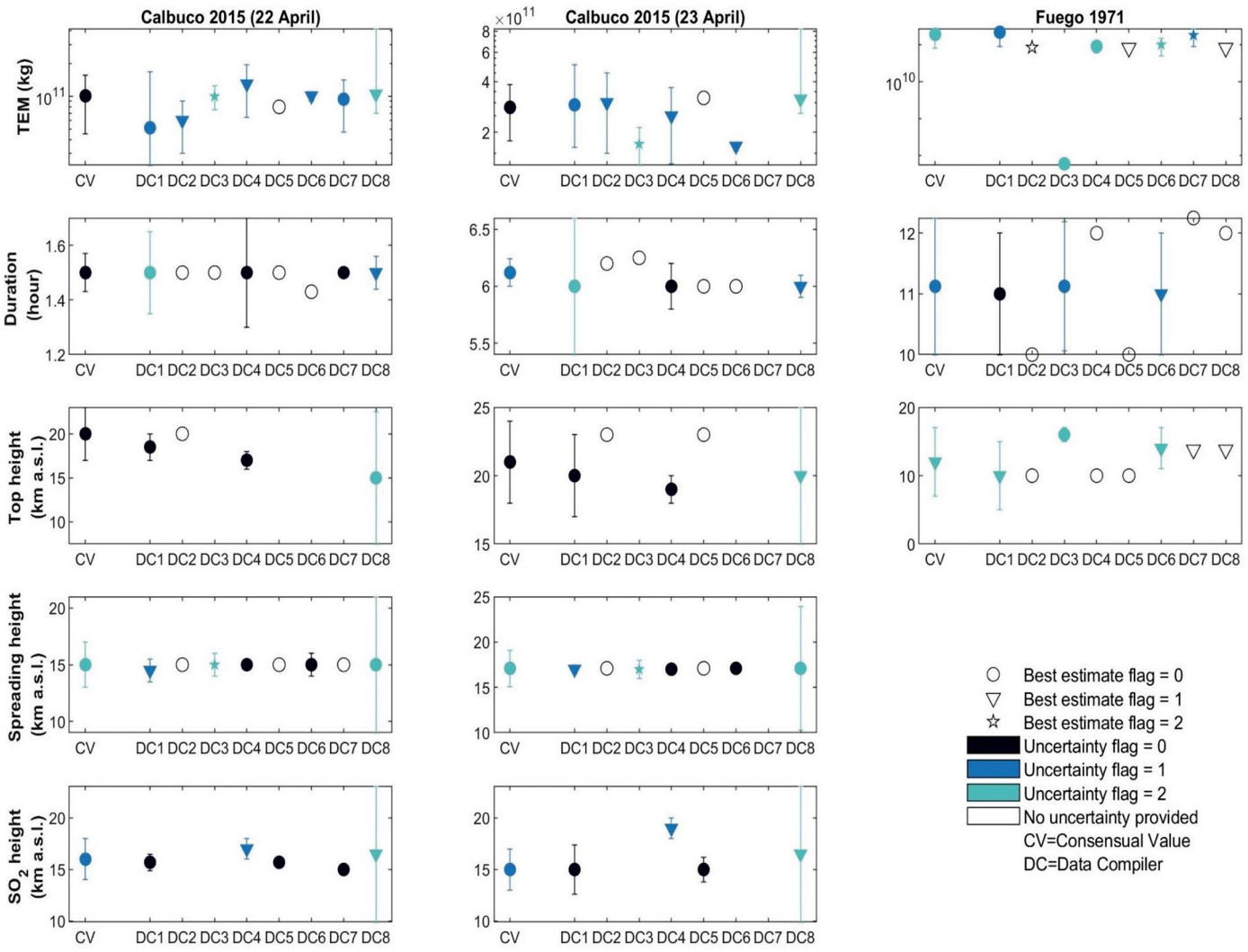

Fig. 8. Consensual values (CV) of key eruption source parameters vs. those originally compiled by individual data compilers (DCs) for the Calbuco 2015 (first 2 columns) and Fuego 1971 (last column) eruptions. The first row shows the total erupted mass (TEM), the second row shows the duration, and the bottom three rows show the different column heights. The symbol shape relates to the interpretation flag value for the best estimate whereas the symbol color relates to the interpretation flag of the uncertainty.

references used among the DCs and the interpretation of these references. As a consequence, the uncertainty provided covered all possible interpretations and we were highly confident that the true value for TEM lies within the uncertainties provided. In general, more DCs provided uncertainty information for TEM than for other parameters. This reflects the fact that uncertainty estimates for TEM are commonly explicitly provided in individual references, which is not the case for other parameters requiring the DC to evaluate uncertainty using discrepancies between different sources, heavily interpret these sources, or take educated guesses. TEM is one of the most uncertain parameters among those provided which is likely why efforts to provide uncertainty on it are more common in the literature.

Results for the TEM provided for the 1971 Fuego eruption are highly variable in terms of best estimate, uncertainty, and their associated flags. First, most of the best estimates provided agree within a factor of 3, with the exception of the estimate of one DC which is three orders of magnitude lower. This is the result of a trivial mistake, with the corresponding DC forgetting to convert the volume estimate found into a mass estimate using the deposit density. Although such mistakes are relatively rare, they are inevitable when reading hundreds of references to find ESPs of dozens of eruptions. This highlights again the value of having two DC independently gathering key ESPs for each eruption. Most DCs used the Rose et al. (1973) study to find a volume and density for the deposit. However, this study provides no details on how isopach maps were integrated to obtain a volume, and the $6x10^7$ m^3 volume quoted is reported as a minimum volume, with the mention that the true volume "could easily be twice the minimum quoted" with no further explanation. As a consequence, DCs used different strategies to report what the best estimate is, from using the minimum volume quoted to rounding it up to doubling it, with only 3 DCs out of 8 reporting a flag 0 for the best estimate. However, one DC found an additional study with a volume estimate for this eruption. In a study testing three methods to estimate a volume from isopach map, Sulpizio (2005) reanalysed the erupted volume of a large number of eruptions including the Fuego 1971 eruption using isopach maps of Rose et al. (1973). In addition to his clear methods, the range of volume found by Sulpizio ($1.4\text{-}1.8x10^8$ m^3) is in excellent agreement with the unsupported claim by Rose et al. (1973) that the best volume estimate was twice their minimum estimate. As a consequence, we deemed that the best volume estimate was $1.4x10^8$ m^3 and attributed a flag of 0 to the best estimate, with two studies supporting this value. This represents an example where an initially wide range of approaches from DCs with high flag values resulted in a flag value of 0, because the approach of one of the DCs prevailed, in this case because the additional reference found enabled more confidence in estimating the erupted volume. As for the uncertainty, we decided to use the minimum volume estimate to propose a lower bound. The difference between our chosen value ($1.4x10^8$ m^3) and the highest estimate of Sulpizio (2005) was very small and it was decided there was not enough information to

provide an upper bound on the uncertainty, in particular given the lack of information on density uncertainty to convert volume into TEM. For the same reason, we attributed a flag 2 to the uncertainty provided.

In comparison to results from the Calbuco 2015 examples, there is a relatively large range of estimates for duration for Fuego 1971, mostly caused by the fact that two different references (Rose et al., 1973; Bonis and Salazar, 1973) quote durations of 10 and 12 hours respectively. DCs who found both references generally proposed a value of 11±1 hour, which was the approach that prevailed. Last, constraining a value for plume height also proved challenging with individual DC values ranging from 10 to 16 km a.s.l. or 6.2 to 12.2 km a.v.l., and most DCs not providing any uncertainty. The only information that DCs could find regarding the eruptive plume height is the following quote from Bonis and Salazar (1973): "eruption clouds reached over 10,000 m in height". With no other contextual information available, each DC had to interpret or guess the following information: i) Is the value quoted a.v.l. or a.s.l.? ii) Is the value quoted most representative of the ash top height or ash umbrella height? iii) How high does "over 10, 000 m" mean? iv) Is the height quoted more representative of the maximum reached during the eruption or of a time-averaged value, which is what we aim to provide in IVESPA? Given these considerations the range of values proposed by DCs can be regarded as low, and we settled for an ash top height value of 12±5 km a.s.l. with a flag 1 for the best estimate and 2 for the uncertainty. The flag value for the best estimate could easily be 2, but individual DCs did not initially think about all potential interpretations of the quote raised above and none of them suggested a flag value of 2, so that it was decided to maintain a value of 1. It is our hope that the true value cannot lie outside the range provided, but if Bonis and Salazar (1973) provided an a.v.l. height for the umbrella height that is representative of the the time-averaged height, this would mean that the 10 km value quoted could correspond to a ca. 17 km value in terms of average top height a.s.l.. This represents our upper bound but the height is said to be "over" this value so our uncertainty choice could have been even more conservative.

4.2. Difference among data compiler estimates across all events

For each event of IVESPA, estimates of parameters were provided by at least two DCs, and the results were discussed and combined to produce a final consensual value. Comparing the initial estimates with the consensual estimate reveals significant differences for each of the key ESPs (Fig. 9). For each parameter, we also calculated the 2.5th and 97.5th quantile of the distribution of the ratio between DC values and final consensual values. Dotted lines in Fig. 9 correspond to these two ratios, with 95% of the data falling in between. Unsurprisingly, the parameter with the most discrepancy is the TEM, with 95% of the consensual values falling between 30% and 220% of initial DCs estimates, whereas the parameter with the least discrepancy is the top height, with 95% of the consensual values falling between 70% and 140% of initial DCs estimates. For TEM, the consensual values reached show up to three orders of magnitude difference with initial DC estimates in a few cases. Most of these extreme discrepancies correspond to either mis-reporting of a value or incorrect data processing (e.g. volume to mass conversion) by one of the DCs (as illustrated for Fuego 1971 in the previous section). After discussion between the two or more DCs working on the same event, such trivial discrepancies are often easily resolved which explains the counter-intuitive result that events with the highest discrepancies commonly have interpretation flag values of 0. The greatest discrepancies for top height reach a factor of 3. In contrast with TEM, top heights with the most extreme discrepancies often have flag values of 1 or 2. Although mis-reporting or mis-processing (e.g. in converting an a.v.l. height into a.s.l.) of heights did happen, discussion on how to interpret plume height data was the main reason for initial discrepancies between DC estimates, resulting in higher flag values (also see Fig. 5). Last, duration had discrepancies almost as significant as the TEM, with 95% of the consensual values falling between 30% and 200% of initial DCs estimates. Large discrepancies commonly exist in values found in the literature because of different definitions and methodologies applied (see section 2.2.2), and these definitions and methods are sometimes not documented. This results in discrepancies in values reported by different DCs. However, it should be noted that many events with a flag 2 (significant interpretation required) fall close to the 1:1 line showing that for the events requiring the most interpretation, DCs commonly agreed. Furthermore, events with the highest discrepancy commonly have flag values of 0 or 1, showing that trivial reporting or incorrect interpretation were often the cause of discrepancy and were resolved easily.

All in all, Fig. 9 shows:

1. Having at least two expert DCs independently compiling key ESPs of each event is valuable in order to highlight discrepancies in

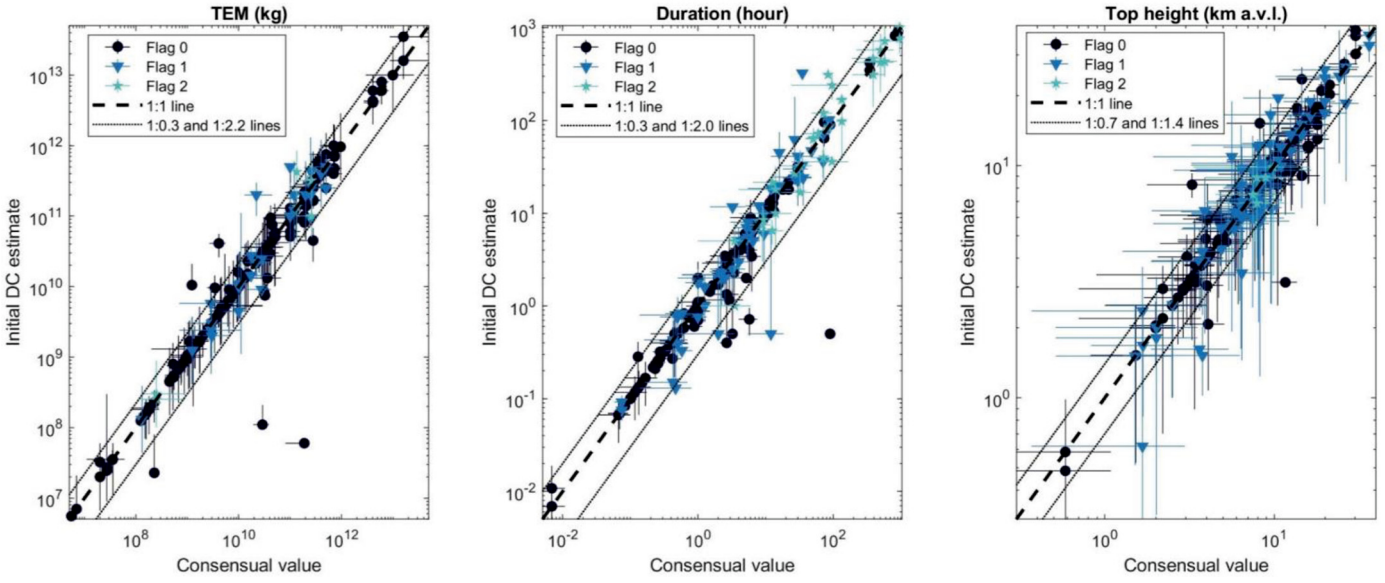

Fig. 9. Scatter plots of values initially compiled by data compilers (DCs) vs final consensual values provided in the database for the TEM (left), duration (center), and the column height (right). Symbol color relates to the value of the interpretation flag for the best estimate. Thick dashed lines correspond to the 1:1 lines and thin dotted lines which slopes are the 2.5th and 97.5th quantiles of the ratio of DC estimate to consensual value (the corresponding slopes are reported in legend).

approach, difference in literature sources consulted, and can help identify transcription and conversion errors that would not be apparent with only one DC.
2. The scatter in data between the DC values and the consensual values highlights the role of the individual level of interpretation required for both best estimates and uncertainty values. The interpretation flags allow us to report this level of interpretation in a consistent way.

These two features of IVESPA (multiple DCs vetting each event and interpretation flags) ensure a higher quality of the data provided as well as better information on the amount of interpretation and discussion that went into each value provided. In the long-term, we hope that these steps will be complemented by user feedback and contributions to the online IVESPA database.

4.3. Comparison with previous ESP datasets

Several ESP datasets have been produced over the past few decades (e.g. Table 1). Comparison of the ESPs estimated in this study with those estimated in Mastin (2014), Aubry et al. (2017a) and the IAVCEI THM original database are presented in Fig. 10. We chose these three datasets for comparison because they are relatively recent and like IVESPA, all events have atmospheric conditions available. The majority of TEM estimated in IVESPA fall on or close to a 1:1 line with those from Mastin (2014). However, there are a couple of examples where the parameters estimated herein fall at a distance of one order of magnitude from the 1:1 line. These examples have a flag 0, indicating that these discrepancies relate to data source rather than interpretation. The IVESPA data largely fall on a 1:1 line with that estimated previously by Aubry et al. (2017a), a result of these authors compiling a large portion of the data for IVESPA and of the relatively close ESP definitions used for IVESPA and in Aubry et al. (2017a), e.g. plume height aiming to be representative of a time-averaged value rather than the maximum reached over the eruption duration. Such similarities also hold for the duration and top height.

There is slightly more discrepancy when comparing IVESPA estimates of duration with those previously published by Mastin (2014), with some occasions where there is more than one order of magnitude difference between the parameters. Differences are also observed between data within the IVESPA dataset and previous datasets when considering plume height. While there is little difference for the majority of examples, there are some notable deviations from the 1:1 line, particularly when comparing IVESPA data with that from Mastin (2014). As for duration, these examples were given a flag of 0, whereby the published data required no interpretation, and therefore, we attribute these differences to be due to the use of different data sources.

5. Future developments and applications

5.1. Potential future developments of IVESPA version 1.0

While IVESPA version 1.0 is the most comprehensive dataset of its kind (see Table 1), a number of lessons were learnt during its

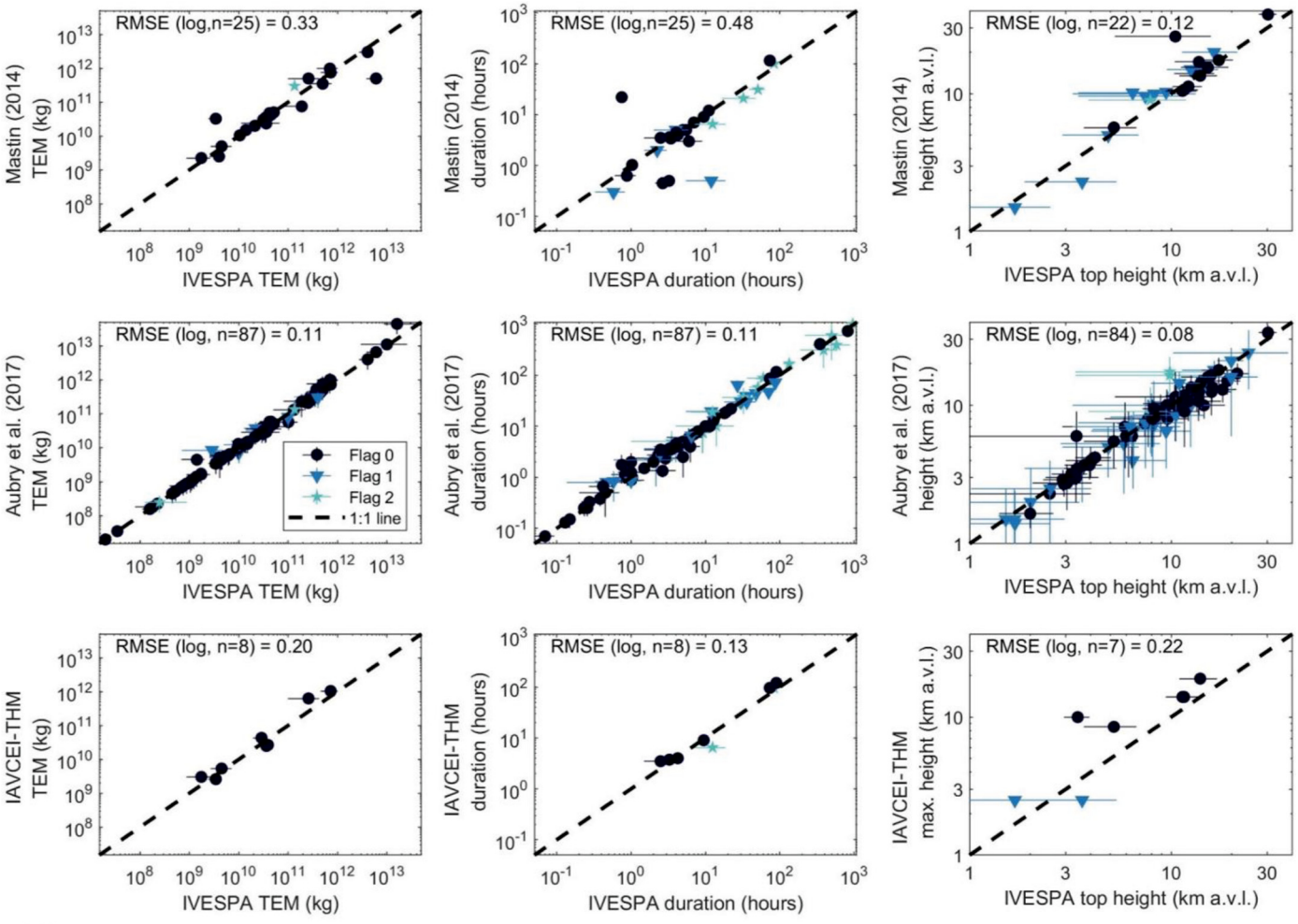

Fig. 10. Scatter plots of consensual key ESPs from published literature of independently estimated eruption source parameters in IVESPA versus previously published ESP datasets. Plots show results for the Mastin (2014), Aubry et al. (2017a) and IAVCEI THM dataset from top to bottom, and for TEM, duration and top height from left to right. Dashed lines show the 1:1 line. The root mean squared error, calculated on a log scale, is reported in each panel along with the number of events used to calculate it.

production that can be used to inform future developments of the database and other similar efforts. First, a number of relatively straightforward parameters can and will be added to IVESPA as part of future developments. These parameters include:

- A categorical parameter indicating the methods used to integrate the isopach or isomass maps and obtain a deposit volume or mass (e.g. power-law, exponential, Weibull; see Bonadonna et al., 2015a) in the reference(s) used to provide the TEM estimate and its uncertainty in IVESPA.
- A flag parameter indicating whether PDCs occurred for the events for which we could not constrain the PDC mass.
- The mass of SO_2 erupted by each event, which would enable synergy between IVESPA and volcanic SO_2 databases (e.g. Carn et al., 2016), and in turn better link the volcanology and the volcano-climate interaction communities.
- Petrological parameters including bulk and glass composition, and crystal content. These provide constraints for rheology, temperature and crystal content of magma that are necessary for conduit models that may be used as input to eruption column models (e.g. Hess et al., 1995; La Spina and Burton, 2015; Wallace et al., 2015).
- Atmospheric profiles from direct observations, in addition to those from climate reanalyses compiled for IVESPA version 1.0. One of the easiest datasets to take advantage of to add direct observations of atmospheric profiles is the atmospheric soundings compiled by the University of Wyoming (http://www.weather.uwyo.edu/upperair/sounding.html). While atmospheric soundings are not available for the older events, and the weather station(s) used may be distant from the volcano of interest, this dataset should cover at least half of the events within IVESPA.

Although relatively simple, the compilation of these parameters for over 130 events is time-consuming and they were suggested too late in the IVESPA production process to be included in version 1.0.

Second, within the database, ESPs and their uncertainty are taken directly from the published record. For different eruptions, they are calculated in different ways which may lead to systematic bias in IVESPA. One potential solution in future efforts is to collect the raw data used to derive ESPs, and re-analyze ESPs and their uncertainties using methodologies consistent across the database. In particular, raw thickness or mass/area measurements, or alternatively isopach and isomass maps could be collected for all events for which they are available in IVESPA. This would enable a consistent reanalysis of TEM with a rigorous propagation of uncertainties at each step of the TEM calculation (see section 2.2.1) and using state of the art methods, e.g. for drawing of isopach/isomass maps and their integration to obtain a volume or mass (e.g. Engwell et al., 2015; Yang and Bursik, 2016). Similar efforts could be conducted for investigating uncertainties around plume heights from satellite instruments, through ensuring the same methodology and assumptions are made when assessing plume heights for different events. For example, the Infrared Atmospheric Sounding Interferometer (IASI), with the first instrument launched in 2006, has been used to estimate the heights of SO_2 emissions from multiple eruptions (e.g. Carboni et al., 2016). However, IASI-derived SO_2 heights have not been found for all of the events in IVESPA that occurred since IASI became operational, and the retrieval scheme and data selection (e.g. excluding or including distal measurements) may differ between different studies. The addition of SO_2 heights from IASI retrievals could thus provide a new specific height measurement in IVESPA with a great level of consistency. Similar reanalysis of satellite products could be applied to Geostationary Satellites, commonly used to derive the top and spreading heights using the temperature method.

Third, in this study, field-derived TEM and duration were used to estimate MER, and as such, the resultant MER is an average across an event and does not account for variations through an eruption, where peak MER can be very high. Direct measurements of MER are scarce and very difficult as shown in Gouhier and Donnadieu (2008) using ground-based Doppler radar. More recently, efforts to measure MER from other methods have focussed on the use of umbrella cloud or downwind plume growth rates (Costa et al., 2013a; Pouget et al., 2013, 2016a; Hargie et al., 2019). Bear-Crozier et al. (2020) compared umbrella growth MER with column height MER, and suggested that umbrella growth MER yields a more nuanced picture of MER variations than does the column height method. While application of such methods is only possible for eruptions with spreading umbrella clouds, analysis of variance in MER of these examples could help better inform uncertainties on MER without using deposit mass, and we plan to include MER estimates derived from umbrella growth rate and other methods (e.g. ground-based radar measurements, Freret-Lorgeril et al., 2018) in future versions of IVESPA. In relation to MER, the TEM currently provided in IVESPA are derived from ground deposits sampled as soon as possible after the eruption. However, distal deposits may lack a significant amount of the far-travelled fine ash fraction. To overcome this issue, satellite measurements have been used to assess the fine ash mass lost in the atmosphere and better constrain the actual TEM. In Gouhier et al. (2019) the systematic analysis of the airborne fine ash fraction for 22 eruptions allowed quantification of the airborne fine ash flow rate. Including these parameters in IVESPA would complement the field-derived TEM estimate provided and reduce uncertainties in MER.

Finally, the eruptions contained within this database consist of a relatively small subset of eruption types, and the parameters collected do not allow for description of the full range of eruptive behaviour. For example, we provide a single, time-averaged value for the three types of column height provided (section 2.2.3). However, observations of numerous eruptions show that spreading can occur at multiple heights, and that plumes are commonly not steady-state resulting in a variation in plume height with time (e.g. Arason et al., 2011). Future iterations of the database could include time series of plume height data and information on plumes when spreading occurs at multiple levels. Of particular importance for weak plumes (e.g. discussion in Mastin (2014), Devenish (2016), Aubry and Jellinek (2018)), distinguishing between the bottom, center and top height of the downwind spreading plume (Fig. 2) is critical for ECM evaluation and this distinction could be added in future versions of the database. In addition, we focus on explosive eruptive events, but analysis of height of SO_2 could extend to a broader range of eruptions including effusive eruptions (e.g. Hyman et al., 2018), providing more insight into the behaviour of gas emission and dispersion during eruptions.

5.2. Presenting eruption source parameters in the published record

There are a number of community endorsed publications which provide recommendations on best practice for collection and analysis of tephra deposits (Bonadonna et al., 2013; Wallace et al., 2020). However, while guidelines exist for data collection, few recommendations exist for best practice of presenting eruption observations and characteristic data in the published record. The production of IVESPA involved analysis of field and eruption observational data from more than 300 papers and data sources (section 2.1.2). The information sourced, and its format can vary significantly across these studies. Here, we highlight challenges in the way information is presented in the published record, with the aim to inform future publication of field and observation data so that data can be fully utilised in similar future studies.

First, only a small number of publications and resources exist that contain field measurements and eruption observations that can be easily extracted and used for modelling purposes (the IAVCEI tephra database is one such example). Presentation of raw field and observational data (e.g. tephra thickness and locations, height time series, grain size information at different locations) and associated metadata, alongside eruption IDs such as the GVP eruption ID, would enable direct comparison of datasets from different eruptions, making future studies on

defining empirical relationships between eruption characteristics more efficient.

Second, column height is a commonly described parameter in the literature, however in some cases, it is not clear whether values presented relate to a.s.l. or a.v.l. height which could relate to errors in plume height of several kilometres. In addition, it is not always stated what part of the column the measured height refers to (see Fig. 2), and the location of the measurement, for example directly above the volcano, or at some distance downwind. Moreover, as the column height may change with time it is important to know when and how the column height is estimated (e.g. during the phase of greatest intensity, or during all eruptive phases). Finally, a number of publications report a minimum column height, and where possible it would be advantageous to also include information that constrains the maximum plume height. Consistently reporting on the details of the measurements would enable reduction of uncertainty when comparing different datasets, and when categorising data.

Third, while characteristics such as column height are defined numerically, duration is often presented in a more descriptive manner, making it difficult for the reader to interpret the start and end time of an eruptive event, and therefore an accurate assessment of duration. In a number of the examples used in this study, it was difficult to define whether presented duration related to, for example, the sustained ash emission, paroxysmal ash emission or seismic duration, resulting in greater uncertainty flags. Consequently, it is important to add the methodology used in the estimation of the duration. Furthermore, the combined use of different sensors (e.g. thermal and visible cameras, satellites, geophysical sensors) could be valuable to discriminate the different eruptive phases and estimate the duration for each of them (Corradini et al., 2020).

Last, uncertainty is calculated by different methods for different parameters, and a number of methods are applied for estimation of various types of uncertainty for the same parameter (for example, uncertainty of TEM may be related to number of measurements, statistical method applied for interpolation of data, assessment of how much of the distal/ proximal deposit is missing), but these uncertainties are rarely propagated. Ensuring that enough information is presented to allow the reader to understand how uncertainty was defined would enable more consistent use of data across studies. Where not possible to present uncertainties, presenting metadata (e.g. number of data points) would enable the reader to make an informed assessment of potential uncertainties on data.

Based on these observations, we compile in Table 5, recommendations for presenting observational data on volcanic eruptions in literature.

Table 5
Suggestions for information to report when publishing ESP information

Parameter	Unit	Parameter considerations
Column height	km a.s.l. or a.v.l. (clearly defined)	- Note what height refers to, e.g. top of column, top of the spreading umbrella, bottom of the umbrella (see Fig. 2) - Detail technique used - When using satellite imagery, note location plume height derived, e.g. close to vent or at distance downwind - When a minimum plume height given, provide any observations constraining plume max height
Total erupted mass	kg	- Note density used if converting from volume to mass - Detail number of measurements - Detail technique used for integrating measurement data - If possible, make raw measurements available
Total erupted volume	Cubic m or km	- Detail number of measurements - Detail technique used for integrating measurement data - If possible, make raw measurements available
Duration	hr:min:sec	- Note start time of eruption, and the activity that this is used to define this (e.g. start of ash emission, seismic information) - Note end time of event and activity used to define this (e.g end of ash emission, end of ashfall, seismic information) - Note time zone time information presented in, and ideally include UTC conversions
Uncertainty considerations appropriate for all parameters		
How is uncertainty defined?		
What does uncertainty refer to?		
What are the units of uncertainty?		
What level of confidence (ideally expressed in % or numbers of standard deviation) is associated with the uncertainty provided?		

5.3. Potential future applications of IVESPA

Given the popularity of simple scaling relationships and their critical importance for initialization of VATDMs (see section 1), one of the first contributions of our working group will be a short study evaluating and calibrating existing relationships, including those accounting for atmospheric conditions (e.g. Degruyter and Bonadonna, 2012; Woodhouse et al., 2013; Carazzo et al., 2014; Aubry et al., 2017a), using IVESPA, and potentially proposing a new relationship which better explains the data. This ongoing work will account for uncertainties constrained in IVESPA, derive relationships for the three different types of heights available (top, spreading and SO_2) and shed light on the dependence of these relationships on parameters such as the eruption style or the occurrence of PDCs.

Beyond this preliminary and relatively simple application of IVESPA, the primary objective of our database is to support the development and evaluation of ECMs of various complexities (0D, 1D, 3D). Consequently, it is our hope that the database will be applied by the volcanology community to answer some of the key questions pertaining to the modelling of eruptive column including:

- To what extent are sophisticated ECMs better than relatively simple ones at linking the column height to the MER?
- What are the most important factors (e.g. wind speed profile, TGSD, eruption style) modulating the relationship between plume height and MER?
- Can we improve constraints on empirical parameters used in ECMs, in particular entrainment rates in 1D models, using observations of natural eruptions?
- Can any of our ECMs predict column height (or invert MER) within observational uncertainty?

Critically, with significant efforts devoted to providing and informing uncertainties in IVESPA, the above questions can and should now be systematically answered with an extensive approach to account for uncertainty propagation in ECMs. Strategies such as Monte Carlo sampling (e.g. Aubry et al., 2017b; Aubry and Jellinek, 2018; Michaud-Dubuy et al., 2020) or history matching (Woodhouse et al., 2015) can easily be applied to computationally inexpensive ECMs (0D, 1D) whereas more efficient methods such as conjugate unscented transformation (Pouget et al., 2016b) may be required for more expensive ECMs (e.g. 1D with aggregation scheme, 3D). Ultimately, we hope that ECM evaluation efforts by individual groups will serve as a testbed to implement evaluation exercises in future ECM intercomparison projects (Costa et al., 2016a). The richness of IVESPA may benefit from the use of machine learning methods and advanced statistical methods (e.g. Gouhier et al., 2019) that may complement or outcompete scaling relationships (0D ECMs) at linking the MER to plume height.

The scope of the database goes beyond informing ECM, with the data collated having the potential to aid definition of ESPs for eruption scenarios at volcanoes for which there is little information. Beyond direct

application to ECM evaluation and development, IVESPA can also be used to answer a large variety of questions. For example, the SO_2 and spreading height compiled can be compared with heights derived from the deposit isopleth (e.g. Carey and Sparks, 1986; Rossi et al., 2019), which are known to be representative of the maximum top height reached during an eruption. Such comparisons could in turn be used to better constrain the height of SO_2 injection to be used in climate modelling studies of ancient eruptions for which only the height derived from isopleth is known (e.g. Vidal et al., 2015b). Similarly, investigating how ESP and atmospheric conditions govern the relationship between the tephra top height, tephra spreading height, and SO_2 height is of interest to the broader volcanology community. Another example of potential application of IVESPA derives from our compilation of both uncertainty on TEM and the metadata provided alongside it (see section 2.2.1), in particular the number of measurements used in estimating mass, and their minimum and maximum locations from the vent. For example, deposits characterised by a smaller number of measurements are likely to be less certain than those with a large number. While some studies have assessed uncertainties in erupted mass measurements (e.g. Klawonn et al., 2014a, 2014b; Bonadonna et al., 2015a), these have typically been applied to individual deposits and eruptions, and as yet no simple relation exists that can be applied taking account of available deposit metadata, e.g. number and distribution of measurements, to estimate uncertainty. IVESPA thus offers an opportunity to assess such relationships across a large number of eruptive events.

6. Conclusions

We have built a new observational database - the Independent Volcanic Eruption Source Parameter Archive (IVESPA, version 1.0) - the primary motivation of which is to support the evaluation and development of eruptive column models (ECMs). IVESPA has been endorsed by the IAVCEI commission on Tephra Hazard Modelling (THM) and is supported by the British Geological Survey which hosts the database website (ivespa.co.uk). It will be maintained, updated as new events become available, and is open to the community for feedback and suggestions. For a current count of 134 eruptive events:

- IVESPA systematically contains the total erupted mass of tephra-fallout, duration, heights (top, spreading and SO_2 height) and atmospheric condition profiles. These parameters enable testing of any 0D ECM (scaling relationships between height, mass eruption rate (MER), and, for some of them, averaged wind and stratification) and the majority of 1D ECMs.
- IVESPA contains the total grain size distribution (TGSD), which is an input required by some 1D ECMs and by 3D ECMs, whenever it has been reconstructed.
- When available in the literature, IVESPA also provides a number of other relevant parameters such as the eruption style or the tephra mass derived from pyroclastic density currents (see Table 4).

IVESPA systematically provides uncertainty estimates associated with each eruption source parameter (ESP) provided in the database. We have also made efforts to provide a high-quality database by having two members of our working group independently search for the value of key ESPs for each event before reaching a consensual value. We show that important differences can arise between the initial estimates of our working group members, as well as between IVESPA and existing datasets with independently estimated ESPs. In particular, these differences can be caused by experts using different references for estimating ESP or interpreting these references differently. To address this issue and further inform the reliability of the data provided for each event, IVESPA contains flags that indicate how much interpretation of the literature was required in providing key ESP values and their uncertainties (Fig. 1). Our approach with two experts independently vetting each ESP value is also crucial to addressing difficulties in compiling ESP values from the literature. We also used lessons learnt from the creation of IVESPA to recommend best practice for presenting ESP information in the literature. Beyond efforts made to extensively inform uncertainties, IVESPA covers an unprecedented range of ESPs including MER, atmospheric conditions and TGSDs. This will be valuable to test and develop ECMs across a wide range of eruptive conditions.

Declaration of Competing Interest

The authors declare that they have no known competing financial interests or personal relationships that could have appeared to influence the work reported in this paper.

Acknowledgements

We thank Sarah Ogburn, Joe Dufek, Ben Andrews and Fabio Dioguardi for their comments which significantly improved the manuscript, and Tim Horscroft and Jim Gardner for inviting us to submit this paper. This work would not have been possible without the efforts of the volcanological community in studying volcanic deposits and eruptions that occurred over the past century. We thank the many experts who provided complementary information on eruptions in IVESPA, including Olga Girina, Marco Pistolesi, David Kratzmann, Marina Belousova, Alexander Belousov, Benjamin Bernard, Daniele Andronico, Jessica Larsen, Michael Ort, and Peter Webley. We acknowledge extensive use of the Volcanoes of the World database made available by the Global Volcanism Program. NCEP Reanalysis data is provided by the NOAA/OAR/ESRL PSL, Boulder, Colorado, USA, from their website at https://psl.noaa.gov/. Support for the Twentieth Century Reanalysis Project version 3 dataset is provided by the U.S. Department of Energy, Office of Science Biological and Environmental Research, by the NOAA Climate Program Office, and by the NOAA Physical Sciences Laboratory. We thank the ECMWF for producing and making available the ERA-5 and ERA-20C reanalyses at https://www.ecmwf.int/en/forecasts/datasets/browse-reanalysis-datasets. We thank the IAVCEI THM Commission for their endorsement of this project. T.J.A. acknowledges support from the Royal Society through a Newton International Fellowship (grant number NIF\R1\180809), from the European Union's Horizon 2020 research and innovation programme under the Marie Skłodowska-Curie grant agreement No 835939, and from the Sidney Sussex College through a Junior Research Fellowship. S.L.E. acknowledges European Union's Horizon 2020 project EUROVOLC (grant agreement No. 731070) and the British Geological Survey NC-Innovation grant NE/R000069/1. S.L.E. publishes with permission of the CEO, British Geological Survey. I.A.T. and R.G.G. acknowledge the support of the Centre for Observation and Modelling of Earthquakes, Volcanoes and Tectonics (COMET). A.S. acknowledges funding from the Natural Environment Research Council (NERC) V-PLUS grant NE/S00436X/1. Any use of trade, firm, or product names is for descriptive purposes only and does not imply endorsement by the U.S. Government.

Authors statement

All authors: Data Curation, Validation, Methodology, Writing - Original Draft, Writing - Review & Editing. **Thomas J. Aubry and Samantha Engwell:** Conceptualization, Formal analysis, Project administration, Funding acquisition.

Data availability

All data, including atmospheric profiles, TGSDs, and notes on DC discussions, is available on the IVESPA website (ivespa.co.uk). Further notes detailing the data collection for each eruption are available upon request from T.J.A. (ta460@cam.ac.uk).

Appendix A

The full list of references and the events they were used for are available on IVESPA website. This appendix simply lists these references to ensure that a citation is associated with this study: Global Volcanism Program (1970, 1971a, b, c, 1973, 1974, 1975, 1980a, b, 1982a, b, 1984, 1985a, b, 1986a, b, c, d, 1990, 1991, 1992a, b, c, 1993, 1995a, b, 1996a, b, c, 1997, 1998, 1999a, b, c, 2000a, b, 2001, 2002, 2003a, b, c, 2005, 2006a, b, c, 2008a, b, 2009, 2011, 2014, 2015a, b, 2016a, b, 2017a, b, c, d), Belousova and Belousov (2001), Cassidy et al. (2015), Castro et al. (2010), Izbekov et al. (2009), Mankowski et al. (2001), Montalbano et al. (2017), Suzuki et al. (2014), Thordarson et al. (2011), Vidal et al. (2015b), Hayer et al. (2016), Thorarinsson (1949), Koyaguchi (1996), Lynch et al. (1996), Newhall et al. (1996), Rybin et al. (2012), Scott et al. (1996), Hoblitt et al. (1996), Le Pennec et al. (2002), Romero et al. (2013, 2016a, 2016b), Bonadonna et al. (2002), Larsen et al. (2015), Naranjo (1993), SERNAGEOMIN (2015), IAVCEI Commission on Tephra Hazard Modelling original database (2001), Hadikusumo (1961), Coltelli et al. (2006), Luigi Lodato e Boris Behncke (2006), Belousov et al. (2003), Hall et al. (2004), Höskuldsson et al. (2018), Schneider and Thompson (2000), Gilbert (2012), Moxey (2005), Unema (2001), Bluth et al. (1995), Brantley (1990), Christiansen and Peterson (1981), Eichelberger et al. (1995), Harris et al. (1981), Miller et al. (1995), Neal et al. (1995), Rose et al. (1995), Rowley (1981), Scott et al. (2008), U.S. Geological Survey (2005), Voight et al. (1981), Waitt et al. (1995), Wallace et al. (2006), Webster et al. (2006), Alfano et al. (2011), Alfano et al. (2016), Aloisi et al. (2002), Andronico et al. (2005, 2008, 2009a, 2009b, 2014a, 2014b, 2015, 2018), Armienta et al. (2002), Atlas et al. (2006), Baldridge et al. (1973), Barberi et al. (1990b), Barton et al. (1992), Belousov et al. (2017), Belousov and Belousova (1998), Belousov (1996), Bernard et al. (2016a, 2016b), Biass et al. (2014), Bitar et al. (2010), Bonaccorso et al. (2014), Bonadonna et al. (2011, 2015a, 2015b), Bonadonna and Houghton (2005), Bonadonna and Costa (2012, 2013), Bonis and Salazar (1973), Bourdier et al. (1997), Brazier et al. (1982), Calvari et al. (2006, 2011), Caplan-Auerbach et al. (2010), Carboni et al. (2016), Carey et al. (1990), Carey and Sigurdsson (1982), Carn and Lopez (2011), Carn et al. (2009), Carter et al. (2008), Caudron et al. (2015), Chung et al. (1981), Collini et al. (2013), Coombs et al. (2013), Corradini et al. (2010, 2016), Costa et al. (2013b, 2016b), Cronin et al. (1998), Danielsen (1981), Davies et al. (1978), Dean et al. (1994), Denniss et al. (1998), Deruelle et al. (1996), Durant and Rose (2009), Durant et al. (2012), Edwards et al. (2018), Ekstrand et al. (2013), Elissondo et al. (2016), Eychenne et al. (2012, 2013, 2015), Flemming and Inness (2013), Fee et al. (2010), Flentje et al. (2010), Folch et al. (2008), Gaunt et al. (2016), Gardner et al. (1994), Geshi and Oikawa (2008), Girault et al. (2014), Girina (2013), Gorshkov (1959), Gronvold et al. (1983), Gudmundsson et al. (1992, 2012), Gudnason et al. (2017), Guffanti et al. (2005), Guo et al. (2004a, 2004b), Gurenko et al. (2005), Hall et al. (2013, 2015), Hashimoto et al. (2012), Hildreth and Drake (1992), Hill et al. (1998), Holasek et al. (1996), Höskuldsson et al. (2007), Hreinsdóttir et al. (2014), Hurst and Turner (1999), Jude-Eton et al. (2012), Kaneko et al. (2016), Kilgour et al. (2013), Koyaguchi and Ohno (2001), Kozono et al. (2013), Kratzmann et al. (2009, 2010), Kristiansen et al. (2015), Kristiansen et al. (2010), Krotkov et al. (1999), Krueger et al. (1990, 2008), Kylling (2016), Lacasse et al. (2004), La Femina et al. (2004), Lara (2010), Larsen et al. (2009, 2013), Le Pennec et al. (2012), Lucic et al. (2016), Luhr et al. (1984), Maeno et al. (2014, 2016, 2019), Major and Lara (2013), Malik (2011), Marchese et al. (2014), Martin-Del Pozzo et al. (2008), Marzano et al. (2013), Mastin (2007), Mastin et al. (2013b), Matoza et al. (2007), Matson (1984), McCarthy et al. (2008), Meinel and Meinel (1963), Melson et al. (1990), Métrich et al. (2004, 2005), Miller and Chouet (1994), Miyabuchi et al. (2018), Moiseenko and Malik (2014, 2015), Mossop (1964), Moune et al. (2007), Murrow et al. (1980), Myers et al. (2014), Nairn and Self (1978), Nakada et al. (2005a, 2005b, 2013), Nakagawa et al. (2002), Naranjo et al. (1986), Norini et al. (2009), Nye et al. (2002), Oddsson et al. (2012), Oikawa et al. (2016), Pallister et al. (2005), Pardini et al. (2018), Petersen et al. (2012), Pistolesi et al. (2015), Pioli et al. (2019), Plechov et al. (2008), Poret et al. (2017, 2018a, 2018b), Portnyagin et al. (2014), Prata et al. (2010, 2015), Prata and Grant (2001), Reckziegel et al. (2016), Ridolfi et al. (2008), Ripepe and Harris (2008), Rizi et al. (2000), Robock and Matson (1983), Roggensack et al. (1997), Romero et al. (2016a, 2016b, 2017), Rose et al. (1973, 1978, 2003, 2008), Rose and Durant (2009), Rosi et al. (2006), Ruprecht and Bachmann (2010), Rutherford et al. (1985), Rybin et al. (2011), Sadofsky et al. (2008), Saito et al. (2010), Samaniego et al. (2008), Scaillet and Evans (1999), Scasso et al. (1994), Schneider et al. (1999), Schneider and Hoblitt (2013), Scollo et al. (2007, 2008), Scott and McGimsey (1994), Self and Rampino (2012), Sellitto et al. (2016), Shcherbakov et al. (2011, 2013), Shepherd et al. (1979), Shibata and Kinoshita (2016), Sigurdsson et al. (1984, 1987), Slezin (2015), Solikhin et al. (2015), Sparks et al. (1997b), Spilliaert et al. (2006), Steffke et al. (2010), Stelling et al. (2002), Stohl et al. (2011), Sulpizio (2005), Surono et al. (2012), Suzuki et al. (2013), Takarada et al. (2016), Thorarinsson (1950), Thorarinsson and Sigvaldason (1972), Troncoso et al. (2017), Trusdell et al. (2005), Underwood et al. (2013), Urai and Ishizuka (2011), Van Manen et al. (2010), Varekamp et al. (1984), Vernier et al. (2016), Voight (1990), Wallace et al. (2013), Watt et al. (2009), Waythomas et al. (2010), Williams and Self (1983), Wolf and Eichelberger (1997), Woods and Kienle (1994), Wright et al. (2005), Zen and Hadikusumo (1964), Zharinov and Demyanchuk (2011).

References

Alfano, F., Bonadonna, C., Volentik, A.C., Connor, C.B., Watt, S.F., Pyle, D.M., Connor, L.J., 2011. Tephra stratigraphy and eruptive volume of the May, 2008, Chaitén eruption, Chile. Bull. Volcanol. 73 (5), 613–630. https://doi.org/10.1007/s00445-010-0428-x.

Alfano, F., Bonadonna, C., Watt, S., Connor, C., Volentik, A., Pyle, D.M., 2016. Reconstruction of total grain size distribution of the climactic phase of a long-lasting eruption: the example of the 2008–2013 Chaitén eruption. Bull. Volcanol. 78 (7), 1–21. https://doi.org/10.1007/s00445-016-1040-5.

Aloisi, M., D'Agostino, M., Dean, K.G., Mostaccio, A., Neri, G., 2002. Satellite analysis and PUFF simulation of the eruptive cloud generated by the Mount Etna paroxysm of 22 July 1998. J. Geophys. Res. Solid Earth 107 (B12). https://doi.org/10.1029/2001JB000630 ECV-9.

Andronico, D., Branca, S., Calvari, S., Burton, M., Caltabiano, T., Corsaro, R.A., Del Carlo, P., Garfì, G., Lodato, L., Miraglia, L., et al., 2005. A multi-disciplinary study of the 2002–03 Etna eruption: insights into a complex plumbing system. Bull. Volcanol. 67 (4), 314–330. https://doi.org/10.1007/s00445-004-0372-8.

Andronico, D., Scollo, S., Caruso, S., Cristaldi, A., 2008. The 2002–03 Etna explosive activity: tephra dispersal and features of the deposits. J. Geophys. Res. Solid Earth 113 (B4). https://doi.org/10.1029/2007JB005126.

Andronico, D., Scollo, S., Cristaldi, A., Ferrari, F., 2009a. Monitoring ash emission episodes at Mt. Etna: the 16 November 2006 case study. J. Volcanol. Geotherm. Res. 180 (2-4), 123–134. https://doi.org/10.1016/j.jvolgeores.2008.10.019.

Andronico, D., Spinetti, C., Cristaldi, A., Buongiorno, M., 2009b. Observations of Mt. Etna volcanic ash plumes in 2006: an integrated approach from ground-based and polar satellite NOAA-AVHRR monitoring system. J. Volcanol. Geotherm. Res. 180 (24), 135–147. https://doi.org/10.1016/j.jvolgeores.2008.11.013 Models and products of mafic explosive activity.

Andronico, D., Scollo, S., Cristaldi, A., Castro, M.D.L., 2014a. Representivity of incompletely sampled fall deposits in estimating eruption source parameters: a test using the 12–13 January 2011 lava fountain deposit from Mt. Etna volcano, Italy. Bull. Volcanol. 76 (10), 861. https://doi.org/10.1007/s00445-014-0861-3.

Andronico, D., Scollo, S., Castro, M.D.L., Cristaldi, A., Lodato, L., Taddeucci, J., 2014b. Eruption dynamics and tephra dispersal from the 24 November 2006 paroxysm at South-East crater,Mt Etna, Italy. J. Volcanol. Geotherm. Res. 274, 78–91. https://doi.org/10.1016/j.jvolgeores.2014.01.009.

Andronico, D., Scollo, S., Cristaldi, A., 2015. Unexpected hazards from tephra fallouts at Mt Etna: The 23 November 2013 lava fountain. J. Volcanol. Geotherm. Res. 304, 118–125. https://doi.org/10.1016/j.jvolgeores.2015.08.007.

Andronico, D., Behncke, B., De Beni, E., Cristaldi, A., Scollo, S., Lopez, M., Lo Castro, M.D., 2018. Magma budget from lava and tephra volumes erupted during the 25-26 October 2013 Lava Fountain at Mt Etna. Front. Earth Sci. 6, 116. https://doi.org/10.3389/feart.2018.00116.

Arason, P., Petersen, G.N., Bjornsson, H., 2011. Observations of the altitude of the volcanic plume during the eruption of Eyjafjallajökull, April-May 2010. Earth Syst. Sci. Data 3 (1), 9–17.

Armienta, M., De la Cruz-Reyna, S., Morton, O., Cruz, O., Ceniceros, N., 2002. Chemical variations of tephra-fall deposit leachates for three eruptions from Popocatepetl volcano.

J. Volcanol. Geotherm. Res. 113 (1), 61–80. https://doi.org/10.1016/S0377-0273(01)00251-7.
Atlas, Z., Dixon, J., Sen, G., Finny, M., Martin-Del Pozzo, A., 2006. Melt inclusions from Volcán Popocatépetl and Volcán de Colima, Mexico: nelt evolution due to vaporsaturated crystallization during ascent. J. Volcanol. Geotherm. Res. 153 (3), 221–240. https://doi.org/10.1016/j.jvolgeores.2005.06.010.
Aubry, T.J., Jellinek, A.M., 2018. New insights on entrainment and condensation in volcanic plumes: Constraints from independent observations of explosive eruptions and implications for assessing their impacts. Earth Planet. Sci. Lett. 490, 132–142.
Aubry, T.J., Jellinek, A.M., Carazzo, G., Gallo, R., Hatcher, K., Dunning, J., 2017a. A new analytical scaling for turbulent wind-bent plumes: comparison of scaling laws with analog experiments and a new database of eruptive conditions for predicting the height of volcanic plumes. J. Volcanol. Geotherm. Res. 343, 233–251.
Aubry, T.J., Carazzo, G., Jellinek, A.M., 2017b. Turbulent entrainment into volcanic plumes: new constraints from laboratory experiments on buoyant jets rising in a stratified crossflow. Geophys. Res. Lett. 44 (20), 10–198.
Baldridge, W.S., McGetchin, T.R., Frey, F.A., Jarosewich, E., 1973. Magmatic evolution of Hekla, Iceland. Contrib. Mineral. Petrol. 42 (3), 245–258. https://doi.org/10.1007/BF00371589.
Barberi, F., Macedonio, G., Pareschi, M., et al., 1990a. Mapping the tephra fallout risk: an example from Vesuvius, Italy. Nature 344, 142–144. https://doi.org/10.1038/344142a0.
Barberi, F., Martini, M., Rosi, M., 1990b. Nevado del Ruiz volcano (Colombia): pre-eruption observations and the November 13, 1985 catastrophic event. J. Volcanol. Geotherm. Res. 42 (1-2), 1–12. https://doi.org/10.1016/0377-0273(90)90066-O.
Barton, I.J., Prata, A.J., Watterson, I.G., Young, S.A., 1992. Identification of the Mount Hudson volcanic cloud over SE Australia. Geophys. Res. Lett. 19 (12), 1211–1214. https://doi.org/10.1029/92GL01122.
Bear-Crozier, A., Pouget, S., Bursik, M., Jansons, E., Denman, J., Tupper, A., Rustowicz, R., 2020. Automated detection and measurement of volcanic cloud growth: towards a robust estimate of mass flux, mass loading and eruption duration. Nat. Hazards 101 (1), 1–38.
Belousov, A., 1996. Deposits of the 30 March 1956 directed blast at Bezymianny volcano, Kamchatka, Russia. Bull. Volcanol. 57 (8), 649–662. https://doi.org/10.1007/s004450050118.
Belousov, A.B., Belousova, M.G., 1998. Bezymyannyi eruption on March 30, 1956 (Kamchatka): sequence of events and debris avalanche deposits. Volcanol Seismol 20, 29–47.
Belousov, A.B., Belousova, M.G., Grushin, S.Y., Krestov, P.B., 2003. Historic eruptions of the Chikurachki volcano (Paramushir, Kurile Islands). Volcanol. Seismol 3, 15–34.
Belousov, A.B., Belousova, M.G., Kozlov, D.N., 2017. The distribution of tephra deposits and reconstructing the parameters of 1973 eruption on Tyatya Volcano, Kunashir I., Kuril Islands. J. Volcanol. Seismol. 11 (4), 285–294. https://doi.org/10.1134/S0742046317040029.
Belousova, M., Belousov, A., 2001. Frequent basaltic plinian eruptions in the history of Chikurachki volcano, Kurile islands, Russia. XXVI EGS General Assembly. http://www.kscnet.ru/ivs/lavdi/staff/belousov/chikabs.pdf.
Bernard, B., Battaglia, J., Proaño, A., Hidalgo, S., Vásconez, F., Hernandez, S., Ruiz, M., 2016a. Relationship between volcanic ash fallouts and seismic tremor: quantitative assessment of the 2015 eruptive period at Cotopaxi volcano. Ecuador. Bull. Volcanol. 78 (11), 80. https://doi.org/10.1007/s00445-016-1077-5.
Bernard, J., Eychenne, J., Le Pennec, J.-L., Narváez, D., 2016b. Mass budget partitioning during explosive eruptions: insights from the 2006 paroxysm of Tungurahua volcano. Ecuador. Geochem. Geophys. Geosyst. 17 (8), 3224–3240.
Biass, S., Bonadonna, C., 2011. A quantitative uncertainty assessment of eruptive parameters derived from tephra deposits: the example of two large eruptions of Cotopaxi volcano, Ecuador. Bull. Volcanol. 73 (1), 73–90.
Biass, S., Scaini, C., Bonadonna, C., Folch, A., Smith, K., Höskuldsson, A., 2014. A multi-scale risk assessment for tephra fallout and airborne concentration from multiple Icelandic volcanoes – Part 1: Hazard assessment. Nat. Hazards Earth Syst. Sci. 14, 2265–2287. https://doi.org/10.5194/nhess-14-2265-2014.
Bitar, L., Duck, T., Kristiansen, N., Stohl, A., Beauchamp, S., 2010. Lidar observations of Kasatochi volcano aerosols in the troposphere and stratosphere. J. Geophys. Res. Atmos. 115 (D2). https://doi.org/10.1029/2009JD013650.
Bluth, G.J., Scott, C.J., Sprod, I.E., Schnetzler, C.C., Krueger, A.J., Walter, L.S., 1995. Explosive emissions of sulfur dioxide from the 1992 Crater Peak eruptions, Mount Spurr volcano. Alaska. US Geol. Surv. Bull 2139, 37–46.
Bonaccorso, A., Calvari, S., Linde, A., Sacks, S., 2014. Eruptive processes leading to the most explosive lava fountain at Etna volcano: The 23 November 2013 episode. Geophys. Res. Lett. 41 (14), 4912–4919. https://doi.org/10.1002/2014GL060623.
Bonadonna, C., Costa, A., 2012. Estimating the volume of tephra deposits: a new simple strategy. Geology https://doi.org/10.1130/G32769.1 G32769–1.
Bonadonna, C., Costa, A., 2013. Plume height, volume, and classification of explosive volcanic eruptions based on the Weibull function. Bull. Volcanol. 75 (8), 742. https://doi.org/10.1007/s00445-013-0742-1.
Bonadonna, C., Houghton, B., 2005. Total grain-size distribution and volume of tephrafall deposits. Bull. Volcanol. 67 (5), 441–456. https://doi.org/10.1007/s00445-004-0386-2.
Bonadonna, C., Mayberry, G.C., Calder, E.S., Sparks, R.S.J., Choux, C., Jackson, P., ... Ryan, G., 2002. Tephra fallout in the eruption of Soufrière Hills Volcano, Montserrat. Geol. Soc. Lond. Mem. 21 (1), 483–516. https://doi.org/10.1144/GSL.MEM.2002.021.01.22.
Bonadonna, C., Genco, R., Gouhier, M., Pistolesi, M., Cioni, R., Alfano, F., Hoskuldsson, A., Ripepe, M., 2011. Tephra sedimentation during the 2010 Eyjafjallajökull eruption (Iceland) from deposit, radar, and satellite observations. J. Geophys. Res. Solid Earth 116 (B12). https://doi.org/10.1029/2011JB008462.
Bonadonna, C., Cioni, R., Pistolesi, M., Connor, C., Scollo, S., Pioli, L., Rosi, M., 2013. Determination of the largest clast sizes of tephra deposits for the characterization of explosive eruptions: a study of the IAVCEI commission on tephra hazard modelling. Bull. Volcanol. 75 (1), 680.
Bonadonna, C., Biass, S., Costa, A., 2015a. Physical characterization of explosive volcanic eruptions based on tephra deposits: propagation of uncertainties and sensitivity analysis. J. Volcanol. Geotherm. Res. 296, 80–100. https://doi.org/10.1016/j.jvolgeores.2015.03.009.
Bonadonna, C., Cioni, R., Pistolesi, M., Elissondo, M., Baumann, V., 2015b. Sedimentation of long-lasting wind-affected volcanic plumes: the example of the 2011 rhyolitic Cordón Caulle eruption, Chile. Bull. Volcanol. 77 (2), 13. https://doi.org/10.1007/s00445-015-0900-8.
Bonadonna, C., Pistolesi, M., Cioni, R., Degruyter, W., Elissondo, M., Baumann, V., 2015c. Dynamics of wind-affected volcanic plumes: The example of the 2011 Cordón Caulle eruption, Chile. J. Geophys. Res. Solid Earth 120 (4), 2242–2261.
Bonis, S., Salazar, O., 1973. The 1971 and 1973 eruptions of Volcan Fuego, Guatemala, and some socio-economic considerations for the volcanologist. Bull. Volcanol. 37 (3), 394–400. https://doi.org/10.1007/BF02597636.
Bourdier, J.-L., Pratomo, I., Thouret, J.-C., Boudon, G., Vincent, P.M., 1997. Observations, stratigraphy and eruptive processes of the 1990 eruption of Kelut volcano, Indonesia. J. Volcanol. Geotherm. Res. 79 (3), 181–203. https://doi.org/10.1016/S0377-0273(97)00031-0.
Brantley, S.R., 1990. The Eruption of Redoubt Volcano, Alaska, December 14, 1989–August 31, 1990.
Brazier, S., Davis, A.N., Sigurdsson, H., Sparks, R.S.J., 1982. Fall-out and deposition of volcanic ash during the 1979 explosive eruption of the Soufriere of St. Vincent. J. Volcanol. Geotherm. Res. 14 (3–4), 335–359. https://doi.org/10.1016/0377-0273(82)90069-5.
Bursik, M., Jones, M., Carn, S., Dean, K., Patra, A., Pavolonis, M., ... Bjornsson, H., 2012. Estimation and propagation of volcanic source parameter uncertainty in an ash transport and dispersal model: application to the Eyjafjallajokull plume of 14–16 April 2010. Bull. Volcanol. 74 (10), 2321–2338.
Calvari, S., Spampinato, L., Lodato, L., 2006. The 5 April 2003 vulcanian paroxysmal explosion at Stromboli volcano (Italy) from field observations and thermal data. J. Volcanol. Geotherm. Res. 149 (1-2), 160–175. https://doi.org/10.1016/j.jvolgeores.2005.06.006.
Calvari, S., Salerno, G.G., Spampinato, L., Gouhier, M., La Spina, A., Pecora, E., Harris, A.J.L., Labazuy, P., Biale, E., Boschi, E., 2011. An unloading foam model to constrain Etna's 11–13 January 2011 lava fountaining episode. J. Geophys. Res. 116, B11207. https://doi.org/10.1029/2011JB008407.
Caplan-Auerbach, J., Bellesiles, A., Fernandes, J.K., 2010. Estimates of eruption velocity and plume height from infrasonic recordings of the 2006 eruption of Augustine Volcano, Alaska. J. Volcanol. Geotherm. Res. 189 (1–2), 12–18. https://doi.org/10.1016/j.jvolgeores.2009.10.002.
Carazzo, G., Girault, F., Aubry, T., Bouquerel, H., Kaminski, E., 2014. Laboratory experiments of forced plumes in a density-stratified crossflow and implications for volcanic plumes. Geophys. Res. Lett. 41 (24), 8759–8766.
Carboni, E., Grainger, R., Mather, T.A., Pyle, D.M., Dudhia, A., Thomas, G., ... Balis, D., 2016. The vertical distribution of volcanic SO2 plumes measured by IASI. Atmos. Chem. Phys. 16. https://doi.org/10.5194/acpd-15-24643-2015.
Carey, S.N., Sigurdsson, H., 1982. Influence of particle aggregation on deposition of distal tephra from the May 18, 1980, eruption of Mount St. Helens volcano. J. Geophys. Res. Solid Earth 87 (B8), 7061–7072. https://doi.org/10.1029/JB087iB08p07061.
Carey, S., Sparks, R.S.J., 1986. Quantitative models of the fallout and dispersal of tephra from volcanic eruption columns. Bull Volcanol 48, 109–125. https://doi.org/10.1007/BF01046546.
Carey, S., Sigurdsson, H., 1989. The intensity of plinian eruptions. Bull. Volcanol. 51, 28–40. https://doi.org/10.1007/BF01086759.
Carey, S., Sigurdsson, H., Gardner, J.E., Criswell, W., 1990. Variations in column height and magma discharge during the May 18, 1980 eruption of Mount St. Helens. J. Volcanol. Geotherm. Res. 43 (1–4), 99–112. https://doi.org/10.1016/0377-0273(90)90047-J.
Carn, S., Lopez, T., 2011. Opportunistic validation of sulfur dioxide in the Sarychev Peak volcanic eruption cloud. Atmos. Meas. Tech. 4 (9), 1705–1712. https://doi.org/10.5194/amt-4-1705-2011.
Carn, S.A., Pallister, J.S., Lara, L., Ewert, J.W., Watt, S., Prata, A.J., Thomas, R.J., Villarosa, G., 2009. The unexpected awakening of Chaitén volcano, Chile. Eos. Trans. AGU 90 (24), 205–206. https://doi.org/10.1029/2009EO240001.
Carn, S.A., Clarisse, L., Prata, A.J., 2016. Multi-decadal satellite measurements of global volcanic degassing. J. Volcanol. Geotherm. Res. 311, 99–134.
Carter, A.J., Girina, O., Ramsey, M.S., Demyanchuk, Y.V., 2008. ASTER and field observations of the 24 December 2006 eruption of Bezymianny volcano. Russia. Remote Sens. Environ. 112 (5), 2569–2577. https://doi.org/10.1016/j.rse.2007.12.001.
Cassidy, M., Helo, C., Castro, J., Muir, D., Troll, V., 2015. The magmatic conditions, from storage to surface preceding effusive and explosive eruptions at Kelud volcano. AGU Fall Meeting Abstracts. http://adsabs.harvard.edu/abs/2015AGUFM.V13B3107C.
Castro, J., Lowenstern, J., Pallister, J., Eichelberger, J., 2010. Simultaneous explosive and effusive activity at Chaitén volcano, Chile. AGU Fall Meeting Abstracts. URL 2010AGUFM.V34B.08C.
Caudron, C., Taisne, B., Garcés, M., Alexis, L.P., Mialle, P., 2015. On the use of remote infrasound and seismic stations to constrain the eruptive sequence and intensity for the 2014 Kelud eruption. Geophys. Res. Lett. 42 (16), 6614–6621. https://doi.org/10.1002/2015GL064885.
Cerminara, M., Ongaro, T.E., Neri, A., 2016. Large Eddy Simulation of gas–particle kinematic decoupling and turbulent entrainment in volcanic plumes. J. Volcanol. Geotherm. Res. 326, 143–171.
Christiansen, R.L., Peterson, D.W., 1981. Chronology of the 1980 eruptive activity. US Geol. Surv. Prof. Pap. 1250, 17–30.

Chung, Y.S., Gallant, A., Fanaki, F., Millan, M., 1981. On the observations of Mount St Helens volcanic emissions: research note. Atmosphere-Ocean 19 (2), 172–178. https://doi.org/10.1080/07055900.1981.9649108.

Collini, E., Osores, M.S., Folch, A., Viramonte, J.G., Villarosa, G., Salmuni, G., 2013. Volcanic ash forecast during the June 2011 Cordón Caulle eruption. Nat. Hazards 66 (2), 389–412. https://doi.org/10.1007/s11069-012-0492-y.

Coltelli, M., Puglisi, G., Guglielmino, F., Palano, M., 2006. Application of differential SAR interferometry for studying eruptive event of 22 July 1998 at Mt. Etna Quaderni di Geofisica.

Compo, G.P., Whitaker, J.S., Sardeshmukh, P.D., Matsui, N., Allan, R.J., Yin, X., ... Brönnimann, S., 2011. The twentieth century reanalysis project. Q. J. R. Meteorol. Soc. 137 (654), 1–28.

Coombs, M., Sisson, T., Bleick, H., Henton, S., Nye, C., Payne, A., Cameron, C., Larsen, J., et al., 2013. Andesites of the 2009 eruption of Redoubt Volcano, Alaska. J. Volcanol. Geotherm. Res. 259, 349–372. https://doi.org/10.1016/j.jvolgeores.2012.01.002.

Corradini, S., Merucci, L., Prata, A., Piscini, A., 2010. Volcanic ash and SO2 in the 2008 Kasatochi eruption: retrievals comparison from different IR satellite sensors. J. Geophys. Res. Atmos. 115 (D2). https://doi.org/10.1029/2009JD013634.

Corradini, S., Montopoli, M., Guerrieri, L., Ricci, M., Scollo, S., Merucci, L., ... Grainger, R.G., 2016. A multi-sensor approach for volcanic ash cloud retrieval and eruption characterization: the 23 November 2013 Etna lava fountain. Remote Sens. 8 (1), 58. https://doi.org/10.3390/rs8010058.

Corradini, S., Guerrieri, L., Lombardo, V., Merucci, L., Musacchio, M., Prestifilippo, M., ... Stelitano, D., 2018. Proximal monitoring of the 2011–2015 Etna lava fountains using MSG-SEVIRI data. Geosciences 8 (4), 140.

Corradini, S., Guerrieri, L., Stelitano, D., Salerno, G., Scollo, S., Merucci, L., ... Caltabiano, T., 2020. Near real-time monitoring of the Christmas 2018 Etna eruption using SEVIRI and products validation. Remote Sens. 12 (8), 1336.

Costa, A., Folch, A., Macedonio, G., 2013a. Density-driven transport in the umbrella region of volcanic clouds: implications for tephra dispersion models. Geophys. Res. Lett. 40 (18), 4823–4827.

Costa, F., Andreastuti, S., de Maisonneuve, C.B., Pallister, J.S., 2013b. Petrological insights into the storage conditions, and magmatic processes that yielded the centennial 2010 Merapi explosive eruption. J. Volcanol. Geotherm. Res. 261, 209–235. https://doi.org/10.1016/j.jvolgeores.2012.12.025.

Costa, A., Suzuki, Y.J., Cerminara, M., Devenish, B.J., Ongaro, T.E., Herzog, M., ... Engwell, S., 2016a. Results of the eruptive column model inter-comparison study. J. Volcanol. Geotherm. Res. 326, 2–25.

Costa, A., Pioli, L., Bonadonna, C., 2016b. Assessing tephra total grain-size distribution: Insights from field data analysis. Earth Planet. Sci. Lett. 443, 90–107. https://doi.org/10.1016/j.epsl.2016.02.040.

Cronin, S., Hedley, M., Neall, V., Smith, R., 1998. Agronomic impact of tephra fallout from the 1995 and 1996 Ruapehu Volcano eruptions, New Zealand. Environ. Geol. 34 (1), 21–30. https://doi.org/10.1007/s002540050253.

Crosweller, H.S., Arora, B., Brown, S.K., Cottrell, E., Deligne, N.I., Guerrero, N.O., Hobbs, L., Kiyosugi, K., Loughlin, S.C., Lowndes, J., Nayembil, M., 2012. Global database on large magnitude explosive volcanic eruptions (LaMEVE). J. Appl. Volcanol. 1 (1), 4.

D'Amours, R., 1994. Current and future capabilities in forecasting the trajectories, transport, and dispersion of volcanic ash clouds at the Canadian Meteorological Centre. Volcanic Ash and Aviation Safety: Proceedings of the First International Symposium on Volcanic Ash and Aviation Safety. Vol. 2047, pp. 325–332.

Danielsen, E.F., 1981. Trajectories of the Mount St. Helens eruption plume. Science 211 (4484), 819–821. https://doi.org/10.1126/science.211.4484.819.

Davies, D.K., Quearry, M.W., Bonis, S.B., 1978. Glowing avalanches from the 1974 eruption of the volcano Fuego, Guatemala. Geol. Soc. Am. Bull. 89 (3), 369–384. https://doi.org/10.1130/0016-7606(1978)89<369:GAFTEO>2.0.CO;2.

Dean, K., Bowling, S.A., Shaw, G., Tanaka, H., 1994. Satellite analyses of movement and characteristics of the Redoubt Volcano plume, January 8, 1990. J. Volcanol. Geotherm. Res. 62 (1–4), 339–352. https://doi.org/10.1016/0377-0273(94)90040-X.

Degruyter, W., Bonadonna, C., 2012. Improving on mass flow rate estimates of volcanic eruptions. Geophys. Res. Lett. 39 (16).

Degruyter, W., Bonadonna, C., 2013. Impact of wind on the condition for column collapse of volcanic plumes. Earth Planet. Sci. Lett. 377, 218–226.

Denniss, A.M., Harris, A.J.L., Rothery, D.A., Francis, P.W., Carlton, R.W., 1998. Satellite observations of the April 1993 eruption of Lascar volcano. Int. J. Remote Sens. 19 (5), 801–821. https://doi.org/10.1080/014311698215739.

Deruelle, B., Oscar Figueroa, A., Eduardo Medina, T., Jose Viramonte, G., Mario Maragaño, C., 1996. Petrology of pumices of April 1993 eruption of Lascar (Atacama, Chile). Terra Nova 8 (2), 191–199. https://doi.org/10.1111/j.1365-3121.1996.tb00744.x.

Devenish, B.J., 2016. Estimating the total mass emitted by the eruption of Eyjafjallajökull in 2010 using plume-rise models. J. Volcanol. Geotherm. Res. 326, 114–119.

Draxler, R.R., Hess, G.D., 1998. An overview of the HYSPLIT_4 modeling system of trajectories, dispersion, and deposition. Aust. Meteor. Mag. 47, 295–308.

Durant, A.J., Rose, W.I., 2009. Sedimentological constraints on hydrometeor-enhanced particle deposition: 1992 Eruptions of Crater Peak, Alaska. J. Volcanol. Geotherm. Res. 186 (1–2), 40–59. https://doi.org/10.1016/j.jvolgeores.2009.02.004.

Durant, A.J., Villarosa, G., Rose, W.I., Delmelle, P., Prata, A.J., Viramonte, J.G., 2012. Long-range volcanic ash transport and fallout during the 2008 eruption of Chaitén volcano, Chile. Physics Chem. Earth A/B/C 45, 50–64. https://doi.org/10.1016/j.pce.2011.09.004.

Edwards, M.J., Pioli, L., Andronico, D., Scollo, S., Ferrari, F., Cristaldi, A., 2018. Shallow factors controlling the explosivity of basaltic magmas: The 17–25 May 2016 eruption of Etna Volcano (Italy). J. Volcanol. Geotherm. Res. 357, 425–436. https://doi.org/10.1016/j.jvolgeores.2018.05.015.

Eichelberger, J., Keith, T., Miller, T., Nye, C., 1995. The 1992 eruptions of Crater Peak vent, Mount Spurr volcano, Alaska: chronology and summary. U.S. Geol. Surv. Bull. 2139, 1–18.

Ekstrand, A., Webley, P., Garay, M., Dehn, J., Prakash, A., Nelson, D., Dean, K., Steensen, T., 2013. A multi-sensor plume height analysis of the 2009 Redoubt eruption. J. Volcanol. Geotherm. Res. 259, 170–184. https://doi.org/10.1016/j.jvolgeores.2012.09.008.

Elissondo, M., Baumann, V., Bonadonna, C., Pistolesi, M., Cioni, R., Bertagnini, A., Biasse, S., Herrero, J.-C., Gonzalez, R., 2016. Chronology and impact of the 2011 Cordón Caulle eruption, Chile. Nat. Hazards Earth Syst. Sci. 16 (3), 675–704. https://doi.org/10.5194/nhess-16-675-2016.

Engwell, S.L., Sparks, R.S.J., Aspinall, W.P., 2013. Quantifying uncertainties in the measurement of tephra fall thickness. J. Appl. Volcanol. 2 (1), 5.

Engwell, S.L., Aspinall, W.P., Sparks, R.S.J., 2015. An objective method for the production of isopach maps and implications for the estimation of tephra deposit volumes and their uncertainties. Bull. Volcanol. 77 (7), 61.

Engwell, S.L., Mastin, L.G., Tupper, A., Kibler, J., Acethorp, P., Lord, G., Filgueira, R., 2021. Near-real-time volcanic cloud monitoring: insights into global explosive volcanic eruptive activity through analysis of Volcanic Ash Advisories. Bull. Volcanol. 83 (9). https://doi.org/10.1007/s00445-020-01419-y.

Eychenne, J., Le Pennec, J.L., Troncoso, L., Gouhier, M., Nedelec, J.M., 2012. Causes and consequences of bimodal grain-size distribution of tephra fall deposited during the August 2006 Tungurahua eruption (Ecuador). Bull. Volcanol. 74 (1), 187–205. https://doi.org/10.1007/s00445-011-0517-5.

Eychenne, J., Le Pennec, J.-L., Ramón, P., Yepes, H., 2013. Dynamics of explosive paroxysms at open-vent andesitic systems: high-resolution mass distribution analyses of the 2006 Tungurahua fall deposit (Ecuador). Earth Planet. Sci. Lett. 361, 343–355. https://doi.org/10.1016/j.epsl.2012.11.002.

Eychenne, J., Cashman, K., Rust, A., Durant, A., 2015. Impact of the lateral blast on the spatial pattern and grain size characteristics of the 18 May 1980 Mount St. Helens fallout deposit. J. Geophys. Res. Solid Earth 120 (9), 6018–6038. https://doi.org/10.1002/2015JB012116.

Eyring, V., Bony, S., Meehl, G.A., Senior, C.A., Stevens, B., Stouffer, R.J., Taylor, K.E., 2016a. Overview of the Coupled Model Intercomparison Project Phase 6 (CMIP6) experimental design and organization. Geosci. Model Dev. 9 (5), 1937–1958.

Eyring, V., Cox, P.M., Flato, G.M., et al., 2019. Taking climate model evaluation to the next level. Nature Clim Change 9, 102–110. https://doi.org/10.1038/s41558-018-0355-y.

Fee, D., Steffke, A., Garces, M., 2010. Characterization of the 2008 Kasatochi and Okmok eruptions using remote infrasound arrays. J. Geophys. Res.-Atmos. 115 (D2). https://doi.org/10.1029/2009JD013621.

Femina, La, Peter, C., Connor, Charles B., Hill, Brittain E., Strauch, Wilfried, Saballos, J. Armando, 2004. Magma–tectonic interactions in Nicaragua: the 1999 seismic swarm and eruption of Cerro Negro volcano. J. Volcanol. Geotherm. Res. 137 (1-3), 187–199. https://doi.org/10.1016/j.jvolgeores.2004.05.006.

Flemming, J., Inness, A., 2013. Volcanic sulfur dioxide plume forecasts based on UV satellite retrievals for the 2011 Grímsvötn and the 2010 Eyjafjallajökull eruption. J. Geophys. Res.-Atmos. 118 (17), 10–172. https://doi.org/10.1002/jgrd.50753.

Flentje, H., Claude, H., Elste, T., Gilge, S., Köhler, U., Plass-Dülmer, C., Steinbrecht, W., Thomas, W., Werner, A., Fricke, W., 2010. The Eyjafjallajökull eruption in April 2010-detection of volcanic plume using in-situ measurements, ozone sondes and lidar-ceilometer profiles. Atmos. Chem. Phys. 10 (20), 10085–10092. https://doi.org/10.5194/acp-10-10085-2010.

Folch, A., Jorba, O., Viramonte, J., 2008. Volcanic ash forecast-application to the May 2008 Chaitén eruption. Nat. Hazards Earth Syst. Sci. 8 (4), 927–940. https://doi.org/10.5194/nhess-8-927-2008.

Freret-Lorgeril, V., Donnadieu, F., Scollo, S., Provost, A., Fréville, P., Guéhenneux, Y., ... Coltelli, M., 2018. Mass Eruption Rates of Tephra Plumes During the 2011–2015 Lava Fountain Paroxysms at Mt. Etna From Doppler Radar Retrievals. Front. Earth Sci. 6, 73.

Freret-Lorgeril, V., Donnadieu, F., Eychenne, J., Soriaux, C., Latchimy, T., 2019. In situ terminal settling velocity measurements at Stromboli volcano: input from physical characterization of ash. J. Volcanol. Geotherm. Res. 374, 62–79.

Gardner, C.A., Neal, C.A., Waitt, R.B., Janda, R.J., 1994. Proximal pyroclastic deposits from the 1989–1990 eruption of Redoubt Volcano, Alaska—Stratigraphy, distribution, and physical characteristics. J. Volcanol. Geotherm. Res. 62 (1–4), 213–250. https://doi.org/10.1016/0377-0273(94)90035-3.

Gaunt, H., Bernard, B., Hidalgo, S., Proano, A., Wright, H., Mothes, P., Criollo, E., Kueppers, U., 2016. Eruptive dynamics inferred from textural analysis of ash time series: the 2015 reawakening of Cotopaxi volcano. J. Volcanol. Geotherm. Res. 328, 134–146. https://doi.org/10.1016/j.jvolgeores.2016.10.013.

Geshi, N., Oikawa, T., 2008. Phreatomagmatic eruptions associated with the caldera collapse during the Miyakejima 2000 eruption. Japan. J. Volcanol. Geotherm. Res. 176 (4), 457–468. https://doi.org/10.1016/j.jvolgeores.2008.04.013.

Gilbert, D.J., 2012. Pre-Eruptive Conditions at Lonquimay and Puyehue-Cordon Caulle Volcanoes, Chile: Framework for Tectonic Influences. Ph.D. thesis. Christian-Albrechts Universität Kiel.

Girault, F., Carazzo, G., Tait, S., Ferrucci, F., Kaminski, É., 2014. The effect of total grain-size distribution on the dynamics of turbulent volcanic plumes. Earth Planet. Sci. Lett. 394, 124–134. https://doi.org/10.1016/j.epsl.2014.03.021.

Girina, O.A., 2013. Chronology of Bezymianny volcano activity, 1956–2010. J. Volcanol. Geotherm. Res. 263, 22–41. https://doi.org/10.1016/j.jvolgeores.2013.05.002.

Global Volcanism Program, 1970. (CSLP 43-70), Hekla.

Global Volcanism Program, 1971a. Report on Cerro Negro (Nicaragua). Center for Short-Lived Phenomena, Smithsonian Institution.

Global Volcanism Program, 1971b. Report on Fuego (Guatemala). Smithsonian Institution.

Global Volcanism Program, 1971c. (CSLP 43-70), Hekla.

Global Volcanism Program, 1973. (CSLP 92-73), Report on Chachadake [Tiatia].
Global Volcanism Program, 1974. Report on Fuego (Guatemala). Center for Short-Lived Phenomena, Smithsonian Institution.
Global Volcanism Program, 1975. (March), Bulletin report on Tongariro (New Zealand).
Global Volcanism Program, 1980a. Report on Hekla (Iceland). In: Squires, D. (Ed.), Scientific Event Alert Network Bulletin, 5:8. Smithsonian Institution https://doi.org/10.5479/si.GVP.SEAN198008-372070.
Global Volcanism Program, 1980b. Report on St. Helens (United States). In: Squires, D. (Ed.), Scientific Event Alert Network Bulletin. 5:5. Smithsonian Institution.
Global Volcanism Program, 1982a. Report on El Chichon (Mexico). In: McClelland, L. (Ed.), Scientific Event Alert Network Bulletin. 7:3. Smithsonian Institution.
Global Volcanism Program, 1982b. Report on El Chichon (Mexico). In: McClelland, L. (Ed.), Scientific Event Alert Network Bulletin. 7:4. Smithsonian Institution.
Global Volcanism Program, 1984. Report on Bezymianny (Russia). In: McClelland, L. (Ed.), Scientific Event Alert Network Bulletin, 9:10. Smithsonian Institution https://doi.org/10.5479/si.GVP.SEAN198410-300250.
Global Volcanism Program, 1985a. Report on Nevado del Ruiz (Columbia). In: McClelland, L. (Ed.), Scientific Event Alert Network Bulletin. 10:11. Smithsonian Institution https://doi.org/10.5479/si.GVP.SEAN198511-351020.
Global Volcanism Program, 1985b. Report on Ruapehu (New Zealand). In: Wunderman, R. (Ed.), Bulletin of the Global Volcanism Network. 20:10 https://doi.org/10.5479/si.GVP.BGVN199510-241100 Smithsonian Institution.
Global Volcanism Program, 1986a. Report on Cerro Negro (Nicaragua). Center for Short-Lived Phenomena, Smithsonian Institution.
Global Volcanism Program, 1986b. Report on Cerro Negro (Nicaragua). Center for Short-Lived Phenomena, Smithsonian Institution.
Global Volcanism Program, 1986c. Report on Cerro Negro (Nicaragua). Center for Short-Lived Phenomena, Smithsonian Institution.
Global Volcanism Program, 1986d. Report on Chikurachki (Russia). In: McClelland, L. (Ed.), Scientific Event Alert Network Bulletin. 11:11. Smithsonian Institution.
Global Volcanism Program, 1990. Report on Kelut (Indonesia). In: McClelland, L. (Ed.), Bulletin of the Global Volcanism Network. 15:1. Smithsonian Institution.
Global Volcanism Program, 1991. Report on Cerro Hudson (Chile). In: McClelland, L. (Ed.), Bulletin of the Global Volcanism Network, 16:7 https://doi.org/10.5479/si.GVP.BGVN199107-358057 Smithsonian Institution.
Global Volcanism Program, 1992a. Report on Cerro Negro (Nicaragua). In: McClelland, L. (Ed.), Bulletin of the Global Volcanism Network. 17:3 Smithsonian Institution.
Global Volcanism Program, 1992b. Report on Cerro Negro (Nicaragua). In: McClelland, L. (Ed.), Bulletin of the Global Volcanism Network. 17:4 Smithsonian Institution.
Global Volcanism Program, 1992c. Report on Spurr (United States). In: McClelland, L. (Ed.), Bulletin of the Global Volcanism Network, 17:5 https://doi.org/10.5479/si.GVP.BGVN199205-313040 Smithsonian Institution.
Global Volcanism Program, 1993. Report on Lascar (Chile). In: Venzke, E. (Ed.), Bulletin of the Global Volcanism Network, 18:4. Smithsonian Institution https://doi.org/10.5479/si.GVP.BGVN199304-355100.
Global Volcanism Program, 1995a. Report on Cerro Negro (Nicaragua). In: Wunderman, R. (Ed.), Bulletin of the Global Volcanism Network. 20:11 Smithsonian Institution.
Global Volcanism Program, 1995b. Report on Ruapehu (New Zealand). In: Wunderman, R. (Ed.), Bulletin of the Global Volcanism Network, 20:9. Smithsonian Institution https://doi.org/10.5479/si.GVP.BGVN199509-241100.
Global Volcanism Program, 1996a. Report on Soufriere Hills (United Kingdom). In: Wunderman, R. (Ed.), Bulletin of the Global Volcanism Network, 21:9. Smithsonian Institution https://doi.org/10.5479/si.GVP.BGVN199609-360050.
Global Volcanism Program, 1996b. Report on popocatepetl (Mexico). In: Wunderman, R. (Ed.), Bulletin of the Global Volcanism Network. 21:4. Smithsonian Institution https://doi.org/10.5479/si.GVP.BGVN199604-341090.
Global Volcanism Program, 1996c. Report on Popocatepetl (Mexico). In: Wunderman, R. (Ed.), Bulletin of the Global Volcanism Network. 21:10 https://doi.org/10.5479/si.GVP.BGVN199610-341090 Smithsonian Institution.
Global Volcanism Program, 1997. Report on Popocatepetl (Mexico). In: Wunderman, R. (Ed.), Bulletin of the Global Volcanism Network. 22:7 https://doi.org/10.5479/si.GVP.BGVN199610-341090 Smithsonian Institution.
Global Volcanism Program, 1998. Report on Etna (Italy). In: Wunderman, R. (Ed.), Bulletin of the Global Volcanism Network, 23:11. Smithsonian Institution.
Global Volcanism Program, 1999a. Report on Cerro Negro (Nicaragua). In: Wunderman, R. (Ed.), Bulletin of the Global Volcanism Network, 24:11 https://doi.org/10.5479/si.GVP.BGVN199911-344070 Smithsonian Institution.
Global Volcanism Program, 1999b. Report on Shishaldin (United States). In: Wunderman, R. (Ed.), Bulletin of the Global Volcanism Network, 24:4 https://doi.org/10.5479/si.GVP.BGVN199904-311360 Smithsonian Institution.
Global Volcanism Program, 1999c. Report on Shishaldin (United States). In: Wunderman, R. (Ed.), Bulletin of the Global Volcanism Network, 24:8 https://doi.org/10.5479/si.GVP.BGVN199908-311360 Smithsonian Institution.
Global Volcanism Program, 2000a. Report on Cerro Negro (Nicaragua). In: Wunderman, R. (Ed.), Bulletin of the Global Volcanism Network, 25:5 https://doi.org/10.5479/si.GVP.BGVN200005-344070 Smithsonian Institution.
Global Volcanism Program, 2000b. Report on Miyakejima (Japan). In: Wunderman, R. (Ed.), Bulletin of the Global Volcanism Network, 25:7 https://doi.org/10.5479/si.GVP.BGVN200007-284040 Smithsonian Institution.
Global Volcanism Program, 2001. Report on Tungurahua (Ecuador). In: Wunderman, R. (Ed.), Bulletin of the Global Volcanism Network, 26:7 https://doi.org/10.5479/si.GVP.BGVN200107-352080 Smithsonian Institution.
Global Volcanism Program, 2002. Report on Reventador (Ecuador). In: Wunderman, R. (Ed.), Bulletin of the Global Volcanism Network. 27:11 https://doi.org/10.5479/si.GVP.BGVN200211-352010 Smithsonian Institution.
Global Volcanism Program, 2003a. Report on Anatahan (United States). In: Venzke, E. (Ed.), Bulletin of the Global Volcanism Network. 28:5 Smithsonian Institution.
Global Volcanism Program, 2003b. Report on Anatahan (United States). In: Venzke, E. (Ed.), Bulletin of the Global Volcanism Network. 28:5 Smithsonian Institution.
Global Volcanism Program, 2003c. Report on Stromboli (Italy). In: Venzke, E. (Ed.), Bulletin of the Global Volcanism Network, 28:4 https://doi.org/10.5479/si.GVP.BGVN200304-211040 Smithsonian Institution.
Global Volcanism Program, 2005. Report on Bezymianny (Russia). In: Wunderman, R. (Ed.), Bulletin of the Global Volcanism Network, 30:3. Smithsonian Institution https://doi.org/10.5479/si.GVP.BGVN200503-300250.
Global Volcanism Program, 2006a. Report on Augustine (United States). In: Wunderman, R. (Ed.), Bulletin of the Global Volcanism Network, 31:1 https://doi.org/10.5479/si.GVP.BGVN200601-313010 Smithsonian Institution.
Global Volcanism Program, 2006b. Report on Bezymianny (Russia). In: Wunderman, R. (Ed.), Bulletin of the Global Volcanism Network, 31:11 https://doi.org/10.5479/si.GVP.BGVN200611-300250 Smithsonian Institution.
Global Volcanism Program, 2006c. Report on Tungurahua (Ecuador). In: Wunderman, R. (Ed.), Bulletin of the Global Volcanism Network, 31:7 https://doi.org/10.5479/si.GVP.BGVN200607-352080 Smithsonian Institution.
Global Volcanism Program, 2008a. Report on Chaiten (Chile). In: Wunderman, R. (Ed.), Bulletin of the Global Volcanism Network, 33:4 https://doi.org/10.5479/si.GVP.BGVN200804-358041 Smithsonian Institution.
Global Volcanism Program, 2008b. Report on Kasatochi (United States). In: Wunderman, R. (Ed.), Bulletin of the Global Volcanism Network, 33:7 https://doi.org/10.5479/si.GVP.BGVN200807-311130 Smithsonian Institution.
Global Volcanism Program, 2009. Report on Bezymianny (Russia). In: Wunderman, R. (Ed.), Bulletin of the Global Volcanism Network, 34:11 Smithsonian Institution.
Global Volcanism Program, 2011. Report on Merapi (Indonesia). In: Wunderman, R. (Ed.), Bulletin of the Global Volcanism Network. 36:1 Smithsonian Institution.
Global Volcanism Program, 2014. Report on Kelut (Indonesia). In: Wunderman, R. (Ed.), Bulletin of the Global Volcanism Network, 39:2 https://doi.org/10.5479/si.GVP.BGVN201402-263280 Smithsonian Institution.
Global Volcanism Program, 2015a. Report on Calbuco (Chile). In: Venzke, E. (Ed.), Bulletin of the Global Volcanism Network, 40:6 https://doi.org/10.5479/si.GVP.BGVN201506-358020 Smithsonian Institution.
Global Volcanism Program, 2015b. Report on Ontakesan (Japan). In: Wunderman, R. (Ed.), Bulletin of the Global Volcanism Network, 40:3 https://doi.org/10.5479/si.GVP.BGVN201503-283040 Smithsonian Institution.
Global Volcanism Program, 2016a. Report on Cotopaxi (Ecuador). In: Venzke, E. (Ed.), Bulletin of the Global Volcanism Network. 41:4 Smithsonian Institution.
Global Volcanism Program, 2016b. Report on Villarrica (Chile). In: Crafford, A.E., Venzke, E. (Eds.), Bulletin of the Global Volcanism Network, 41:11 https://doi.org/10.5479/si.GVP.BGVN201611-357120 Smithsonian Institution.
Global Volcanism Program, 2017a. Report on Asosan (Japan). In: Crafford, A.E., Venzke, E. (Eds.), Bulletin of the Global Volcanism Network, 42:5. Smithsonian Institution https://doi.org/10.5479/si.GVP.BGVN201705-282110.
Global Volcanism Program, 2017b. Report on Etna (Italy). In: Crafford, A.E., Venzke, E. (Eds.), Bulletin of the Global Volcanism Network, 42:9. Smithsonian Institution https://doi.org/10.5479/si.GVP.BGVN201709-211060.
Global Volcanism Program, 2017c. Report on Tungurahua (Ecuador). In: Crafford, A.E., Venzke, E. (Eds.), Bulletin of the Global Volcanism Network, 42:5 https://doi.org/10.5479/si.GVP.BGVN201705-352080 Smithsonian Institution.
Global Volcanism Program, 2017d. Report on Tungurahua (Ecuador). In: Crafford, A.E., Venzke, E. (Eds.), Bulletin of the Global Volcanism Network, 42:5 https://doi.org/10.5479/si.GVP.BGVN201705-352080 Smithsonian Institution.
Gorshkov, G.S., 1959. Gigantic eruption of the volcano Bezymianny. Bull. Volcanol. 20 (1), 77–109. https://doi.org/10.1007/BF02596572.
Gouhier, M., Donnadieu, F., 2008. Mass estimations of ejecta from Strombolian explosions by inversion of Doppler radar measurements. J. Geophys. Res. Solid Earth 113 (B10).
Gouhier, M., Eychenne, J., Azzaoui, N., Guillin, A., Deslandes, M., Poret, M., Costa, A., Husson, P., 2019. Low efficiency of large volcanic eruptions in transporting very fine ash into the atmosphere. Sci. Rep. 9 (1), 1–12.
Gouhier, M., Deslandes, M., Guéhenneux, Y., Hereil, P., Cacault, P., Josse, B., 2020. Operational response to volcanic ash risks using HOTVOLC satellite-based system and MOCAGE-accident model at the Toulouse VAAC. Atmosphere 11 (8), 864.
Gronvold, K., Larsen, G., Einarsson, P., Thorarinsson, S., Saemundsson, K., 1983. The Hekla eruption 1980–1981. Bull. Volcanol. 46 (4), 349–363. https://doi.org/10.1007/BF02597770.
Gudmundsson, A., Oskarsson, N., Gronvold, K., Saemundsson, K., Sigurdsson, O., Stefansson, R., Gislason, S.R., Einarsson, P., Brandsdottir, B., Larsen, G., et al., 1992. The 1991 eruption of Hekla, Iceland. Bull. Volcanol. 54 (3), 238–246. https://doi.org/10.1007/BF00278391.
Gudmundsson, M.T., Thordarson, T., Höskuldsson, Á., Larsen, G., Björnsson, H., Prata, F.J., Oddsson, B., Magnússon, E., Högnadóttir, T., Petersen, G.N., et al., 2012. Ash generation and distribution from the April–May 2010 eruption of Eyjafjallajökull, Iceland. Sci. Rep. 2. https://doi.org/10.1038/srep00572.
Gudnason, J., Thordarson, T., Houghton, B.F., Larsen, G., 2017. The opening subplinian phase of the Hekla 1991 eruption: properties of the tephra fall deposit. Bull. Volcanol. 79 (5), 34. https://doi.org/10.1007/s00445-017-1118-8.
Guffanti, M., Ewert, J.W., Gallina, G.M., Bluth, G.J., Swanson, G.L., 2005. Volcanic-ash hazard to aviation during the 2003–2004 eruptive activity of Anatahan volcano, Commonwealth of the Northern Mariana Islands. J. Volcanol. Geotherm. Res. 146 (1–3), 241–255. https://doi.org/10.1016/j.jvolgeores.2004.12.011.
Gunn, L.S., Blake, S., Jones, M.C., Rymer, H., 2014. Forecasting the duration of volcanic eruptions: an empirical probabilistic model. Bull. Volcanol. 76 (1), 780.

Guo, S., Bluth, G.J., Rose, W.I., Watson, I.M., Prata, A.J., 2004a. Re-evaluation of SO2 release of the 15 June 1991 Pinatubo eruption using ultraviolet and infrared satellite sensors. Geochem. Geophys. Geosyst. 5 (4). https://doi.org/10.1029/2003GC000654.

Guo, S., Rose, W.I., Bluth, G.J., Watson, I.M., 2004b. Particles in the great Pinatubo volcanic cloud of June 1991: the role of ice. Geochem. Geophys. Geosyst. 5 (5). https://doi.org/10.1029/2003GC000655.

Gurenko, A., Belousov, A., Trumbull, R., Sobolev, A., 2005. Explosive basaltic volcanism of the Chikurachki volcano (Kurile arc, Russia): insights on pre-eruptive magmatic conditions and volatile budget revealed from phenocryst-hosted melt inclusions and groundmass glasses. J. Volcanol. Geotherm. Res. 147 (3), 203–232. https://doi.org/10.1016/j.jvolgeores.2005.04.002.

Hadikusumo, D., 1961. Report of the volcanological research and volcanic activity in Indonesia for the period 1950–1957. Bull Volcanol Surv Indonesia, Bandung, No 100:122 p.

Hall, M., Ramón, P., Mothes, P., LePennec, J., García, A., Samaniego, P., Yepes, H., 2004. Volcanic eruptions with little warning: the case of Volcán Reventador's Surprise November 3, 2002 Eruption. Ecuador. Rev. Geol. Chile 31 (2), 349–358. https://doi.org/10.4067/S0716-02082004000200010.

Hall, M., Steele, A., Mothes, P., Ruiz, M., 2013. Pyroclastic density currents (PDC) of the 16–17 August 2006 eruptions of Tungurahua volcano, Ecuador: geophysical registry and characteristics. J. Volcanol. Geotherm. Res. 265, 78–93.

Hall, M.L., Steele, A.L., Bernard, B., Mothes, P.A., Vallejo, S.X., Douillet, G.A., ... Ruiz, M.C., 2015. Sequential plug formation, disintegration by Vulcanian explosions, and the generation of granular Pyroclastic Density Currents at Tungurahua volcano (2013–2014), Ecuador. J. Volcanol. Geotherm. Res. 306, 90–103. https://doi.org/10.1016/j.jvolgeores.2015.09.009.

Hargie, K.A., Van Eaton, A.R., Mastin, L.G., Holzworth, R.H., Ewert, J.W., Pavolonis, M., 2019. Globally detected volcanic lightning and umbrella dynamics during the 2014 eruption of Kelud, Indonesia. J. Volcanol. Geotherm. Res. 382, 81–91.

Harris, D.M., Rose, W., Roe, R., Thompson, M., Lipman, P., Mullineaux, D., 1981. Radar observations of ash eruptions. US Geol. Surv. Prof. Pap. 1250, 323–333.

Hashimoto, A., Shimbori, T., Fukui, K., 2012. Tephra fall simulation for the eruptions at Mt. Shinmoe-dake during 26–27 January 2011 with JMANHM. Sola 8, 37–40. https://doi.org/10.2151/sola.2012-010.

Hayer, C., Carboni, E., Ventress, L., Povey, A., Grainger, R., 2016. Satellite observations of the volcanic plume from the 23rd April 2015 eruption of Calbuco volcano. EGU General Assembly Conference Abstracts. vol. 18, p. 17035. http://adsabs.harvard.edu/abs/2016EGUGA.1817035H.

Heffter, J.L., Stunder, B.J., 1993. Volcanic ash forecast transport and dispersion (VAFTAD) model. Weather Forecast. 8 (4), 533–541.

Hersbach, H., Bell, B., Berrisford, P., Hirahara, S., Horányi, A., Muñoz-Sabater, J., ... Simmons, A., 2020. The ERA5 global reanalysis. Q. J. R. Meteorol. Soc. 146 (730), 1999–2049.

Hess, K.-U., Dingweil, D.B., Webb, S.L., 1995. The influence of excess alkalis on the viscosity of a haplogranitic melt. Am. Mineral. 80 (3–4), 297–304. https://doi.org/10.2138/am-1995-3-412.

Hildreth, W., Drake, R., 1992. Volcán Quizapu, Chilean Andes. Bull. Volcanol. 54 (2), 93–125. https://doi.org/10.1007/BF00278002.

Hill, B.E., Connor, C.B., Jarzemba, M.S., La Femina, P.C., Navarro, M., Strauch, W., 1998. 1995 eruptions of Cerro Negro volcano, Nicaragua, and risk assessment for future eruptions. Geol. Soc. Am. Bull. 110 (10), 1231–1241 10.1130/0016-7606(1998)110<1231:EOCNVN>2.3.CO;2.

Hoblitt, R., Wolfe, E., Scott, W., Couchman, M., Pallister, J., Javier, D., 1996. The preclimactic eruptions of Mount Pinatubo, June 1991. Fire and Mud: Eruptions and Lahars of Mount Pinatubo. Philippine Institute of Volcanology and Seismology and University of Washington, Philippines, pp. 457–511.

Holasek, R., Self, S., Woods, A., 1996. Satellite observations and interpretation of the 1991 Mount Pinatubo eruption plumes. J. Geophys. Res. Solid Earth 101 (B12), 27635–27655. https://doi.org/10.1029/96JB01179.

Höskuldsson, Á., Óskarsson, N., Pedersen, R., Grönvold, K., Vogfjörð, K., Ólafsdóttir, R., 2007. The millennium eruption of Hekla in February 2000. Bull. Volcanol. 70 (2), 169–182. https://doi.org/10.1007/s00445-007-0128-3.

Höskuldsson, Á., Janebo, M., Thordarson, T., Andrésdóttir, T.B., Jónsdóttir, I., Guðnason, J., ... Magnúsdóttir, A.Ö., 2018. Total grain size distribution in selected Icelandic eruptions. Retrieved May 20, 2018. http://islenskeldfjoll.is/data/Gosva/Total_Grain_Size_Distribution_in_Selected_Icelandic_Eruptions_01.pdf.

Hreinsdóttir, S., Sigmundsson, F., Roberts, M.J., Björnsson, H., Grapenthin, R., Arason, P., Árnadóttir, T., Hólmjárn, J., Geirsson, H., Bennett, R.A., et al., 2014. Volcanic plume height correlated with magma-pressure change at Grimsvotn volcano. Iceland. Nat. Geosci. 7 (3), 214–218. https://doi.org/10.1038/ngeo2044.

Hurst, A., Turner, R., 1999. Performance of the program ASHFALL for forecasting ashfall during the 1995 and 1996 eruptions of Ruapehu volcano. N. Z. J. Geol. Geophys. 42 (4), 615–622. https://doi.org/10.1080/00288306.1999.9514865.

Hyman, D.M., Bursik, M.I., Legorreta Paulín, G., 2018. Time dependence of passive degassing at Volcán Popocatépetl, Mexico, from infrared measurements: implications for gas pressure distribution and lava dome stability. J. Geophys. Res. Solid Earth 123 (10), 8527–8547.

IAVCEI commission on tephra hazard modelling database. http://www2.ct.ingv.it/iavcei/index.htm.

Izbekov, P., Sisson, T., Wooden, J., Bacon, C., 2009. 2008 Kasatochi Eruption: SHRIMP constraints on concentration of volatiles in melt inclusions. AGU Fall Meeting Abstracts. vol. 1, p. 1775. http://adsabs.harvard.edu/abs/2009AGUFM.V51E1775I.

Jay, J., Costa, F., Pritchard, M., Lara, L.E., Singer, B., Herrin, J., 2014. Locating magma reservoirs using InSAR and petrology before and during the 2011–2012 Cordón Caulle silicic eruption, Earth Planet. Sci. Lett. 395, 254–266.

Jenkins, S., McAneney, J., Magill, C., Blong, R., 2012. Regional ash fall hazard II: Asia-Pacific modelling results and implications. Bull. Volcanol. 74 (7), 1713–1727.

Jessop, D.E., Gilchrist, J., Jellinek, A.M., Roche, O., 2016. Are eruptions from linear fissures and caldera ring dykes more likely to produce pyroclastic flows? Earth Planet. Sci. Lett. 454, 142–153.

Jude-Eton, T., Thordarson, T., Gudmundsson, M., Oddsson, B., 2012. Dynamics, stratigraphy and proximal dispersal of supraglacial tephra during the ice-confined 2004 eruption at Grímsvötn volcano, Iceland. Bull. Volcanol. 74 (5), 1057–1082. https://doi.org/10.1007/s00445-012-0583-3.

Kalnay, E., Kanamitsu, M., Kistler, R., Collins, W., Deaven, D., Gandin, L., ... Zhu, Y., 1996. The NCEP/NCAR 40-year reanalysis project. Bull. Am. Meteorol. Soc. 77 (3), 437–472.

Kaneko, T., Maeno, F., Nakada, S., 2016. 2014 Mount Ontake eruption: characteristics of the phreatic eruption as inferred from aerial observations. Earth Planets Space 68 (1), 1–11. https://doi.org/10.1186/s40623-016-0452-y.

Kilgour, G., Blundy, J., Cashman, K., Mader, H., 2013. Small volume andesite magmas and melt-mush interactions at Ruapehu, New Zealand: evidence from melt inclusions. Contrib. Mineral. Petrol. 166 (2), 371–392. https://doi.org/10.1007/s00410-013-0880-7.

Klawonn, M., Houghton, B.F., Swanson, D.A., Fagents, S.A., Wessel, P., Wolfe, C.J., 2014a. Constraining explosive volcanism: subjective choices during estimates of eruption magnitude. Bull. Volcanol. 76 (2), 793.

Klawonn, M., Houghton, B.F., Swanson, D.A., Fagents, S.A., Wessel, P., Wolfe, C.J., 2014b. From field data to volumes: constraining uncertainties in pyroclastic eruption parameters. Bull. Volcanol. 76 (7), 839.

Koyaguchi, T., 1996. Volume estimation of tephra-fall deposits from the June 15, 1991, eruption of Mount Pinatubo by theoretical and geological methods. Fire and Mud: Eruptions and Lahars of Mount Pinatubo. Philippines University of Washington Press, Seattle, pp. 583–600.

Koyaguchi, T., Ohno, M., 2001. Reconstruction of eruption column dynamics on the basis of grain size of tephra fall deposits: 2. Application to the Pinatubo 1991 eruption. J. Geophys. Res. Solid Earth 106 (B4), 6513–6533. https://doi.org/10.1029/2000JB900427.

Koyaguchi, T., Suzuki, Y.J., 2018. The condition of eruption column collapse: 1. A reference model based on analytical solutions. J. Geophys. Res. Solid Earth 123 (9), 7461–7482.

Koyaguchi, T., Suzuki, Y.J., Takeda, K., Inagawa, S., 2018. The condition of eruption column collapse: 2. Three-dimensional numerical simulations of eruption column dynamics. J. Geophys. Res. Solid Earth 123 (9), 7483–7508.

Kozono, T., Ueda, H., Ozawa, T., Koyaguchi, T., Fujita, E., Tomiya, A., Suzuki, Y., 2013. Magma discharge variations during the 2011 eruptions of Shinmoe-dake volcano, Japan, revealed by geodetic and satellite observations. Bull. Volcanol. 75 (3), 695. https://doi.org/10.1007/s00445-013-0695-4.

Kratzmann, D.J., Carey, S., Scasso, R., Naranjo, J.-A., 2009. Compositional variations and magma mixing in the 1991 eruptions of Hudson volcano, Chile. Bull. Volcanol. 71 (4), 419. https://doi.org/10.1007/s00445-008-0234-x.

Kratzmann, D.J., Carey, S.N., Fero, J., Scasso, R.A., Naranjo, J.-A., 2010. Simulations of tephra dispersal from the 1991 explosive eruptions of Hudson volcano, Chile. J. Volcanol. Geotherm. Res. 190 (3), 337–352. https://doi.org/10.1016/j.jvolgeores.2009.11.021.

Kristiansen, N.I., Stohl, A., Prata, A.J., Richter, A., Eckhardt, S., Seibert, P., ... Stebel, K., 2010. Remote sensing and inverse transport modeling of the Kasatochi eruption sulfur dioxide cloud. J. Geophys. Res.-Atmos. 115 (D2). https://doi.org/10.1029/2009JD013286.

Kristiansen, N.I., Prata, A.J., Stohl, A., Carn, S.A., 2015. Stratospheric volcanic ash emissions from the 13 February 2014 Kelut eruption. Geophys. Res. Lett. 42 (2), 588–596. https://doi.org/10.1002/2014GL062307.

Krotkov, N., Torres, O., Seftor, C., Krueger, A., Kostinski, A., Rose, W., Bluth, G., Schneider, D., Schaefer, S., 1999. Comparison of TOMS and AVHRR volcanic ash retrievals from the August 1992 eruption of Mt. Spurr. Geophys. Res. Lett. 26 (4), 455–458. https://doi.org/10.1029/1998GL900278.

Krueger, A., Walter, L., Schnetzler, C., Doiron, S., 1990. TOMS measurement of the sulfur dioxide emitted during the 1985 Nevado del Ruiz eruptions. J. Volcanol. Geotherm. Res. 41 (1–4), 7–15. https://doi.org/10.1016/0377-0273(90)90081-P.

Krueger, A., Krotkov, N., Carn, S., 2008. El Chichon: the genesis of volcanic sulfur dioxide monitoring from space. J. Volcanol. Geotherm. Res. 175 (4), 408–414. https://doi.org/10.1016/j.jvolgeores.2008.02.026.

Kylling, A., 2016. Ash and ice clouds during the Mt Kelud February 2014 eruption as interpreted from IASI and AVHRR/3 observations. Atmos. Meas. Tech. 9 (5), 2103–2117. https://doi.org/10.5194/amt-9-2103-2016.

La Spina, G., Burton, M., M. de' Micheili Vitturi, Sept. 2015. Temperature evolution during magma ascent in basaltic effusive eruptions: a numerical application to Stromboli volcano. Earth Planet. Sci. Lett. 426, 89–100. https://doi.org/10.1016/j.epsl.2015.06.015.

Lacasse, C., Karlsdóttir, S., Larsen, G., Soosalu, H., Rose, W.I., Ernst, G.G.J., 2004. Weather radar observations of the Hekla 2000 eruption cloud, Iceland. Bull. Volcanol. 66 (5), 457–473. https://doi.org/10.1007/s00445-003-0329-3.

Lara, L.E., 2010. The 2008 eruption of the chaitén volcano, Chile: a preliminary report. Andean Geol. 36 (1), 125–130. https://doi.org/10.5027/andgeoV36n1-a09.

Larsen, J., Sliwinski, M., Nye, C., Cameron, C., Schaefer, J., 2013. The 2008 eruption of Okmok Volcano, Alaska: petrological and geochemical constraints on the subsurface magma plumbing system. J. Volcanol. Geotherm. Res. 264, 85–106. https://doi.org/10.1016/j.jvolgeores.2013.07.003.

Larsen, J., Neal, C., Webley, P., Freymueller, J., Haney, M., McNutt, S., Schneider, D., et al., 2009. Eruption of Alaska volcano breaks historic pattern. Eos. Trans. AGU 90 (20), 173–174.

Larsen, J., Schaefer, J., Neal, C., Kaufman, A., Lu, Z., 2015. The 2008 phreatomagmatic eruption of Okmok Volcano, Aleutian Islands, Alaska: chronology, deposits, and landform changes. Technical Report. Alaska Division of Geological and Geophysical Surveys.

Le Pennec, J.-L., Mothes, P., Hall, M., Ramon, P., Ruiz, G., 2002. Maximum and minimum volume estimates of an ash fall layer from the August 2001 eruption of Mt Tungurahua (Ecuador). pp. 371–374.
Le Pennec, J.-L., Ruiz, G., Ramon, P., Palacios, E., Mothes, P., Yepes, H., 2012. Impact of tephra falls on Andean communities: the influences of eruption size and weather conditions during the 1999–2001 activity of Tungurahua volcano, Ecuador. J. Volcanol. Geotherm. Res. 217, 91–103. https://doi.org/10.1016/j.jvolgeores.2011.06.011.
Lucic, G., Berg, A.-S., Stix, J., 2016. Water-rich and volatile-undersaturated magmas at Hekla volcano, Iceland. Geochem. Geophys. Geosyst. 17 (8), 3111–3130. https://doi.org/10.1002/2016GC006336.
Luhr, J.F., Carmichael, I.S., Varekamp, J.C., 1984. The 1982 eruptions of El Chichón volcano, Chiapas, Mexico: mineralogy and petrology of the anhydritebearing pumices. J. Volcanol. Geotherm. Res. 23 (1–2), 69–108. https://doi.org/10.1016/0377-0273(84)90057-X.
Luigi Lodato e Boris Behncke, 2006. Aggiornamento attività Etna: Osservazioni dall'elicottero della Protezione Civile Nazionale (24 Novembre 2006, ore 14,30). http://sowebapp.ct.ingv.it/oldweb/Report/RPTVGFTR20061124_1430.pdf.
Lynch, J.S., Stephens, G., Matson, M., 1996. Mount Pinatubo: a satellite perspective of the June 1991 eruptions. Fire and Mud: The Eruptions and Lahars of Mount Pinatubo, Philippines. University of Washington Press, Seattle, pp. 637–646.
Maeno, F., Nagai, M., Nakada, S., Burden, R., Engwell, S., Suzuki, Y., Kaneko, T., 2014. Constraining tephra dispersion and deposition from three subplinian explosions in 2011 at Shinmoedake volcano, Kyushu, Japan. Bull. Volcanol. 76 (6), 823. https://doi.org/10.1007/s00445-014-0823-9.
Maeno, F., Nakada, S., Oikawa, T., Yoshimoto, M., Komori, J., Ishizuka, Y., ... Nagai, M., 2016. Reconstruction of a phreatic eruption on 27 September 2014 at Ontake volcano, central Japan, based on proximal pyroclastic density current and fallout deposits. Earth Planets Space 68 (1), 82. https://doi.org/10.1186/s40623-016-0449-6.
Maeno, F., Nakada, S., Yoshimoto, M., Shimano, T., Hokanishi, N., Zaennudin, A., Iguchi, M., 2019. A sequence of a plinian eruption preceded by dome destruction at Kelud volcano, Indonesia, on February 13, 2014, revealed from tephra fallout and pyroclastic density current deposits. J. Volcanol. Geotherm. Res. 382, 24–41. https://doi.org/10.1016/j.jvolgeores.2017.03.002.
Major, J.J., Lara, L.E., 2013. Overview of Chaitén volcano, Chile, and its 2008–2009 eruption. Andean Geol. 40 (2), 196–215. https://doi.org/10.5027/andgeoV40n2-a01.
Malik, N., 2011. The December 24, 2006 eruption of Bezymyannyi volcano, Kamchatka. J. Volcanol. Seismol. 5 (4), 268. https://doi.org/10.1134/S0742046311040051.
Mankowski, L., Riley, C., Rose, W., McGimsey, R., Ernst, G., 2001. Mapping ash grainsize distribution from the August 18, 1992 eruption of Mt. Spurr, AGU Fall Meeting Abstracts.
Marchese, F., Falconieri, A., Pergola, N., Tramutoli, V., 2014. A retrospective analysis of the Shinmoedake (Japan) eruption of 26–27 January 2011 by means of Japanese geostationary satellite data. J. Volcanol. Geotherm. Res. 269, 1–13. https://doi.org/10.1016/j.jvolgeores.2013.10.011.
Martin-Del Pozzo, A., González-Morán, T., Espinasa-Perena, R., Butron, M., Reyes, M., 2008. Characterization of the recent ash emissions at Popocatepetl Volcano, Mexico. J. Volcanol. Geotherm. Res. 170 (1), 61–75. https://doi.org/10.1016/j.jvolgeores.2007.09.004.
Marzano, F.S., Lamantea, M., Montopoli, M., Herzog, M., Graf, H., Cimini, D., 2013. Microwave remote sensing of the 2011 plinian eruption of the Grímsvötn Icelandic volcano. Remote Sens. Environ. 129, 168–184. https://doi.org/10.1016/j.rse.2012.11.005.
Marzano, Frank S., et al., 2016. Near-real-time detection of tephra eruption onset and mass flow rate using microwave weather radar and infrasonic arrays. IEEE Transactions on Geoscience and Remote Sensing https://doi.org/10.1109/TGRS.2016.2578282 n° 99.
Marzano, F.S., Mereu, L., Scollo, S., Donnadieu, F., Bonadonna, C., 2019. Tephra mass eruption rate from ground-based X-band and L-band microwave radars during the November 23, 2013, Etna Paroxysm. IEEE Trans. Geosci. Remote Sens. 58 (5), 3314–3327.
Marzano, et al., 2020. IEEE. Trans. Geosci. Remote Sens. 2020 58 (5), 3314–3327 8939354.
Mastin, L.G., 2007. A user-friendly one-dimensional model for wet volcanic plumes. Geochem. Geophys. Geosyst. 8 (3). https://doi.org/10.1029/2006GC001455.
Mastin, L.G., 2014. Testing the accuracy of a 1-D volcanic plume model in estimating mass eruption rate. J. Geophys. Res.-Atmos. 119 (5), 2474–2495.
Mastin, L.G., Guffanti, M., Servranckx, R., Webley, P., Barsotti, S., Dean, K., ... Schneider, D., 2009. A multidisciplinary effort to assign realistic source parameters to models of volcanic ash-cloud transport and dispersion during eruptions. J. Volcanol. Geotherm. Res. 186 (1-2), 10–21.
Mastin, L.G., Bonadonna, C., Folch, A., Webley, P., Stunder, B., Pavolonis, M., 2013a. Eruption data for ash-cloud model validation. https://vhub.org/resources/2431.
Mastin, L.G., Schwaiger, H., Schneider, D.J., Wallace, K.L., Schaefer, J., Denlinger, R.P., 2013b. Injection, transport, and deposition of tephra during event 5 at Redoubt Volcano, 23March, 2009. J. Volcanol. Geotherm. Res. 259, 201–213. https://doi.org/10.1016/j.jvolgeores.2012.04.025.
Matoza, R.S., Hedlin, M.A., Garcés, M.A., 2007. An infrasound array study of Mount St. Helens. J. Volcanol. Geotherm. Res. 160 (3), 249–262. https://doi.org/10.1016/j.jvolgeores.2006.10.006.
Matson, M., 1984. The 1982 El Chichon volcano eruptions-a satellite perspective. J. Volcanol. Geotherm. Res. 23 (1–2), 1–10. https://doi.org/10.1016/0377-0273(84)90054-4.
McCarthy, E.B., Bluth, G.J.S., Watson, I.M., Tupper, A., 2008. Detection and analysis of the volcanic clouds associated with the 18 and 28 August 2000 eruptions of Miyakejima volcano, Japan. Int. J. Remote Sens. 29 (22), 6597–6620. https://doi.org/10.1080/01431160802168400.
Meinel, M.P., Meinel, A.B., 1963. Late twilight glow of the ash stratum from the eruption of Agung volcano. Science 142 (3592), 582–583. https://doi.org/10.1126/science.142.3592.582.
Melson, W., Allan, J., Jerez, D., Nelen, J., Calvache, M., Williams, S., Fournelle, J., Perfit, M., 1990. Water contents, temperatures and diversity of the magmas of the catastrophic eruption of Nevado del Ruiz, Colombia, November 13, 1985. J. Volcanol. Geotherm. Res. 41 (1–4), 97–126. https://doi.org/10.1016/0377-0273(90)90085-T.
Métrich, N., Allard, P., Spilliaert, N., Andronico, D., Burton, M., 2004. 2001 flank eruption of the alkali-and volatile-rich primitive basalt responsible for Mount Etna's evolution in the last three decades. Earth Planet. Sci. Lett. 228 (1), 1–17. https://doi.org/10.1016/j.epsl.2004.09.036.
Métrich, N., Bertagnini, A., Landi, P., Rosi, M., Belhadj, O., 2005. Triggering mechanism at the origin of paroxysms at Stromboli (Aeolian Archipelago, Italy): the 5 April 2003 eruption. Geophys. Res. Lett. 32 (10). https://doi.org/10.1029/2004GL022257.
Michaud-Dubuy, A., Carazzo, G., Kaminski, E., Girault, F., 2018. A revisit of the role of gas entrapment on the stability conditions of explosive volcanic columns. J. Volcanol. Geotherm. Res. 357, 349–361.
Michaud-Dubuy, A., Carazzo, G., Kaminski, E., 2020. Wind entrainment in jets with reversing buoyancy: implications for volcanic plumes. J. Geophys. Res. Solid Earth 125. https://doi.org/10.1029/2020JB020136 e2020JB020136.
Miller, T., Chouet, B., 1994. The 1989–1990 eruptions of Redoubt Volcano: an introduction. J. Volcanol. Geotherm. Res. 62 (1–4), 1–10. https://doi.org/10.1016/0377-0273(94)90025-6.
Miller, T.P., Neal, C.A., Waitt, R.B., 1995. Pyroclastic flows of the 1992 Crater Peak eruptions: distribution and origin. The 1992 Eruptions Of Crater Peak Vent, Mt. Spurr Volcano, Alaska. 2139 pp. 81–87.
Miyabuchi, Y., Iizuka, Y., Hara, C., Yokoo, A., Ohkura, T., 2018. The September 14, 2015 phreatomagmatic eruption of Nakadake first crater, Aso Volcano, Japan: eruption sequence inferred from ballistic, pyroclastic density current and fallout deposits. J. Volcanol. Geotherm. Res. 351, 41–56. https://doi.org/10.1016/j.jvolgeores.2017.12.009.
Moiseenko, K., Malik, N., 2014. Estimates of total ash content from 2006 and 2009 explosion events at Bezymianny volcano with use of a regional atmospheric modeling system. J. Volcanol. Geotherm. Res. 270, 53–75. https://doi.org/10.1016/j.jvolgeores.2013.11.016.
Moiseenko, K., Malik, N., 2015. Reconstruction of the ashfall at Bezymyanny volcano during the eruption of December 24, 2006 by using a mesoscale model of the atmospheric transport of ash particles. Izv. Atmos. Oceanic Phys. 51 (6), 585–598. https://doi.org/10.1134/S0001433815050072.
Montalbano, S., Namur, O., Schiano, P., Bolle, O., Vander Auwera, J., 2017. Magma storage conditions and processes at Calbuco volcano (Central Southern Volcanic Zone, Chile). Goldschmidt 2017 conference abstract. https://orbi.uliege.be/bitstream/2268/212144/1/Goldschmidt2017_VF1.pdf.
Morton, B.R., Taylor, Geoffrey Ingram, Turner, John Stewart, 1956. Turbulent gravitational convection from maintained and instantaneous sources. Proceedings of the Royal Society of London. Series A. Mathematical and Physical Sciences 234.1196. pp. 1–23.
Mossop, S., 1964. Volcanic dust collected at an altitude of 20 km. Nature 203 (4947), 824–827. https://doi.org/10.1038/203824a0.
Moune, S., Sigmarsson, O., Thordarson, T., Gauthier, P.-J., 2007. Recent volatile evolution in the magmatic system of Hekla volcano. Iceland. Earth Planet. Sci. Lett. 255 (3), 373–389. https://doi.org/10.1016/j.epsl.2006.12.024.
Moxey, L., 2005. A Complete Space-Based Synopsis of Eruption Dynamics: The 2002 Eruption of Reventador Volcano Ecuador. Master's thesis.
Murrow, P., Rose, W., Self, S., 1980. Determination of the total grain size distribution in a vulcanian eruption column, and its implications to stratospheric aerosol perturbation. Geophys. Res. Lett. 7 (11), 893–896. https://doi.org/10.1029/GL007i011p00893.
Myers, M., Geist, D., Rowe, M., Harpp, K., Wallace, P., Dufek, J., 2014. Replenishment of volatile-rich mafic magma into a degassed chamber drives mixing and eruption of Tungurahua volcano. Bull. Volcanol. 76 (11), 872. https://doi.org/10.1007/s00445-014-0872-0.
Nairn, I.A., Self, S., 1978. Explosive eruptions and pyroclastic avalanches from Ngauruhoe in February 1975. J. Volcanol. Geotherm. Res. 3 (1–2), 39–60. https://doi.org/10.1016/0377-0273(78)90003-3.
Nakada, S., Matsushima, T., Yoshimoto, M., Sugimoto, T., Kato, T., Watanabe, T., Chong, R., Camacho, J.T., 2005a. Geological aspects of the 2003–2004 eruption of Anatahan volcano, Northern Mariana Islands. J. Volcanol. Geotherm. Res. 146 (1), 226–240. https://doi.org/10.1016/j.jvolgeores.2004.10.023.
Nakada, S., Nagai, M., Kaneko, T., Nozawa, A., Suzuki-Kamata, K., 2005b. Chronology and products of the 2000 eruption of Miyakejima volcano, Japan. Bull. Volcanol. 67 (3), 205–218. https://doi.org/10.1007/s00445-004-0404-4.
Nakada, S., Nagai, M., Kaneko, T., Suzuki, Y., Maeno, F., 2013. The outline of the 2011 eruption at Shinmoe-dake (Kirishima), Japan. Earth Planets Space 65 (6), 475–488. https://doi.org/10.5047/eps.2013.03.016.
Nakagawa, M., Ishizuka, Y., Kudo, T., Yoshimoto, M., Hirose, W., Ishizaki, Y., ... Abdurakhmanov, A.I., 2002. Tyatya volcano, southwestern Kuril arc: recent eruptive activity inferred from widespread tephra. Island Arc 11 (4), 236–254. https://doi.org/10.1046/j.1440-1738.2002.00368.x.
Naranjo, J.A., 1993. La erupcion del volcan Hudson en 1991 (46 ° S), Region XI, Aisen, Chile. Servicio Nacional de Geologia y Minera Boletin 44, 1–50.
Naranjo, J., Sigurdsson, H., Carey, S., Fritz, W., 1986. Eruption of the Nevada del Ruiz volcano, Colombia, on 13 November 1985: tephra fall and lahars. Science 233, 961–964. https://doi.org/10.1126/science.233.4767.961.
Neal, C., McGimsey, R., Gardner, C., Harbin, M., Nye, C., Keith, T., 1995. Tephra-fall deposits from the 1992 eruptions of Crater Peak, Mount Spurr Volcano, Alaska; a preliminary report on distribution, stratigraphy, and composition. U.S. Geol. Surv. Bull. 2139, 65–79.

Newhall, C.G., Self, S., 1982. The volcanic explosivity index (VEI) an estimate of explosive magnitude for historical volcanism. J. Geophys. Res. Oceans 87 (C2), 1231–1238.
Newhall, C.G., Daag, A.S., Delfin, F., Hoblitt, R.P., McGeehin, J., Pallister, J.S., Regalado, M., Rubin, M., Tubianosa, B.S., Tamayo, R., et al., 1996. Eruptive History of Mount Pinatubo. Fire and Mud: Eruptions and Lahars of Mount Pinatubo, Philippines: Philippine Institute of Volcanology and Seismology and University of Washington. pp. 165–195.
Norini, G., De Beni, E., Andronico, D., Polacci, M., Burton, M., Zucca, F., 2009. The 16 November 2006 flank collapse of the south-east crater at Mount Etna, Italy: Study of the deposit and hazard assessment. J. Geophys. Res. Solid Earth 114 (B2). https://doi.org/10.1029/2008JB005779.
Nye, C., Keith, T., Eichelberger, J., Miller, T., McNutt, S., Moran, S., Schneider, D., Dehn, J., Schaefer, J., 2002. The 1999 eruption of Shishaldin Volcano, Alaska: monitoring a distant eruption. Bull. Volcanol. 64 (8), 507–519. https://doi.org/10.1007/s00445-002-0225-2.
Oddsson, B., Gudmundsson, M.T., Larsen, G., Karlsdóttir, S., 2012. Monitoring of the plume from the basaltic phreatomagmatic 2004 Grímsvötn eruption-application of weather radar and comparison with plume models. Bull. Volcanol. 74 (6), 1395–1407. https://doi.org/10.1007/s00445-012-0598-9.
Ogburn, S.E., Loughlin, S.C., Calder, E.S., 2015. The association of lava dome growth with major explosive activity (VEI≥ 4): DomeHaz, a global dataset. Bull. Volcanol. 77 (5), 40.
Oikawa, T., Yoshimoto, M., Nakada, S., Maeno, F., Komori, J., Shimano, T., ... Ishimine, Y., 2016. Reconstruction of the 2014 eruption sequence of Ontake Volcano from recorded images and interviews. Earth Planets Space 68 (1), 1–13. https://doi.org/10.1186/s40623-016-0458-5.
Pallister, J.S., Trusdell, F.A., Brownfield, I.K., Siems, D.F., Budahn, J.R., Sutley, S.F., 2005. The 2003 phreatomagmatic eruptions of Anatahan volcano-textural and petrologic features of deposits at an emergent island volcano. J. Volcanol. Geotherm. Res. 146 (1), 208–225. https://doi.org/10.1016/j.jvolgeores.2004.11.036.
Pardini, F., Burton, M., Arzilli, F., La Spina, G., Polacci, M., 2018. SO2 emissions, plume heights and magmatic processes inferred from satellite data: The 2015 Calbuco eruptions. J. Volcanol. Geotherm. Res. 361, 12–24. https://doi.org/10.1016/j.jvolgeores.2018.08.001.
Petersen, G., Bjornsson, H., Arason, P., Löwis, S.v., 2012. Two weather radar time series of the altitude of the volcanic plume during the May 2011 eruption of Grímsvötn, Iceland. Earth Syst. Sci. Data 4 (1), 121–127. https://doi.org/10.5194/essd-4-121-2012.
Pioli, L., Bonadonna, C., Pistolesi, M., 2019. Reliability of total grain-size distribution of tephra deposits. Sci. Rep. 9 (1), 1–15. https://doi.org/10.1038/s41598-019-46125-8.
Pistolesi, M., Cioni, R., Bonadonna, C., Elissondo, M., Baumann, V., Bertagnini, A., Chiari, L., Gonzales, R., Rosi, M., Francalanci, L., 2015. Complex dynamics of small-moderate volcanic events: the example of the 2011 rhyolitic Cordón Caulle eruption, Chile. Bull. Volcanol. 77 (1), 3. https://doi.org/10.1007/s00445-014-0898-3.
Plechov, P.Y., Tsai, A.E., Shcherbakov, V.D., Dirksen, O.V., 2008. Opacitization conditions of hornblende in Bezymyannyi volcano andesites (March 30, 1956 eruption). Petrology 16 (1), 19–35. https://doi.org/10.1134/S0869591108010025.
Poli, P., Hersbach, H., Dee, D.P., Berrisford, P., Simmons, A.J., Vitart, F., ... Trémolet, Y., 2016. ERA-20C: an atmospheric reanalysis of the twentieth century. J. Clim. 29 (11), 4083–4097.
Poret, M., Costa, A., Folch, A., Martí, A., 2017. Modelling tephra dispersal and ash aggregation: the 26th April 1979 eruption, La Soufrière St. Vincent. J. Volcanol. Geotherm. Res. 347, 207–220. https://doi.org/10.1016/j.jvolgeores.2017.09.012.
Poret, M., Costa, A., Andronico, D., Scollo, S., Gouhier, M., Cristaldi, A., 2018a. Modeling eruption source parameters by integrating field, ground-based, and satellite-based measurements: The case of the 23 February 2013 Etna Paroxysm. J. Geophys. Res. Solid Earth 123 (7), 5427–5450. https://doi.org/10.1029/2017JB015163.
Poret, M., Corradini, S., Merucci, L., Costa, A., Andronico, D., Montopoli, M., ... Freret-Lorgeril, V., 2018b. Reconstructing volcanic plume evolution integrating satellite and ground-based data: application to the 23 November 2013 Etna eruption. Atmos. Chem. Phys. 18 (7), 4695. https://doi.org/10.5194/acp-18-4695-2018.
Portnyagin, M.V., Hoernle, K., Mironov, N.L., 2014. Contrasting compositional trends of rocks and olivine-hosted melt inclusions from Cerro Negro volcano (Central America): implications for decompression-driven fractionation of hydrous magmas. Int. J. Earth Sci. 103 (7), 1963–1982. https://doi.org/10.1007/s00531-012-0810-3.
Pouget, S., Bursik, M., Webley, P., Dehn, J., Pavolonis, M., 2013. Estimation of eruption source parameters from umbrella cloud or downwind plume growth rate. J. Volcanol. Geotherm. Res. 258, 100–112.
Pouget, S., Bursik, M., Johnson, C.G., Hogg, A.J., Phillips, J.C., Sparks, R.S.J., 2016a. Interpretation of umbrella cloud growth and morphology: implications for flow regimes of short-lived and long-lived eruptions. Bull. Volcanol. 78 (1), 1.
Pouget, S., Bursik, M., Singla, P., Singh, T., 2016b. Sensitivity analysis of a one-dimensional model of a volcanic plume with particle fallout and collapse behavior. J. Volcanol. Geotherm. Res. 326, 43–53.
Prata, A.J., Grant, I.F., 2001. Retrieval of microphysical and morphological properties of volcanic ash plumes from satellite data: application to Mt Ruapehu, New Zealand. Q. J. R. Meteorol. Soc. 127 (576), 2153–2179. https://doi.org/10.1002/qj.49712757615.
Prata, A.J., Gangale, G., Clarisse, L., Karagulian, F., 2010. Ash and sulfur dioxide in the 2008 eruptions of Okmok and Kasatochi: insights from high spectral resolution satellite measurements. J. Geophys. Res.-Atmos. 115 (D2). https://doi.org/10.1029/2009JD013556.
Prata, A., Siems, S., Manton, M., 2015. Quantification of volcanic cloud top heights and thicknesses using A-train observations for the 2008 Chaitén eruption. J. Geophys. Res. Atmos. 120 (7), 2928–2950. https://doi.org/10.1002/2014JD022399.
Prata, F., Woodhouse, M., Huppert, H.E., Prata, A., Thordarson, T., Carn, S., 2017. Atmospheric processes affecting the separation of volcanic ash and SO2 in volcanic eruptions: inferences from the May 2011 Grímsvötn eruption. Atmos. Chem. Phys. 17 (17), 10709–10732.
Pyle, D.M., 1989. The thickness, volume and grainsize of tephra fall deposits. Bull. Volcanol. 51 (1), 1–15.
Reckziegel, F., Bustos, E., Mingari, L., Báez, W., Villarosa, G., Folch, A., Collini, E., Viramonte, J., Romero, J., Osores, S., 2016. Forecasting volcanic ash dispersal and coeval resuspension during the April–May 2015 Calbuco eruption. J. Volcanol. Geotherm. Res. 321, 44–57. https://doi.org/10.1016/j.jvolgeores.2016.04.033.
Ridolfi, F., Puerini, M., Renzulli, A., Menna, M., Toulkeridis, T., 2008. The magmatic feeding system of El Reventador volcano (Sub-Andean zone, Ecuador) constrained by texture, mineralogy and thermobarometry of the 2002 erupted products. J. Volcanol. Geotherm. Res. 176 (1), 94–106. https://doi.org/10.1016/j.jvolgeores.2008.03.003.
Ripepe, M., Harris, A.J., 2008. Dynamics of the 5 April 2003 explosive paroxysm observed at Stromboli by a near-vent thermal, seismic and infrasonic array. Geophys. Res. Lett. 35 (7). https://doi.org/10.1029/2007GL032533.
Ripepe, M., Bonadonna, C., Folch, A., Delle Donne, D., Lacanna, G., Marchetti, E., Höskuldsson, A., 2013. Ash-plume dynamics and eruption source parameters by infrasound and thermal imagery: the 2010 Eyjafjallajökull eruption. Earth Planet. Sci. Lett. 366, 112–121. https://doi.org/10.1016/j.epsl.2013.02.005.
Rizi, V., Masci, F., Redaelli, G., Di Carlo, P., Iarlori, M., Visconti, G., Thomason, L.W., 2000. Lidar and SAGE II observations of Shishaldin volcano aerosols and lower stratospheric transport. Geophys. Res. Lett. 27 (21), 3445–3448. https://doi.org/10.1029/2000GL011515.
Robock, Alan, Matson, Michael, 1983. Circumglobal transport of the El Chichón volcanic dust cloud. Science 221 (4606), 195–197. https://doi.org/10.1126/science.221.4606.195.
Roggensack, K., Hervig, R.L., McKnight, S.B., Williams, S.N., 1997. Explosive basaltic volcanism from Cerro Negro volcano: influence of volatiles on eruptive style. Science 277 (5332), 1639–1642. https://doi.org/10.1126/science.277.5332.1639.
Romero, J., Viramonte, J.G., Scasso, R.A., 2013. Indirect tephra volume estimations using theoretical models for some Chilean historical volcanic eruptions with sustained columns. https://www.researchgate.net/publication/258866588_Indirect_tephra_volume_estimations_using_theorical_models_for_some_Chilean_historical_volcanic_eruptions_with_sustained_columns.
Romero, J., Keller, W., Diaz-Alvarado, J., Polacci, M., Inostroza, M., 2016a. The 3 March 2015 eruption of Villarrica volcano, Southern Andes of Chile: overview of deposits and impacts. https://doi.org/10.13140/RG.2.1.3575.1286.
Romero, J., Morgavi, D., Arzilli, F., Daga, R., Caselli, A., Reckziegel, F., Viramonte, J., Díaz-Alvarado, J., Polacci, M., Burton, M., et al., 2016b. Eruption dynamics of the 22–23 April 2015 Calbuco volcano (Southern Chile): analyses of tephra fall deposits. J. Volcanol. Geotherm. Res. 317, 15–29. https://doi.org/10.1016/j.jvolgeores.2016.02.027.
Romero, J.E., Amin Doulillet, G., Vallejo Vargas, S., Bustillos Arequipa, J.E., Troncoso, L., Díaz Alvarado, J., Ramón, P., 2017. Dynamics and style transition of a moderate, Vulcanian-driven eruption at Tungurahua (Ecuador) in February 2014: pyroclastic deposits and hazard considerations. https://doi.org/10.5194/se-8-697-2017.
Rose, W.I., 1972. Notes on the 1902 eruption of Santa Maria volcano, Guatemala. Bull. Volcanol. 36 (1), 29–45.
Rose, W.I., Durant, A.J., 2009. El Chichón volcano, April 4, 1982: volcanic cloud history and fine ash fallout. Nat. Hazards 51 (2), 363. https://doi.org/10.1007/s11069-008-9283-x.
Rose, W., Bonis, S., Stoiber, R., Keller, M., Bickford, T., 1973. Studies of volcanic ash from two recent Central American eruptions. Bull. Volcanol. 37 (3), 338–364. https://doi.org/10.1007/BF02597633.
Rose, W.I., Anderson, A.T., Woodruff, L.G., Bonis, S.B., 1978. The October 1974 basaltic tephra from Fuego volcano: description and history of the magma body. J. Volcanol. Geotherm. Res. 4 (1), 3–53. https://doi.org/10.1016/0377-0273(78)90027-6.
Rose, W.I., Kostinski, A.B., Kelley, L., 1995. Real-time C-band radar observations of 1992 eruption clouds from Crater Peak, Mount Spurr Volcano, Alaska. U.S. Geol. Surv. Bull. 2139, 19–26.
Rose, W., Gu, Y., Watson, I., Yu, T., Blut, G., Prata, A., Krueger, A., Krotkov, N., Carn, S., Fromm, M., et al., 2003. The February–March 2000 eruption of Hekla, Iceland from a satellite perspective. Volcanism Earth's Atmos., 107–132 https://doi.org/10.1029/139GM07.
Rose, W.I., Self, S., Murrow, P.J., Ernst, G.J., Bonadonna, C., Durant, A.J., 2007. Pyroclastic fall deposit from the October 14, 1974 eruption of Fuego Volcano, Guatemala. Volcanol 70, 1043–1067.
Rose, W., Self, S., Murrow, P., Bonadonna, C., Durant, A., Ernst, G., 2008. Nature and significance of small volume fall deposits at composite volcanoes: insights from the October 14, 1974 Fuego eruption, Guatemala. Bull. Volcanol. 70 (9), 1043–1067. https://doi.org/10.1007/s00445-007-0187-5.
Rosi, M., Bertagnini, A., Harris, A.J.L., Pioli, L., Pistolesi, M., Ripepe, M., 2006. A case history of paroxysmal explosion at Stromboli: timing and dynamics of the April 5, 2003 event. Earth Planet. Sci. Lett. 243 (3–4), 594–606. https://doi.org/10.1016/j.epsl.2006.01.035.
Rossi, E., Bonadonna, C., Degruyter, W., 2019. A new strategy for the estimation of plume height from clast dispersal in various atmospheric and eruptive conditions. Earth Planet. Sci. Lett. 505, 1–12.
Rowley, P.D., 1981. Pyroclastic-flow deposits. The 1980 eruptions of Mount St. Helens, Washington. US Geol. Surv. Prof. Paper, 1250. pp. 489–512.
Ruprecht, P., Bachmann, O., 2010. Pre-eruptive reheating during magma mixing at Quizapu volcano and the implications for the explosiveness of silicic arc volcanoes. Geology 38 (10), 919–922. https://doi.org/10.1130/G31110.1.

Rutherford, M.J., Sigurdsson, H., Carey, S., Davis, A., 1985. The May 18, 1980, eruption of Mount St. Helens: 1. Melt composition and experimental phase equilibria. J. Geophys. Res. Solid Earth 90 (B4), 2929–2947. https://doi.org/10.1029/JB090iB04p02929.

Rybin, A., Chibisova, M., Webley, P., Steensen, T., Izbekov, P., Neal, C., Realmuto, V., 2011. Satellite and ground observations of the June 2009 eruption of Sarychev Peak volcano, Matua Island, Central Kuriles. Bull. Volcanol. 73 (9), 1377–1392. https://doi.org/10.1007/s00445-011-0481-0.

Rybin, A., Razjigaeva, N., Degterev, A., Ganzey, K., Chibisova, M., 2012. The Eruptions of Sarychev Peak Volcano. Particularities of Activity and Influence on the Environment. New Achievements in Geoscience, Kurile Arc, p. 179.

Sadofsky, S., Portnyagin, M., Hoernle, K., van den Bogaard, P., 2008. Subduction cycling of volatiles and trace elements through the Central American volcanic arc: evidence from melt inclusions. Contrib. Mineral. Petrol. 155 (4), 433–456. https://doi.org/10.1007/s00410-007-0251-3.

Saito, G., Morishita, Y., Shinohara, H., 2010. Magma plumbing system of the 2000 eruption of Miyakejima volcano, Japan, deduced from volatile and major component contents of olivine-hosted melt inclusions. J. Geophys. Res. Solid Earth 115 (B11). https://doi.org/10.1029/2010JB007433.

Samaniego, P., Eissen, J., Le Pennec, J., Robin, C., Hall, M., Mothes, P., Chavrit, D., Cotten, J., 2008. Pre-eruptive physical conditions of El Reventador volcano (Ecuador) inferred from the petrology of the 2002 and 2004–05 eruptions. J. Volcanol. Geotherm. Res. 176 (1), 82–93. https://doi.org/10.1016/j.jvolgeores.2008.03.004.

Scaillet, B., Evans, B.W., 1999. The 15 June 1991 eruption of Mount Pinatubo. I. Phase equilibria and pre-eruption P–T–fO2–fH2O conditions of the dacite magma. J. Petrol. 40 (3), 381–411. https://doi.org/10.1093/petroj/40.3.381.

Scasso, R.A., Corbella, H., Tiberi, P., 1994. Sedimentological analysis of the tephra from the 12–15 August 1991 eruption of Hudson volcano. Bull. Volcanol. 56 (2), 121–132. https://doi.org/10.1007/BF00304107.

Schneider, D.J., Hoblitt, R.P., 2013. Doppler weather radar observations of the 2009 eruption of Redoubt Volcano, Alaska. J. Volcanol. Geotherm. Res. 259, 133–144. https://doi.org/10.1016/j.jvolgeores.2012.11.004.

Schneider, D.J., Thompson, G., 2000. Volcanic Clouds from the 1999 Eruption of Shishaldin Volcano: Comparison of Satellite and Seismic Observations, manuscript submitted to Bulletin of VOlcanology in May 2020. https://osf.io/2hfcx.

Schneider, D.J., Rose, W.I., Coke, L.R., Bluth, G.J., Sprod, I.E., Krueger, A.J., 1999. Early evolution of a stratospheric volcanic eruption cloud as observed with TOMS and AVHRR. J. Geophys. Res. Atmos. 104 (D4), 4037–4050. https://doi.org/10.1029/1998JD200073.

Scollo, S., Del Carlo, P., Coltelli, M., 2007. Tephra fallout of 2001 Etna flank eruption: analysis of the deposit and plume dispersion. J. Volcanol. Geotherm. Res. 160 (1), 147–164. https://doi.org/10.1016/j.jvolgeores.2006.09.007.

Scollo, S., Tarantola, S., Bonadonna, C., Coltelli, M., Saltelli, A., 2008. Sensitivity analysis and uncertainty estimation for tephra dispersal models. J. Geophys. Res. Solid Earth 113 (B6). https://doi.org/10.1029/2006JB004864.

Scollo, S., Prestifilippo, M., Pecora, E., Corradini, S., Merucci, L., Spata, G., Coltelli, M., 2014. Eruption column height estimation of the 2011-2013 Etna lava fountains. Ann. Geophys. 57 (2), 0214. https://doi.org/10.4401/ag-6396.

Scollo, S., Boselli, A., Coltelli, M., Leto, G., Pisani, G., Prestifilippo, M., ... Wang, X., 2015. Volcanic ash concentration during the 12 August 2011 Etna eruption. Geophys. Res. Lett. 42 (8), 2634–2641.

Scott, W., McGimsey, R., 1994. Character, mass, distribution, and origin of tephra-fall deposits of the 1989–1990 eruption of Redoubt Volcano, south-central Alaska. J. Volcanol. Geotherm. Res. 62 (1–4), 251–272. https://doi.org/10.1016/0377-0273(94)90036-1.

Scott, W.E., Hoblitt, R.P., Torres, R.C., Self, S., Martinez, M.M.L., Nillos, T., 1996. Pyroclastic flows of the June 15, 1991, climactic eruption of Mount Pinatubo. Fire and mud: Eruptions and lahars of Mount Pinatubo, Philippines. pp. 545–570.

Scott, W.E., Sherrod, D.R., Gardner, C.A., 2008. Overview of the 2004 to 2006, and continuing, eruption of Mount St. Helens, Washington. A Volcano Rekindled: The Renewed Eruption of Mount St. Helens, 2004–2006. vol. 1750. US Geological Survey. pp. 3–22.

Searcy, C., Dean, K.G., Stringer, W., 1998. PUFF: a volcanic ash tracking and prediction model, Journal of Volcanology and. Geothermal Res. 80, 1–16.

Self, S., Rampino, M., 2012. The 19631964 eruption of Agung volcano (Bali, Indonesia). Bull. Volcanol. 74 (6), 1521–1536. https://doi.org/10.1007/s00445-012-0615-z.

Sellitto, P., di Sarra, A., Corradini, S., Boichu, M., Herbin, H., Dubuisson, P., ... Rusalem, J., 2016. Synergistic use of Lagrangian dispersion and radiative transfer modelling with satellite and surface remote sensing measurements for the investigation of volcanic plumes: the Mount Etna eruption of 25–27 October 2013. Atmos. Chem. Phys. https://doi.org/10.5194/acp-16-6841-2016.

SERNAGEOMIN, 2015. Informe de resumen crisis volcán Villarrica febrero-marzo 2015. Technical Report. Servicio Nacional de Geología y Minería.

Settle, M., 1978. Volcanic eruption clouds and the thermal power output of explosive eruptions. J. Volcanol. Geotherm. Res. 3 (3-4), 309–324.

Shcherbakov, V.D., Plechov, P.Y., Izbekov, P.E., Shipman, J.S., 2011. Plagioclase zoning as an indicator of magma processes at Bezymianny volcano, Kamchatka. Contrib. Mineral. Petrol. 162 (1), 83–99. https://doi.org/10.1007/s00410-010-0584-1.

Shcherbakov, V.D., Neill, O.K., Izbekov, P.E., Plechov, P.Y., 2013. Phase equilibria constraints on pre-eruptive magma storage conditions for the 1956 eruption of Bezymianny Volcano, Kamchatka, Russia. J. Volcanol. Geotherm. Res. 263, 132–140. https://doi.org/10.1016/j.jvolgeores.2013.02.010.

Shepherd, J.B., Aspinall, W.P., Rowley, K.C., Pereira, J., Sigurdsson, H., Fiske, R.S., Tomblin, J.F., 1979. The eruption of Soufrière volcano, St Vincent April–June 1979. Nature 282 (5734), 24–28. https://doi.org/10.1038/282024a0.

Shibata, T., Kinoshita, T., 2016. Volcanic aerosol layer formed in the tropical upper troposphere by the eruption of Mt. Merapi, Java, in November 2010 observed by the spaceborne lidar CALIOP. Atmos. Res. 168, 49–56. https://doi.org/10.1016/j.atmosres.2015.09.002.

Shimano, T., Nishimura, T., Chiga, N., Shibasaki, Y., Iguchi, M., Miki, D., Yokoo, A., 2013. Development of an automatic volcanic ash sampling apparatus for active volcanoes. Bull. Volcanol. 75 (12), 773.

Sigurdsson, H., Carey, S.N., Espindola, J.M., 1984. The 1982 eruptions of El Chichón volcano, Mexico: stratigraphy of pyroclastic deposits. J. Volcanol. Geotherm. Res. 23 (1–2), 11–37. https://doi.org/10.1016/0377-0273(84)90055-6.

Sigurdsson, H., Carey, S.N., Fisher, R.V., 1987. The 1982 eruptions of El Chichón volcano, Mexico (3): Physical properties of pyroclastic surges. Bull. Volcanol. 49 (2), 467–488. https://doi.org/10.1007/BF01245474.

Slezin, Y.B., 2015. The Bezymyannyi, Shiveluch, and St. Helens volcanoes: a comparative revision of their catastrophic eruptions during the 20th century. J. Volcanol. Seismol. 9 (5), 289–294. https://doi.org/10.1134/S0742046315050073.

Solikhin, A., Thouret, J.-C., Liew, S.C., Gupta, A., Sayudi, D.S., Oehler, J.-F., Kassouk, Z., 2015. High-spatial-resolution imagery helps map deposits of the large (VEI 4) 2010 Merapi volcano eruption and their impact. Bull. Volcanol. 77 (3), 20. https://doi.org/10.1007/s00445-015-0908-0.

Sparks, R.S.J., 1986. The dimensions and dynamics of volcanic eruption columns. Bull. Volcanol. 48 (1), 3–15.

Sparks, R.S.J., Bursik, M.I., Carey, S.N., Gilbert, J., Glaze, L.S., Sigurdsson, H., Woods, A.W., 1997a. Volcanic Plumes. Wiley.

Sparks, R.S.J., Gardeweg, M.C., Calder, E.S., Matthews, S.J., 1997b. Erosion by pyroclastic flows on Lascar Volcano, Chile. Bull. Volcanol. 58 (7), 557–565. https://doi.org/10.1007/s004450050162.

Spilliaert, N., Allard, P., Métrich, N., Sobolev, A., 2006. Melt inclusion record of the conditions of ascent, degassing, and extrusion of volatile-rich alkali basalt during the powerful 2002 flank eruption of Mount Etna (Italy). J. Geophys. Res. Solid Earth 111 (B4). https://doi.org/10.1029/2005JB003934.

Steffke, A., Fee, D., Garces, M., Harris, A., 2010. Eruption chronologies, plume heights and eruption styles at Tungurahua Volcano: integrating remote sensing techniques and infrasound. J. Volcanol. Geotherm. Res. 193 (3), 143–160.

Stelling, P., Beget, J., Nye, C., Gardner, J., Devine, J., George, R., 2002. Geology and petrology of ejecta from the 1999 eruption of Shishaldin Volcano, Alaska. Bull. Volcanol. 64 (8), 548–561. https://doi.org/10.1007/s00445-002-0229-y.

Stohl, A., Hittenberger, M., Wotawa, G., 1998. Validation of the Lagrangian particle dispersion model FLEXPART against large scale tracer experiments. Atmos. Environ. 32, 4245–4264.

Stohl, A., Prata, A.J., Eckhardt, S., Clarisse, L., Durant, A., Henne, S., ... Stebel, K., 2011. Determination of time-and height-resolved volcanic ash emissions and their use for quantitative ash dispersion modeling: the 2010 Eyjafjallajökull eruption. Atmos. Chem. Phys. 11, 4333–4351. https://doi.org/10.5194/acp-11-4333-2011.

Sulpizio, R., 2005. Three empirical methods for the calculation of distal volume of tephra-fall deposits. J. Volcanol. Geotherm. Res. 145 (3), 315–336. https://doi.org/10.1016/j.jvolgeores.2005.03.001.

Surono, Jousset, P., Pallister, J., Boichu, M., Buongiorno, M.F., Budisantoso, A., Costa, F., Andreastuti, S., Prata, F., Schneider, D., Clarisse, L., et al., 2012. The 2010 explosive eruption of Java's Merapi volcano—a 100-year event. J. Volcanol. Geotherm. Res. 241, 121–135. https://doi.org/10.1016/j.jvolgeores.2012.06.018.

Suzuki, Y.J., Iguchi, M., 2019. Determination of the mass eruption rate for the 2014 Mount Kelud eruption using three-dimensional numerical simulations of volcanic plumes. J. Volcanol. Geotherm. Res. 382, 42–49.

Suzuki, Y., Yasuda, A., Hokanishi, N., Kaneko, T., Nakada, S., Fujii, T., 2013. Syneruptive deep magma transfer and shallow magma remobilization during the 2011 eruption of Shinmoe-dake, Japan-constraints from melt inclusions and phase equilibria experiments. J. Volcanol. Geotherm. Res. 257, 184–204. https://doi.org/10.1016/j.jvolgeores.2013.03.017.

Suzuki, Y., Iguchi, M., Maeno, F., Nakada, S., Hashimoto, A., Shimbori, T., Ishii, K., 2014. 3D numerical simulations of volcanic plume and tephra dispersal: reconstruction of the 2014 Kelud eruption. AGU Fall meeting abstracts. vol. 1, p. 02. http://adsabs.harvard.edu/abs/2014AGUFM.V53E.02S.

Suzuki, Y.J., Costa, A., Cerminara, M., Eposti Ongaro, T., Herzog, M., Van Eaton, A.R., Denby, L.C., 2016. Inter-comparison of three-dimensional models of volcanic plumes. J. Volcanol. Geotherm. Res. 326, 26–42. https://doi.org/10.1016/j.jvolgeores.2016.06.011.

Syahbana, D.K., Kasbani, K., Suantika, G., Prambada, O., Andreas, A.S., Saing, U.B., ... Suparman, Y., 2019. The 2017–19 activity at Mount Agung in Bali (Indonesia): Intense unrest, monitoring, crisis response, evacuation, and eruption. Sci. Rep. 9 (1), 1–17.

Takarada, S., Oikawa, T., Furukawa, R., Hoshizumi, H., Itoh, J.I., Geshi, N., Miyagi, I., 2016. Estimation of total discharged mass from the phreatic eruption of Ontake Volcano, central Japan, on September 27, 2014. Earth Planets Space 68 (1), 138. https://doi.org/10.1186/s40623-016-0511-4.

Taylor, I.A., Carboni, E., Ventress, L.J., Mather, T.A., Grainger, R.G., 2019. An adaptation of the CO_2 slicing technique for the Infrared Atmospheric Sounding Interferometer to obtain the height of tropospheric volcanic ash clouds. Atmos. Measur. Techn. 12 (7), 3853–3883.

Thorarinsson, S., 1949. The tephra-fall from Hekla on March 29th, 1947: Reykjavik, Societas Scientiarum Islandica, v. II, 3: The tephra-fall from Hekla on March 29, 1947 68 p.

Thorarinsson, S., 1950. The eruption of Mt. Hekla 1947–1948. Bull. Volcanol. 10 (1), 157–168. https://doi.org/10.1007/BF02596085.

Thorarinsson, S., Sigvaldason, G.E., 1972. The Hekla eruption of 1970. Bull. Volcanol. 36 (2), 269–288. https://doi.org/10.1007/BF02596870.

Thordarson, T., Hayward, C., Hartley, M., Sigmarsson, O., Höskuldsson, Á., Larsen, G., 2011. The 14 April–22 May 2010 summit eruption at Eyjafjallajökull volcano, Iceland: volatile contents and magma degassing. Geophys. Res. Abstr. 13, EGU201112046.
Troncoso, L., Bustillos, J., Romero, J.E., Guevara, A., Carrillo, J., Montalvo, E., Izquierdo, T., 2017. Hydrovolcanic ash emission between August 14 and 24, 2015 at Cotopaxi volcano (Ecuador): Characterization and eruption mechanisms. J. Volcanol. Geotherm. Res. 341, 228–241. https://doi.org/10.1016/j.jvolgeores.2017.05.032.
Trusdell, F.A., Moore, R.B., Sako, M., White, R.A., Koyanagi, S.K., Chong, R., Camacho, J.T., 2005. The 2003 eruption of Anatahan volcano, Commonwealth of the Northern Mariana Islands: chronology, volcanology, and deformation. J. Volcanol. Geotherm. Res. 146 (1), 184–207. https://doi.org/10.1016/j.jvolgeores.2004.12.010.
Tupper, A., Wunderman, R., 2009. Reducing discrepancies in ground and satellite-observed eruption heights. J. Volcanol. Geotherm. Res. 186 (1-2), 22–31.
U.S. Geological Survey, 2005. Mount St. Helens From the 1980 Eruption to 2000. U.S. Geological Survey Fact Sheet 036-00.
Underwood, S.J., Feeley, T.C., Clynne, M.A., 2013. Hydrogen isotope investigation of amphibole and glass in dacite magmas erupted in 1980–1986 and 2005 at Mount St. Helens, Washington. J. Petrol. 54 (6), 1047–1070. https://doi.org/10.1093/petrology/egt005.
Unema, J., 2001. Water-Magma Interaction and Plume Processes in the 2008 Okmok Eruption Master's thesis.
Urai, M., Ishizuka, Y., 2011. Advantages and challenges of space-borne remote sensing for Volcanic Explosivity Index (VEI): the 2009 eruption of Sarychev Peak on Matua Island, Kuril Islands, Russia. J. Volcanol. Geotherm. Res. 208 (3-4), 163–168. https://doi.org/10.1016/j.jvolgeores.2011.07.010.
Van Eaton, A.R., Herzog, M., Wilson, C.J.N., McGregor, J., 2012. Ascent dynamics of large phreatomagmatic eruption clouds: the role of microphysics. J. Geophys. Res. 117, B03203. https://doi.org/10.1029/2011JB008892.
Van Eaton, A., Mastin, L., Herzog, M., et al., 2015. Hail formation triggers rapid ash aggregation in volcanic plumes. Nat. Commun. 6, 7860. https://doi.org/10.1038/ncomms8860.
Van Eaton, A.R., Amigo, Á., Bertin, D., Mastin, L.G., Giacosa, R.E., González, J., ... Behnke, S.A., 2016. Volcanic lightning and plume behavior reveal evolving hazards during the April 2015 eruption of Calbuco volcano, Chile. Geophys. Res. Lett. 43 (7), 3563–3571.
Van Manen, S.M., Dehn, J., Blake, S., 2010. Satellite thermal observations of the Bezymianny lava dome 1993–2008: precursory activity, large explosions, and dome growth. J. Geophys. Res. Solid Earth 115 (B8). https://doi.org/10.1029/2009JB006966.
Varekamp, J.C., Luhr, J.F., Prestegaard, K.L., 1984. The 1982 eruptions of El Chichón Volcano (Chiapas, Mexico): character of the eruptions, ash-fall deposits, and gasphase. J. Volcanol. Geotherm. Res. 23 (1–2), 39–68. https://doi.org/10.1016/0377-0273(84)90056-8.
Vernier, J.-P., Fairlie, T.D., Deshler, T., Natarajan, M., Knepp, T., Foster, K., Wienhold, F.G., Bedka, K.M., Thomason, L., Trepte, C., 2016. In situ and spacebased observations of the Kelud volcanic plume: the persistence of ash in the lower stratosphere. J. Geophys. Res. Atmos. 121 (18). https://doi.org/10.1002/2016JD025344.
Versteegeri, P.L., Douglas, D.D., Autrechy, M.C.M., Gallaway, C.R., 1995. Defining a keep-out region for aircraft after a volcanic eruption. In Volcanic ash and aviation safety: Proceedings of the First International Symposium on Volcanic Ash and Aviation Safety. Vol. 2047. DIANE Publishing, p. 297.
Vidal, L., Nesbitt, S., Salio, P., Osores, S., Farias, C., Rodriguez, A., Serra, J., Caranti, G., 2015a. C-band dual-polarization observations of a massive volcanic eruption in South America. AMS. https://ams.confex.com/ams/37RADAR/webprogram/Handout/Paper276312/ID276312_AMSRadarConf2015_Vidal_et_al.pdf.
Vidal, C.M., Komorowski, J.C., Métrich, N., Pratomo, I., Kartadinata, N., Prambada, O., ... Fontijn, K., 2015b. Dynamics of the major plinian eruption of Samalas in 1257 AD (Lombok, Indonesia). Bull. Volcanol. 77 (9), 73.
Voight, B., 1990. The 1985 Nevado del Ruiz volcano catastrophe: anatomy and retrospection. J. Volcanol. Geotherm. Res. 42 (1–2), 151–188. https://doi.org/10.1016/0377-0273(90)90075-Q.
Voight, B., Glicken, H.A.R.R.Y., Janda, R.J., Douglass, P.M., 1981. The 1980 eruptions of Mount St. Helens, Washington. US Geol. Survey Prof. Paper, 1250. pp. 347–377.
Volentik, A.C., Bonadonna, C., Connor, C.B., Connor, L.J., Rosi, M., 2010. Modeling tephra dispersal in absence of wind: Insights from the climactic phase of the 2450 BP Plinian eruption of Pululagua volcano (Ecuador). J. Volcanol. Geotherm. Res. 193 (1–2), 117–136.
Waitt, R.B., Mastin, L.G., Miller, T.P., 1995. Ballistic showers during crater peak eruptions of Mount Spurr volcano, summer 1992. USGS Bull 2139, 89–106.
Wallace, K.L., Neal, C.A., McGimsey, R.G., 2006. Timing, distribution, and character of tephra fall from the 2005–2006 eruption of Augustine volcano. U.S. Geol. Surv. Prof. Pap. 187–217.
Wallace, K., Schaefer, J., Coombs, M., 2013. Character, mass, distribution, and origin of tephra-fall deposits from the 2009 eruption of Redoubt Volcano, Alaska highlighting the significance of particle aggregation. J. Volcanol. Geotherm. Res. 259, 145–169. https://doi.org/10.1016/j.jvolgeores.2012.09.015.
Wallace, P.J., et al., 2015. Volatiles in magmas. The Encyclopedia of Volcanoes. Elsevier, pp. 163–183 Ed. by H. Sigurdsson et al.
Wallace, K., Bursik, M., Kuehn, S., Kurbatov, A., Abbott, P., Bonadonna, C., Cashman, K., Davies, S., Jensen, B., Lane, C., Plunkett, G., Smith, V., Tomlinson, E., Thordarsson, T., Walker, D., 2020. Community Established Best Practice Recommendations for Tephra Studies-from Collection through Analysis. Scientific Data: SDATA-20-01163, in review. .
Watt, S.F., Pyle, D.M., Mather, T.A., Martin, R.S., Matthews, N.E., 2009. Fallout and distribution of volcanic ash over Argentina following the May 2008 explosive eruption of Chaitén, Chile. J. Geophys. Res. Solid Earth 114 (B4). https://doi.org/10.1029/2008JB006219.
Waythomas, C.F., Scott, W.E., Prejean, S.G., Schneider, D.J., Izbekov, P., Nye, C.J., 2010. The 7–8 August 2008 eruption of Kasatochi volcano, central Aleutian Islands, Alaska. J. Geophys. Res. Solid Earth 115 (B12). https://doi.org/10.1029/2010JB007437.
Webster, J.D., Mandeville, C.W., Goldoff, B., Coombs, M.L., Tappen, C., 2006. Augustine volcano-the influence of volatile components in magmas erupted AD 2006 to 2,100 years before present. U.S. Geol. Surv. Prof. Pap. 383–423.
White, J.D., Valentine, G.A., 2016. Magmatic versus phreatomagmatic fragmentation: absence of evidence is not evidence of absence. Geosphere 12 (5), 1478–1488.
Williams, S., Self, S., 1983. The October 1902 plinian eruption of Santa Maria volcano, Guatemala. J. Volcanol. Geotherm. Res. 16 (1–2), 33–56. https://doi.org/10.1016/0377-0273(83)90083-5.
Wilson, L., Walker, G.P.L., 1987. Explosive volcanic eruptions-VI. Ejecta dispersal in plinian eruptions: the control of eruption conditions and atmospheric properties. Geophys. J. Int. 89 (2), 657–679.
Wilson, L., Sparks, R.S.J., Huang, T.C., Watkins, N.D., 1978. The control of volcanic column heights by eruption energetics and dynamics. J. Geophys. Res. Solid Earth 83 (B4), 1829–1836.
Witham, C.S., Hort, M.C., Potts, R., Servranckx, R., Husson, P., Bonnardot, F., 2007. Comparison of VAAC atmospheric dispersion models using the 1 November 2004 Grimsvötn eruption. Meteorol. Appl. J. Forecast. Pract. Appl. Train. Techn. Model. 14 (1), 27–38.
Wolf, K.J., Eichelberger, J.C., 1997. Syneruptive mixing, degassing, and crystallization at Redoubt Volcano, eruption of December, 1989 to May 1990. J. Volcanol. Geotherm. Res. 75 (1–2), 19–37. https://doi.org/10.1016/S0377-0273(96)00055-8.
Woodhouse, M.J., Hogg, A.J., Phillips, J.C., Sparks, R.S.J., 2013. Interaction between volcanic plumes and wind during the 2010 Eyjafjallajökull eruption, Iceland. J. Geophys. Res. Solid Earth 118 (1), 92–109.
Woodhouse, M.J., Hogg, A.J., Phillips, J.C., Rougier, J.C., 2015. Uncertainty analysis of a model of wind-blown volcanic plumes. Bull. Volcanol. 77 (10), 83.
Woods, A.W., Kienle, J., 1994. The dynamics and thermodynamics of volcanic clouds: theory and observations from the April 15 and April 21, 1990 eruptions of Redoubt Volcano, Alaska. J. Volcanol. Geotherm. Res. 62 (1–4), 273–299. https://doi.org/10.1016/0377-0273(94)90037-X.
Wright, R., Carn, S.A., Flynn, L.P., 2005. A satellite chronology of the May–June 2003 eruption of Anatahan volcano. J. Volcanol. Geotherm. Res. 146 (1), 102–116. https://doi.org/10.1016/j.jvolgeores.2004.10.021.
Yang, Q., Bursik, M., 2016. A new interpolation method to model thickness, isopachs, extent, and volume of tephra fall deposits. Bull. Volcanol. 78 (10), 68.
Zen, M., Hadikusumo, D., 1964. Preliminary report on the 1963 eruption of Mt. Agung in Bali (Indonesia). Bull. Volcanol. 27 (1), 269–299. https://doi.org/10.1007/BF02597526.
Zharinov, N.A., Demyanchuk, Y.V., 2011. Assessing the volumes of material discharged by Bezymyannyi Volcano during the 1955–2009 period. J. Volcanol. Seismol. 5 (2), 100–113. https://doi.org/10.1134/S0742046311020072.